Rensselaer Polytechnic Institute

Troy, New York

Rensselaer Polytechnic Institute
Troy, New York 12181

Final Report - Vol. I

Contract No. NAS8-21131

Covering period May 4, 1967-Nov. 3, 1968
NATIONAL AERONAUTICS AND
SPACE ADMINISTRATION

Analysis of Saturn Booster Performance by Conventional Control Theory Techniques

by Edward J. Smith

Other Vols.- N.I.

Submitted on behalf of

Rob Roy
Professor of Systems Division

PRECEDING PAGE BLANK NOT FILMED.

CONTENTS

Page

LIST OF FIGURES

ABSTRACT

An analysis of the stability of the flight control system of the Saturn booster is discussed here. The control law is written in terms of position gyro and rate gyro feedback. Conventional linear feedback theory is used for the analysis with the emphasis on the root locus technique. An eleventh order model is used for plant dynamics; a third order rigid body model, plus a second order model for each of the first four bending modes. The rigid body and bending dynamics are assumed to be decoupled from each other in an open loop sense, but are coupled through the gyro feedback.

The system was analyzed at the 80 second point in the trajectory, which is representative of the maximum aerodynamic pressure region. Gyro feedback gains, which determine the position of the gyro open loop zero, were chosen by use of the Routh-Hurwitz stability criteria. This method yields a stable rigid body mode, but an unstable system when the bending modes are added. At this point in the trajectory system stability is very sensitive to the first and second bending mode dynamics. A low, positive open loop gain produces an unstable system. Some form of compensation was indicated.

A simple second order lag filter inserted in the feedback path was chosen for the compensation. This filter has the effect of changing the exit angle of the locus of closed loop poles from the first and second bending mode open loop poles by 180°. This delays the entry of the loci into the right half plane. The location of the filter open loop poles were chosen to minimize their effect on the rigid body dynamics. The filter improved the stability problem caused by the first two bending modes but introduced a problem with the fourth bending mode.

In the uncompensated system the fourth bending mode locus never left the left half plane, but in the compensated system this locus now changed direction and migrated into the right half plane.

Several gyro gain combinations were investigated by use of techniques described in Parts II and III of this final report series. Several of these combinations produced stable systems. Root locus diagrams for these gains are discussed in this document.

1. INTRODUCTION

Many different techniques are available to a control systems engineer to study the time response of a closed loop feedback system. Each technique offers a distinct viewpoint of the problem. In the analysis of the Saturn Booster Control problem by the R.P.I. group, Modern Control System Analysis techniques have been used to a great extent. The use of state variable notation has simplified the system design, by facilitating the simulation of booster dynamics on the digital computer. While these techniques lend themselves admirably to the analysis of the booster control system, a certain degree of physical insight into the problem is exchanged for computational facility. In order to develop a better physical understanding of the problem, an analysis of the vehicle inner loop dynamics was undertaken using the root locus technique. This analysis provided a reference for comparison of the results obtained by more advanced techniques. By inspecting the trends shown by root locus a better physical picture is obtained of how gyro and compensation filter gain selection alter the control system effect on vehicle dynamical response.

It was felt that the analysis of the inner loop would be more informative if the rigid body dynamics were treated first, and then the bending modes added one at a time. The effect of each bending mode on the rigid body and the previous bending mode, could then be studied.

2. DEVELOPMENT OF A GENERAL CONTROL SYSTEM MODEL

In Appendix A, the closed loop transfer function of the system was first developed in general form. Polynomial coefficients were left in terms of vehicle parameters. At this point no attempt was made to obtain numerical results. Since a root locus plot was desired, the general expression for the closed loop system characteristic equation was obtained. The control law was written in terms of a command input because this led to the simplest transfer function representation of the system. A linear system was assumed, therefore this choice of input had no effect on the time response of the system.

The vehicle equations of motion, as described in the July-August 1967 project progress report, were used for this analysis. The vehicle lateral velocity $\dot{z}$, was eliminated from these equations to reduce the number of variables. This is valid because the control law does not include any parameter that will effectively control this variable and its elimination does not affect the results. The time domain equations were transformed to the s domain to simplify the algebra.

The rigid body dynamics are represented by a third order system. The open loop transfer function for this mode also contains a first order zero. The open loop poles are a result of the aerodynamic forces acting on the vehicle and the location of the vehicle center of gravity and center of pressure. The location of the open loop zero is a function of aerodynamic forces and engine thrusting forces. The rigid body attitude control loop is closed through a position and rate gyro in the feedback loop. These two gyros add another open loop zero to the system and the location of this zero on the s-plane has a great bearing on vehicle response. Overall booster stability is therefore very sensitive to the magnitudes and the ratio of gyro gains.

Each bending mode open loop transfer function has the form of a second order, lightly damped system. Each mode is excited by a forcing function which is functionally related to the engine gimble angle. While the bending modes are assumed to be decoupled from each other in an open loop sense, they are strongly coupled to the rigid body mode and to each other when the control feedback loop is closed. The bending modes are detected by the gyros, and they appear as noise in the gyro outputs. The magnitude of this noise is a function of the vehicle position in the launch trajectory.

3. NUMERICAL EXAMPLE

When the algebraic expression for the system characteristic equation was obtained, a numerical analysis at $t = 80$ seconds into the flight was conducted to obtain specific root locus plots for various gyro gains.

3.1 Rigid Body Mode

Again the rigid body dynamics were treated separately. NASA data, contained in Boeing Report D5-15381-1 was used for all calculations. As mentioned previously, the closed loop system performance was very sensitive to the location of the open loop gyro zero. A unity feedback gain was first selected, corresponding to the use of only a position gyro in the feedback path, to investigate the closed loop rigid body behavior. A root locus diagram for this condition was sketched. This is shown in Figure 1. This diagram indicated that the vehicle is unstable for all values of gain. This result is expected since the center of pressure of the booster is forward of the center of gravity, at this point in the trajectory, and results in aerodynamic instability. This is indicated by the presence of the two open loop rigid body poles located in the right half plane. The need for a stabilizing zero in the left half plane is obvious. This zero, of course, is produced by the use of the position and rate gyros in the feedback loop. The best location of the open loop gyro zero however is not readily apparent. To determine the best location, on a gross basis, three root locus diagrams were sketched indicating the three possible locations for this zero. These are shown in Figure 2. It was determined that the most suitable location for this zero was on the real axis in the left half plane to the left of the open loop pole-zero pattern of the rigid body mode. This location yielded a stable system for the lowest possible loop gain. A Routh-Hurwitz criterion analysis was conducted to determine the value of the gyro gains and the gain ratio that would just meet this condition. Analysis indicated that a displacement gyro gain of $a_o = 0.2$ and a rate gyro gain of $a_1 = 0.4$ with a corresponding gain ratio of 0.5 would satisfy this condition. Root locus diagrams were now constructed by means of a digital computer program that determined the location of the closed loop poles with a precision commensurate with the accuracy of NASA data as contained in Boeing Report D5-15381-1.

A plot of the root locus diagram for the rigid body mode is shown in Figure 3. This plot indicates that the system can be stabilized by the proper choice of forward loop gain. The gyro gain ratio is 0.5. The forward loop gain, which includes vehicle gain and the rate gyro gain, is of course varied from zero to infinity. This is a rather unusual root locus plot. As gain is increased, from zero, the locus migrating from the rigid body open loop poles located on the real axis in the right half plane, leaves the real axis at a gain of $k = 0.185$ and $s = 0.123$, crosses the $j\omega$ axis into the left half plane and reenters the real axis at $s = -0.269$ at a gain of $k = 0.79$. The locus that originated at the open loop pole located at $s = 0.422$ is traced out below the σ axis and upon reentry into this axis at $s = -0.269$, turns right and moves along the real axis to the open loop zero located at $s = -0.046$. The locus that originated at the open loop pole located at $s = 0.014$ is traced out above the σ axis, reenters this axis at $s = -0.269$ turns right, moves along the real axis until the point $s = -0.287$ is reached. This locus again breaks away from the real axis, moves in an arc above this axis around the gyro zero and again reenters the real axis at $s = -0.661$. It now turns right and moves to the zero located at $s = -\infty$.

The locus that originates at the open loop poles located at $s = -0.48$ moves to the right, along the real axis as the gain is increased until the point $s = -0.287$ is reached. Here it turns right, enters the region below the σ axis and moves in an arc to the left, swinging around the gyro zero. This locus reenters the real axis at $s = -0.661$, turns right and migrates to the open loop pole located at $s = -0.5$. The existence of four real axis break away and break in points was verified by taking the partial derivative $\partial k/\partial s$, setting it equal to zero, and factoring the roots of the resultant equation. This locus results in a situation where critical damping can be achieved for two different gains $k = 0.79$ (at $s = -0.269$) and $k = 1.36$ (at $s = -0.661$).

For the gyro feedback gains chosen for this preliminary investigation ($a_o = 0.2$ and $a_1 = 0.4$) the system forward loop gain is $k = 0.468$. This value of gain yields a pair of dominant closed loop poles at $s = -0.26 \pm j\,0.17$. This produces a damping factor of $\delta = 0.126$ at a frequency of 0.172 radians per second. This produces a very lightly damped system oscillating at a low frequency. Both damping and frequency may be improved by raising the gain to $k = 0.685$ to yield a damping factor of $\delta = 0.707$ at a frequency of $\omega = 0.15$ radians per second.

3.2 Rigid Body Plus First Bending Mode

A plot of the root locus diagram for the rigid body plus first bending mode is shown in Figure 4. Here the root locus is plotted for a positive feedback condition due to the negative sign in the characteristic equation (1-KGH).

The adverse effect of the first bending mode dynamics on the response of the vehicle is dramatically illustrated here. When the forward loop gain is increased to only $k = 0.035$, the locus migrating from the open loop poles, associated with the first bending mode and located at $s = -0.067 \pm j\,6.7$, will cross the $j\omega$ axis into the right half plane producing a divergent oscillation in the response. The system gain, resulting from a combination of rigid body open loop gain, rate gyro gain and first bending mode gain, is $k = 0.244$. This of course yields an unstable system. It is obvious that some form of compensation is required to stabilize the vehicle.

3.3 Rigid Body Plus First and Second Bending Mode

The root locus plot of the rigid body mode plus the first and second bending mode is shown in Figure 5. The open loop pole-zero pair arising from the second bending mode dynamics straddle the $j\omega$ axis. Again something unexpected happens. Comparison of Figures 4 and 5 show a difference in the locus from the pair of complex conjugate open loop poles located in the left half plane to the open loop zeros located in the right half plane on the real axis. In Figure 4, the locus migrated from the pole pair located at $s = -0.067 \pm j6.7$ to the zero located at $s = 8.7$. In Figure 5, one would expect that the addition of the pole-zero pair associated with the second bending mode would result in a locus between this pair. This does not occur. Instead a locus exists between the poles associated with the first bending mode and the zeros associated with the second bending mode. A locus also exists between the poles associated with the second bending mode and the zeros associated with the first bending mode.

Two possible explanations can be offered for this odd behavior. Although the bending modes are uncoupled in an open loop manner, they are strongly coupled through the rate and position gyros resulting in a strong interaction between modes. Secondly, the root locus itself is a mechanical technique where the physical proximity of poles and zeros determines the locus. The zeros are highly sensitive to slight changes in the coefficients of the polynomials from which they have been factored. Errors in the fifth and sixth places can change the position of the zeros sufficiently to influence the locus. As system gain is increased instability will occur at $k = 0.175$ when the locus from the pair of complex conjugate open loop poles located at $s = -0.067 \pm j6.7$ crosses the $j\omega$ axis into the right half plane. At a gain of $k = 0.373$ the locus from the open loop poles located at $s = -0.22 \pm j12.3$ also cross the $j\omega$ axis into the right half plane. The system gain resulting from the rigid body, gyro, first and second bending mode gains is $k = 1.24$. This gain results, of course, in an unstable system. Closed loop poles are located at $s = 0.29 \pm j6.66$ and $s = 0.38 \pm j12.2$ for this value of gain. Again the system must be compensated if a stable condition is to be achieved.

3.4 Rigid Body Plus First, Second and Third Bending Mode

The root locus plot of the rigid body plus first, second and third bending modes is shown in Figure 6. Again the open loop pole-zero pair arising from the third bending mode dynamics, straddle the $j\omega$ axis. Again as gain is increased, the closed loop poles due to the third bending mode will migrate from the left half plane to the right half plane. However, the third bending mode has little effect on stability since the $j\omega$ axis crossover does not occur until a gain of $k = 191$ is reached. This value is far above the low gain required to move the locus from the first bending mode poles into the right half plane. The destabilizing effect of the first and second bending modes will dominate the system response.

Determination of the location of the closed loop poles for the gains involved indicate that the first and second bending mode dynamics produce pairs of complex conjugate closed loop poles at $s = 0.38 \pm j12.3$ and $s = 0.29 \pm j6.3$ which produce instability. However at this value of gain, $k = 0.654$, the closed loop poles of the third bending mode are at $s = -0.46 \pm j16.9$ and have not crossed the $j\omega$ axis into the right half plane. This indicates that at the 80 second point in the trajectory, the vehicle is not overly sensitive to vibrations produced by the third bending mode.

3.5 Rigid Body Plus First, Second, Third and Fourth Bending Mode.

The root locus plot of the rigid body plus first, second, third and fourth bending modes is shown in Figure 7. The fourth bending mode dynamics do not produce an open loop pole-zero pair astraddle the $j\omega$ axis, but instead produce a complex conjugate pair of poles in the left half plane and a pair of zeros on the real axis one in the right half plane and one in the left half plane. The locus is traced from the open loop poles located at $s = -0.21 \pm j21.5$ to the real axis. The locus never leaves the left half plane regardless of how high the value of gain is adjusted. It is obvious that the system will not experience instability due to the fourth bending mode dynamics at this point in the trajectory.

In summary, it appears that the first and second bending modes are the principle causes of instability at this point in the trajectory. The need for compensation is apparent. Investigation of the root locus diagram of Figure 7 for the rigid body plus first bending mode, revealed that the entry of the locus into the right half plane could be delayed, until higher values of gain are reached, if the exit angle of the locus from the complex open loop poles located at $s = 0.067 \pm j6.7$ could be rotated by 180°. This can be accomplished by the addition of a second order filter of the form

$$G_c(s) = \frac{\omega_c^2}{s^2 + 2\delta_c \omega_c s + \omega_c^2} \tag{1}$$

into the feedback loop. This filter will degenerate the performance of the rigid body mode, but this trade off is practical, since the rigid body can be made stable by the proper choice of gain. Values of $\omega_c^2 = 50$ and $\delta_c = 0.707$ were chosen for the filter parameters.

4. NUMERICAL EXAMPLE WITH FEEDBACK COMPENSATION FILTER

4.1 Rigid Body Mode

The insertion of the second order lag filter in the feedback loop has little effect upon the performance of the rigid body mode at lower gains. This is apparent from the root locus of Figure 8. The location of the closed loop poles for a gain of $k = 23.4$ (a combination of a filter gain of 50 and a gyro, rigid body and bending mode open loop gain of $k = 0.468$) indicates that the dominant pair of closed loop poles are located at $s = -0.026 \pm j0.18$ due to the rigid body dynamics. The effect of the filter complex conjugate closed loop poles located at $s = -4.8 \pm j4.8$ is negligible on the overall response because the transient due to these poles dies out very quickly compared to the long transient associated with the rigid body poles. However as gain is increased the effect of the filter is more noticeable and the possibility of instability exists for high gain as the locus will move from the left half plane to the right half plane, at a gain of $k = 426$, along the direction of the asymptotes located at 60° and 300°.

4.2 Rigid Body Plus First Bending Mode

Figure 9 shows the effect of the compensation filter on the root locus for the rigid body plus the first bending mode. The filter has the effect of delaying the entry of the locus into the right half plane until higher values of gain are reached. The locus migrating from the open loop poles located at $s = -0.067 \pm j6.7$ again moves from the left half plane to the right half plane but the $j\omega$ axis crossover is accomplished at a higher gain $(k = 36.4)$ than the uncompensated system $(k = 0.0335)$ this results in a "stiffer" system. The dominant pair of closed loop poles due to the rigid body are located at $s = -0.03 \pm j0.18$. All other closed loop poles lie in the left half plane. System gain is $k = 12.2$.

4.3 Rigid Body Plus First and Second Bending Mode

The root locus plot of the rigid body plus the first and second bending modes, with compensation, is shown in Figure 10. Comparison of this locus with the uncompensated system of Figure 9, indicate that the addition of the filter has changed the locus considerably. The proximity of the closed loop filter poles to the $j\omega$ axis has changed the paths of the locus. Whereas in the uncompensated case, the locus migrated from the open loop poles associated with the first bending mode to the open loop zeros associated with the second bending mode, in the compensated case the locus now migrates between first bending mode pole-zero pair and the second bending mode pole-zero pair. The entry of the first bending mode locus into the right half plane is delayed in the compensated case. A gain of $k = 0.175$ was sufficient in the uncompensated case to drive the locus into the right half plane, but with the addition of the filter, a gain of $k = 126$, was needed to produce instability. The second bending mode locus entered the right half plane at a gain of $k = 0.373$ for the uncompensated case and for a gain of $k = 14,320$ for the compensated case. Again a great improvement is evident here and the effect of the second bending mode on system stability is desensitized. The dominant pair of closed loop poles due to the rigid body are located at $s = -0.033 \pm j0.18$. All other closed loop poles are located in the left half plane indicating a nondiverging vehicle time response. System gain is $k = 62.5$ for this condition.

4.4 Rigid Body Plus First, Second and Third Bending Mode

The root locus diagram for the rigid body plus first, second and third bending modes is shown in Figure 11. Comparison of this locus with the uncompensated system of Figure 6 again indicates that the addition of the filter drastically alters the root locus. The compensated system locus behaves as expected. A locus now exists between first bending mode pole-zero pairs, second bending mode pole-zero pairs and third bending mode pole-zero pairs. This was not the case, of course, in the uncompensated system. The entry of the first bending mode locus into the right half plane is again delayed due to the 180° phase shift in locus exist angle produced by the compensation filter. A gain of $k = 0.281$ produced first bending mode instability in the uncompensated case but now a gain of $k = 71$ is required before the locus enters the right half plane. The second bending mode locus enters the right half plane at a gain of $k = 0.208$ for the uncompensated case, but a gain of $k = 2900$ is required before this condition occurs in the compensated case. The third bending mode locus enters the right half plane for a gain of $k = 195$ for the uncompensated case however a gain of $k = 191$ is required before the system goes unstable due to the effect of the third bending mode. The first bending mode is still the prime contributor to vehicle instability, but the improvement in gain required to drive the system unstable is dramatic.

4.5 Rigid Body Plus First, Second, Thrid and Fourth Bending Mode

Finally the root locus for the rigid body plus first, second, third and fourth bending modes is shown in Figure 12. Here a stability problem is introduced by the addition of the compensation filter. In the uncompensated case, the locus from the pair of complex conjugate open loop poles associated with the fourth bending mode migrates to the real axis in the left half plane. The locus never leaves the left half plane and the fourth bending mode can never produce instability regardless of how high the system gain is raised. However, with the addition of the compensation network, the locus now migrates into the right half plane for a gain of $k = 17.3$. A check of the behavior of the first bending mode locus indicates that it does not crossover the $j\omega$ axis until a gain of $k = 36$ is reached. This indicates that in the compensated system the first bending mode no longer determines when the system will go unstable but rather the fourth bending mode now determines system stability. Obviously the filter acts as a destabilizing influence on the fourth bending mode dynamics. The composite system gain, a combination of filter, gyro and rigid body plus bending mode open loop gains, is $k = 32.7$ as indicated in Equation A-132. This produces an unstable system.

5. EFFECT OF CHANGING THE OPEN LOOP GYRO ZERO POSITION

The effect of changing the open loop gyro zero position was investigated next. Four locations at $s = 1.0$, 1.25, 1.64 and 2.33 were chosen. Root locus plots corresponding to these conditions are plotted in Figures 13, 14, 15 and 16. These root locus plots, are similar in shape to the plot shown in Figure 12.

For a position gyro gain of $a_o = 0.8$ and a rate gyro gain of $a_1 = 0.8$, resulting in a gain ratio of one. The locus migrating from the fourth bending mode open loop pole crosses the $j\omega$ axis into the right half plane at a gain of $k = 93.1$. This represents a considerable improvement over the gain of $k = 17.3$ for the case where the gyro gain ratio was 0.5. A check of the first bending mode locus reveals that a gain of $k = 44$ is now required to produce instability due to this mode. This is also an improvement over the gain of $k = 36$ found for a gyro gain ratio of 0.5. It is interesting to note, that moving the gyro zero further to the left along the real axis, as has been accomplished here, desensitizes the system to the effect of the compensation filter on the fourth bending mode locus. This root locus is shown in Figure 13.

The root locus for a gyro gain ratio of 1.25 is shown in Figure 14. Here the position gyro gain was chosen as $a_o = 0.5$ and the rate gyro gain as $a_1 = 0.4$. The locus at the fourth bending mode closed loop poles crosses the $j\omega$ axis, into the right half plane, at a value of gain of $k = 93.5$ indicating a very small change from the value of $k = 93.1$ found for a gain ratio of one. The first bending mode locus crosses the $j\omega$ axis into the right half plane for a gain of $k = 48.7$. This represents an improvement over the gain of $k = 44$ found for a gyro ratio of one. The gains required for instability of the other bending modes are much higher than the first mode and do not contribute to the stability problem.

The root locus for a gyro gain ratio of 1.64 is shown in Figure 15. Here the position gyro gain was chosen as $a_o = 0.82$ and the rate gyro gain as $a_1 = 0.5$. The locus of the fourth bending mode closed loop poles crosses the $j\omega$ axis, into the right half plane, at a value of gain of $k = 93.4$. This value is approximately the same as the gain of $k = 93.5$ obtained for a gyro gain ratio of $k = 1.25$. The gain required to drive the first bending mode unstable is $k = 55.6$, again an improvement over the gain of $k = 48.7$ found for a gyro gain ratio of 1.25.

The root locus diagram for a gyro gain ratio of 2.33 is shown in Figure 16. The position gyro gain is chosen as $a_o = 0.921$ and the rate gyro gain $a_1 = 0.395$. A check of the fourth bending mode locus reveals the system will be unstable for a gain of $k = 77.14$. This indicates a reversal in the trend of the three other gyro gain ratios plotted. Here the gain required for instability is lower than the gain ratio of 1.64 plotted previously. The gain required to drive the first mode unstable is $k = 63.6$. This again represents an improvement over the previous case.

The location of the dominant rigid body closed loop poles for a gain of $k = 63.6$ is at $s = - 1.18 \pm j2.62$ which yields an equivalent second order system damping ratio of $\delta = 0.225$. However the system response is not as lightly damped as this "dominant" second order response would indicate.

Figure 17 shows a plot of the gain required to move the locus of the closed loop poles associated with the first and fourth bending mode across the $j\omega$ axis into the right half plane as a function of the location of the open loop gyro zero. Inspection of this graph indicates that the gain required to drive the system unstable increases, as the gyro zero is shifted to the left along the real axis in the left half plane will improve system performance considerably. However there appears to be an optimum gyro gain ratio where the gain required to produce instability would be the same for the first and fourth bending modes. Further investigation into this area is indicated.

6. SUMMARY

Conventional control techniques have been used to analyze the stability of the Saturn booster at the 80 second point in the trajectory. A linear vehicle was assumed.

The Routh-Hurwitz stability criteria was used to determine the location of the gyro feedback open loop zero. This method yielded a value for both the position ($a_o = 0.2$) and the rate ($a_1 = 0.4$) gyro gains. These gyro gains were then used to evaluate the effect of the first four bending modes. The result of this analysis indicated that the first and second bending modes caused instability with these gains. Third and fourth bending modes were stable.

An appraisal of the problem of first and second bending mode stability indicated that a shift in exit angle of the locus from the first and second bending mode open loop poles, of 180° would delay the entry of the locus into the right half plane until higher loop gains were reached. A simple second order lag filter was used in the feedback path to accomplish this. The open loop poles of this filter were placed at $s = -5 \pm j5$ so that the filter would not affect the rigid body response. The sensitivity of the system to the first bending mode was diminished. The sensitivity to the second bending mode was dramatically diminished, but the sensitivity to the fourth bending mode increased to where the fourth bending mode dominated the stability picture producing an unstable system for low gains.

Further investigation into the effect of the location of the open loop gyro zero revealed that moving the zero to the left along the real axis in the left half plane desensitized the system to the first and fourth bending mode in the compensated system but that an optimum gyro zero position existed. Further work is required in this area to determine the optimum gain.

The author is indebted to Dr. Raymond H. Ash, Jr. of the R.P.I. Staff for the use of his root locus digital plotting routine which he has developed. Without this program it would have been impossible to conduct this analysis with the speed and accuracy required to complete this task.

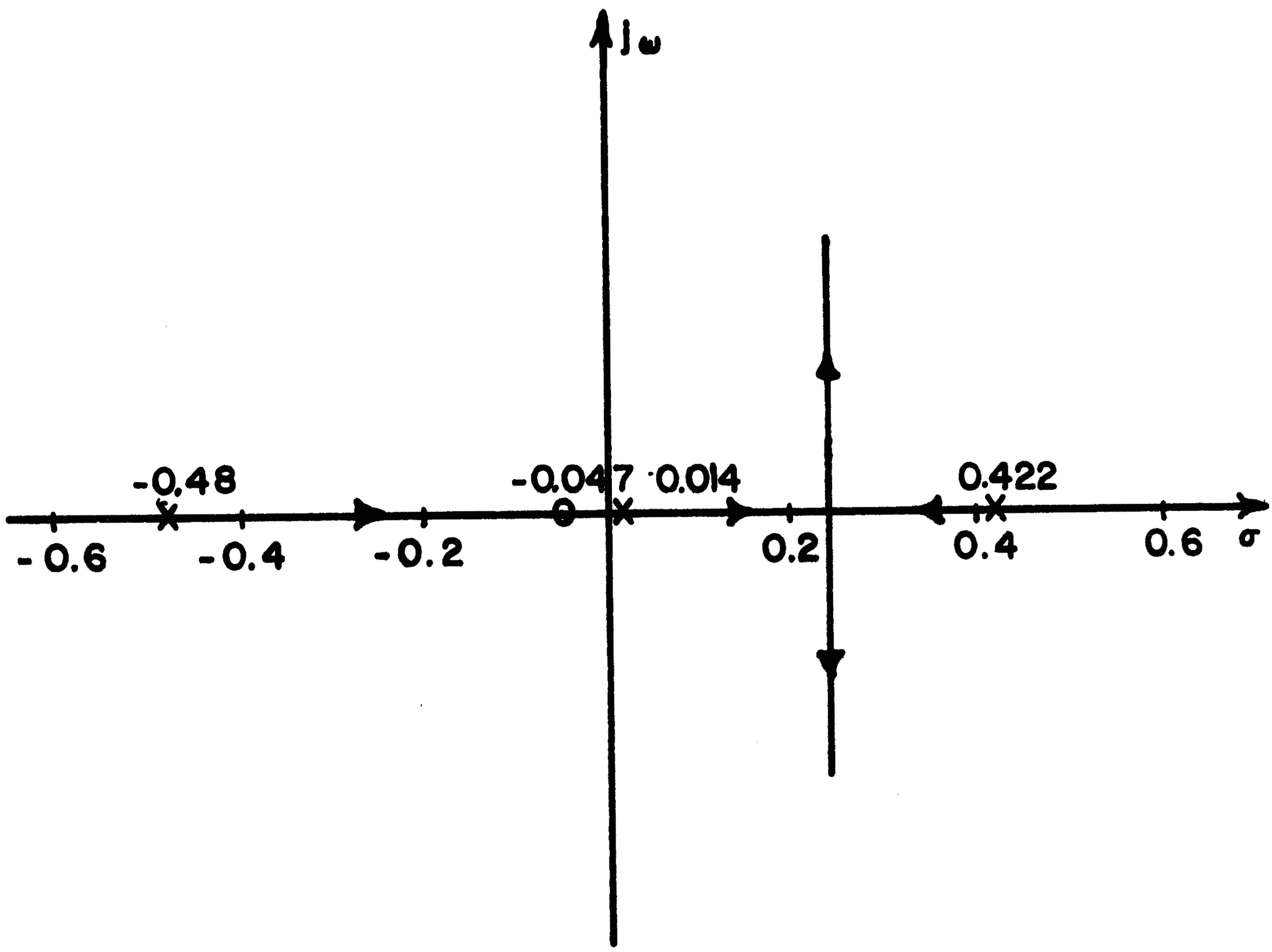

FIGURE I POLE-ZERO PATTERN FOR RIGID BODY MODE WITH UNITY FEEDBACK

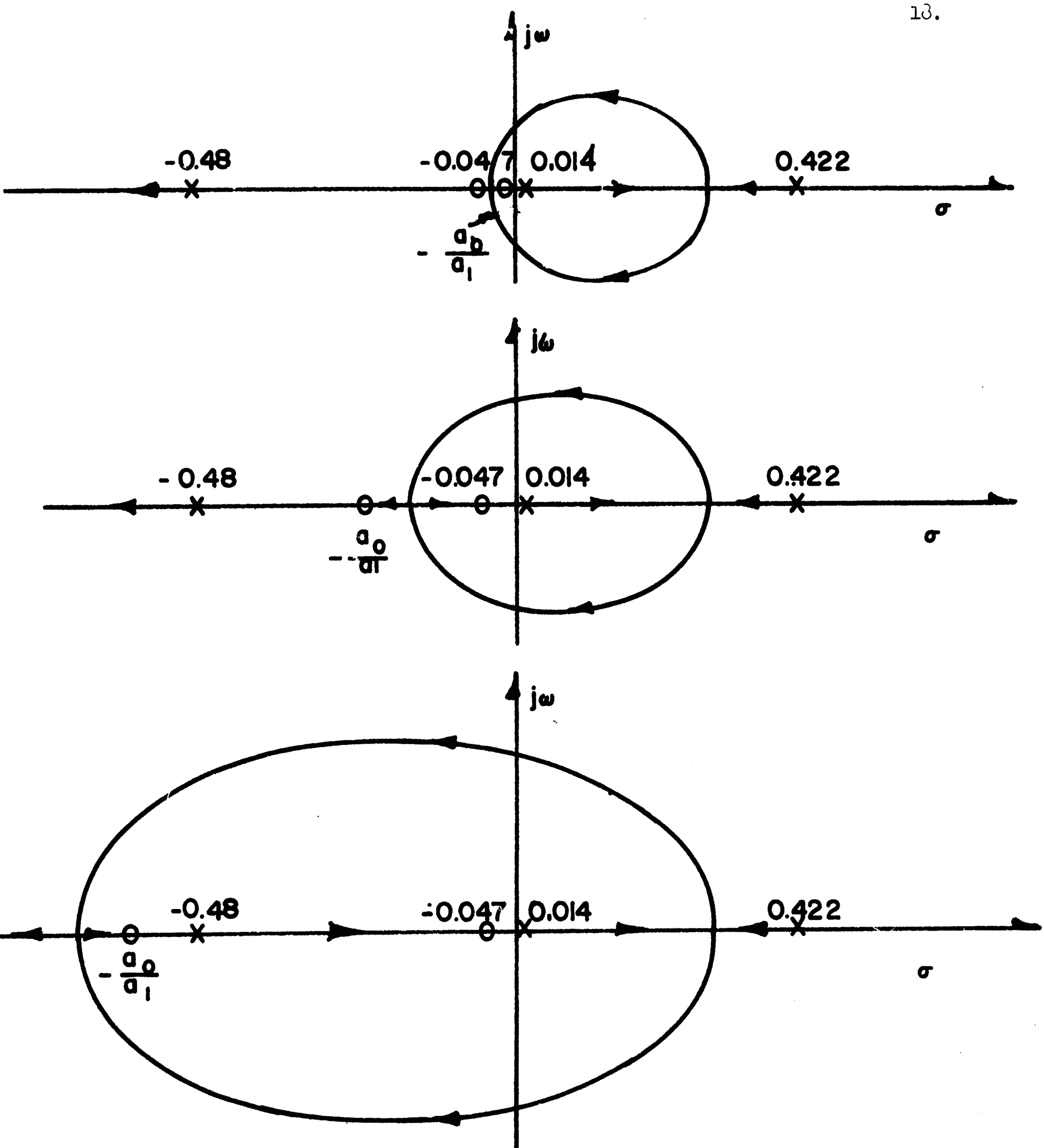

FIGURE 2 POSSIBLE GYRO OPEN LOOP ZERO LOCATIONS ON THE S-PLANE

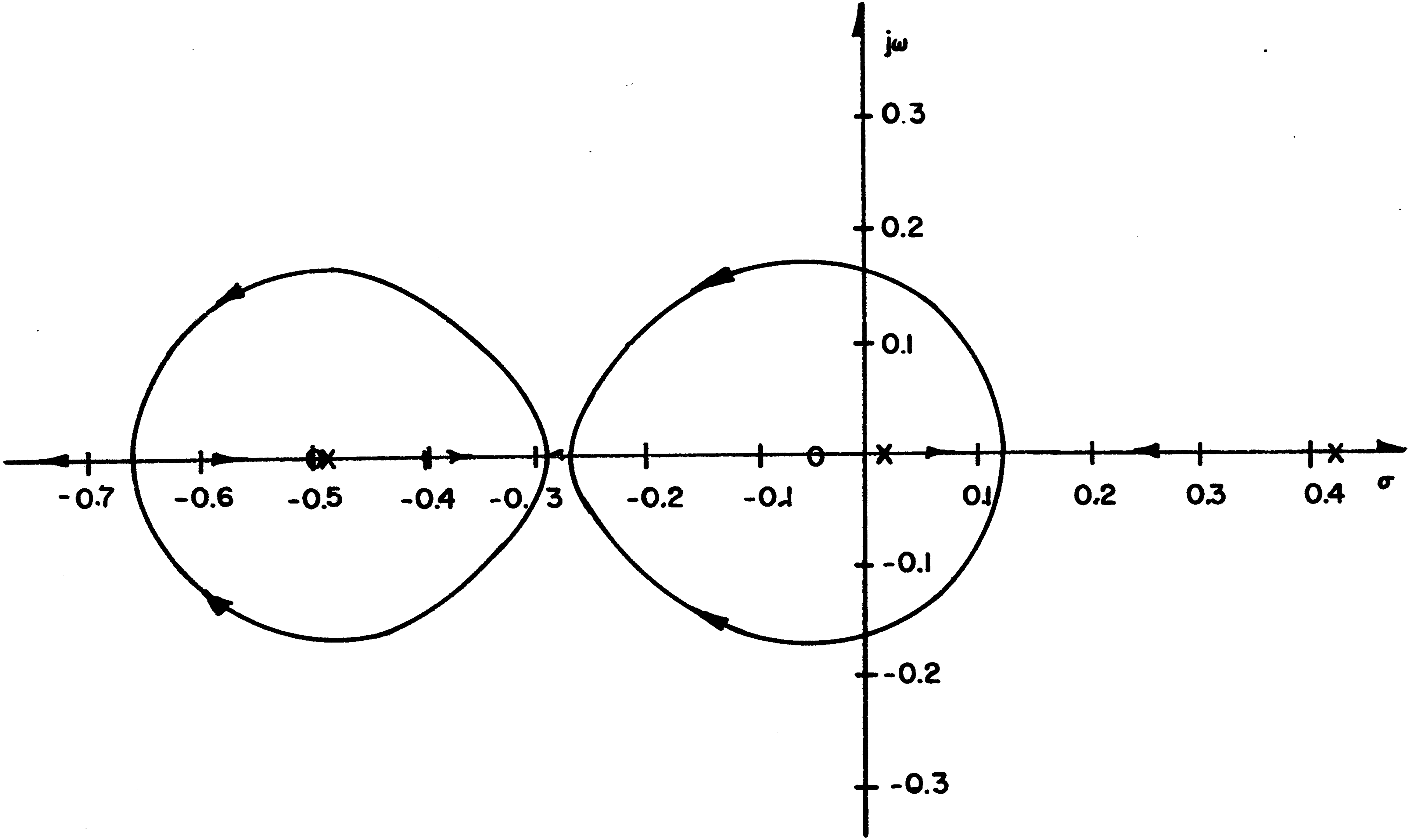

FIGURE 3 ROOT LOCUS PLOT OF RIGID BODY MODE

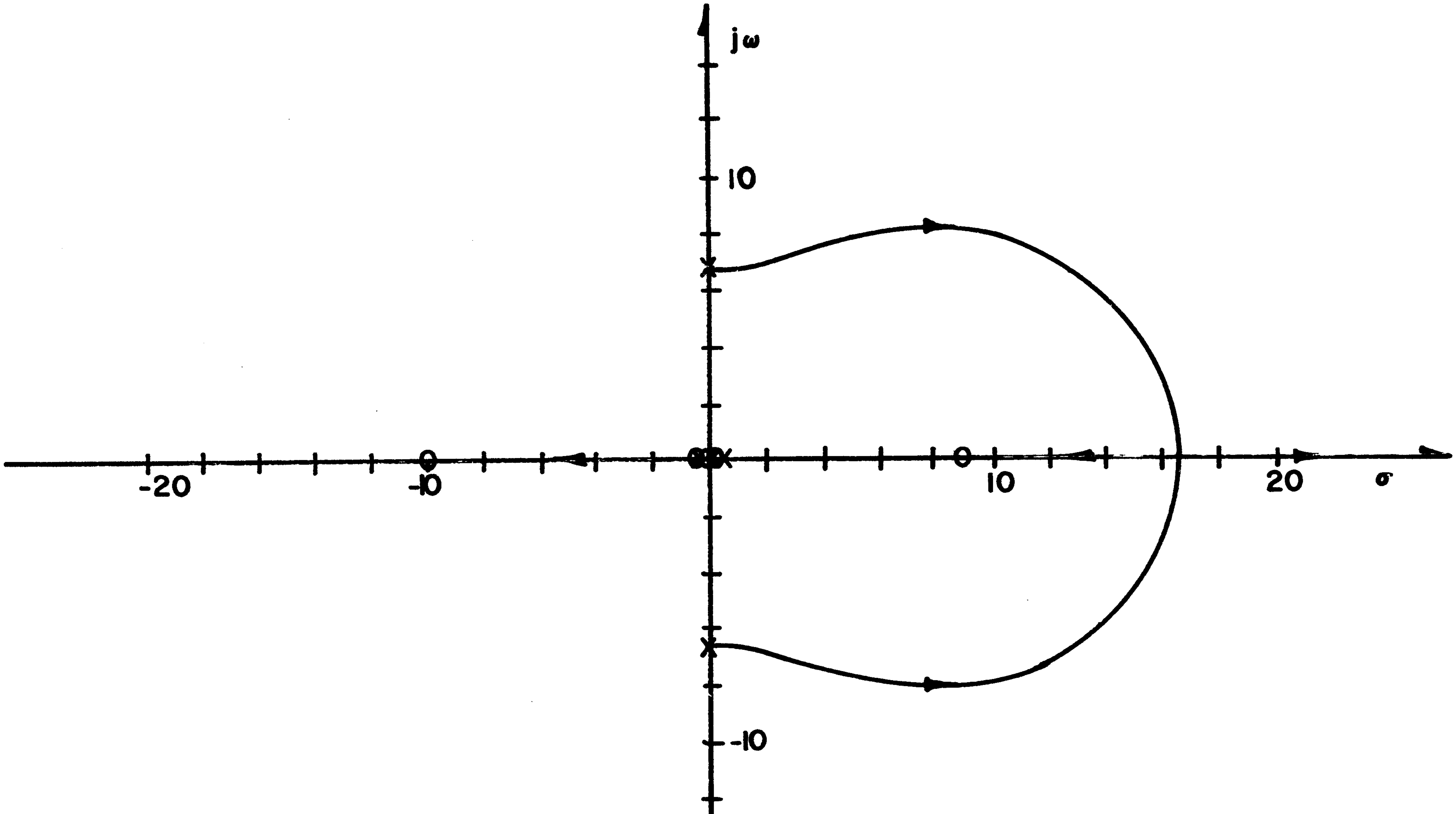

FIGURE 4 ROOT LOCUS PLOT OF RIGID BODY MODE PLUS FIRST BENDING MODE

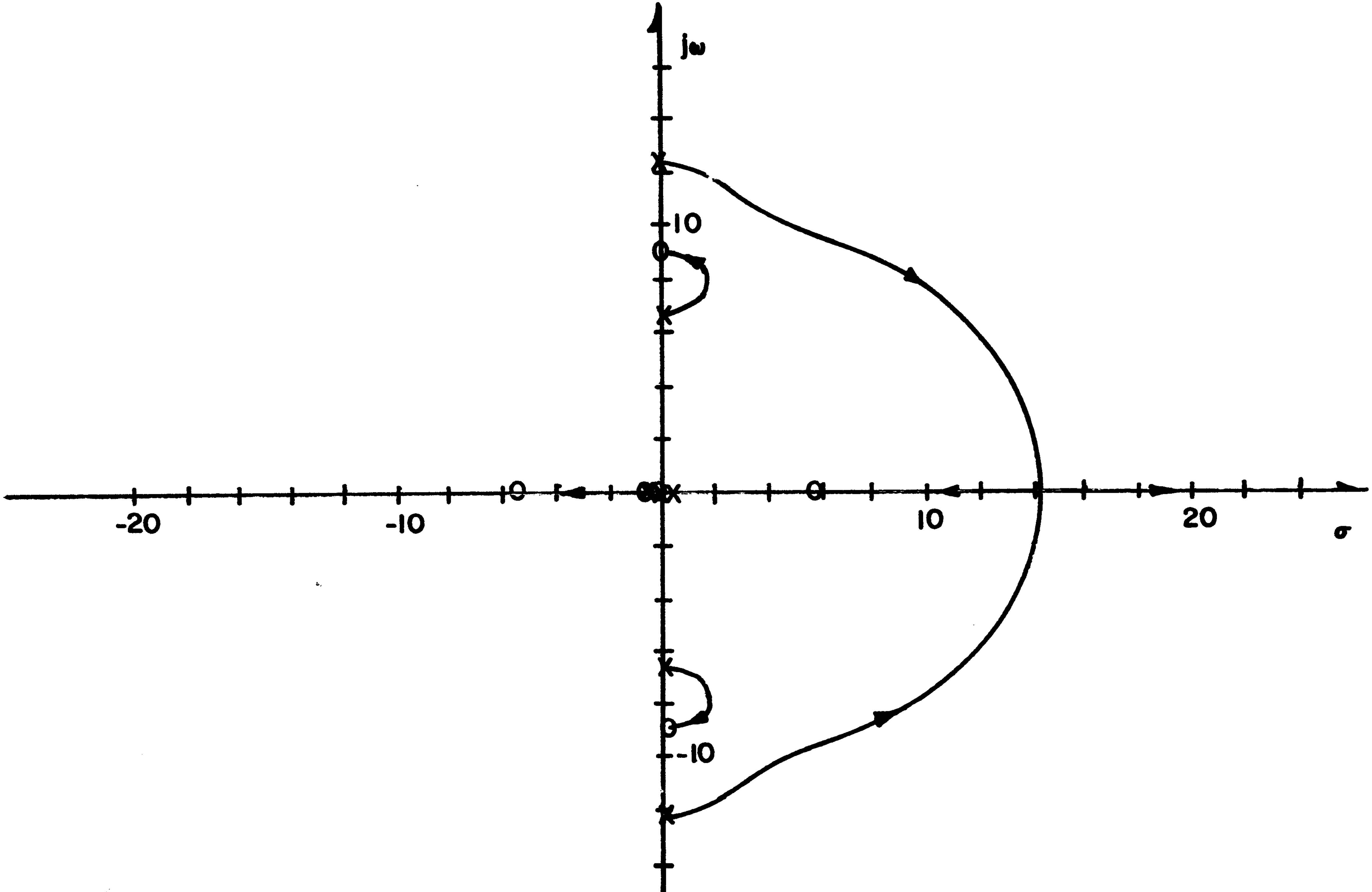

FIGURE 5 ROOT LOCUS PLOT OF RIGID BODY PLUS FIRST AND SECOND BENDING MODE

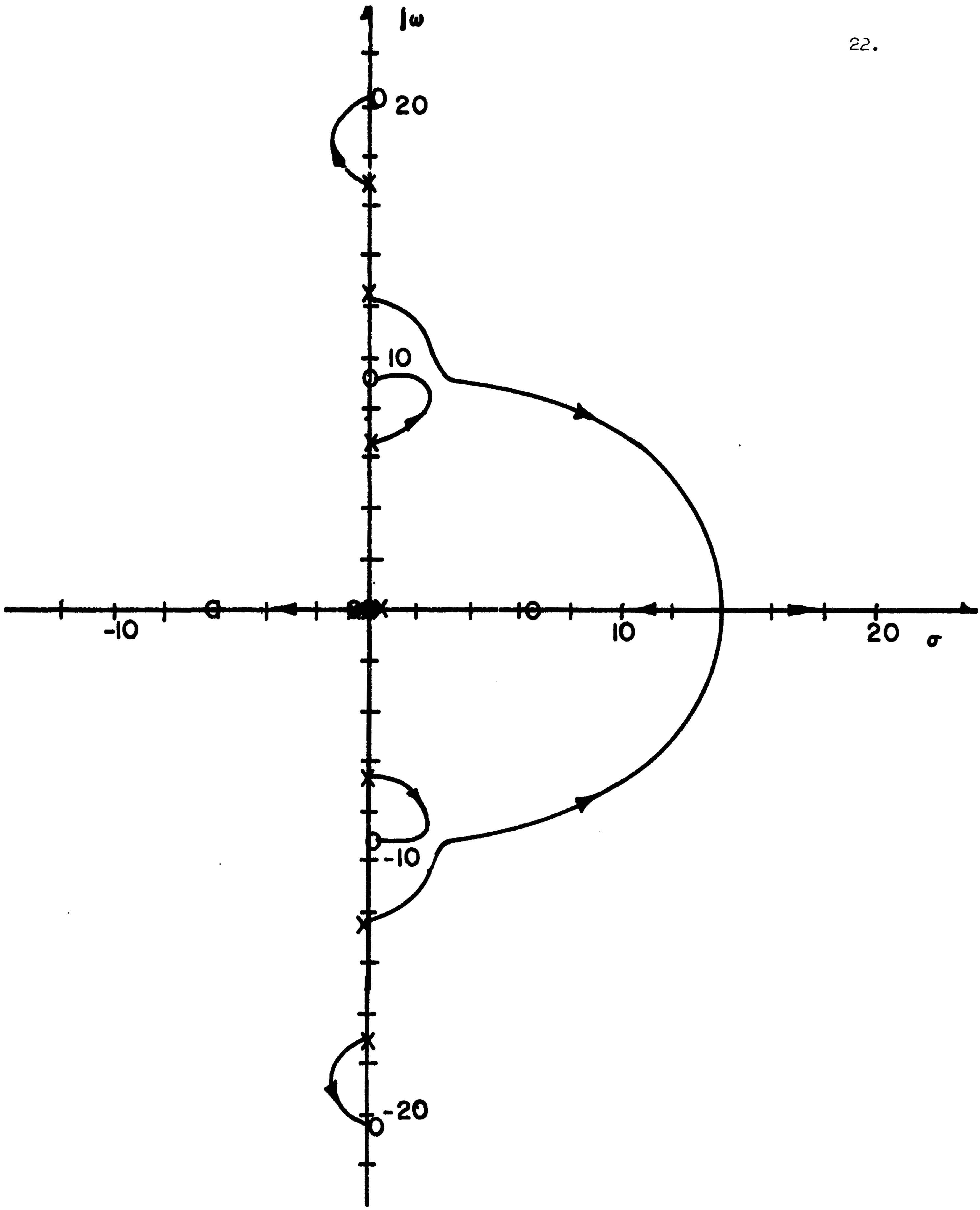

FIGURE 6 ROOT LOCUS PLOT OF RIGID BODY MODE PLUS FIRST, SECOND AND THIRD BENDING MODE

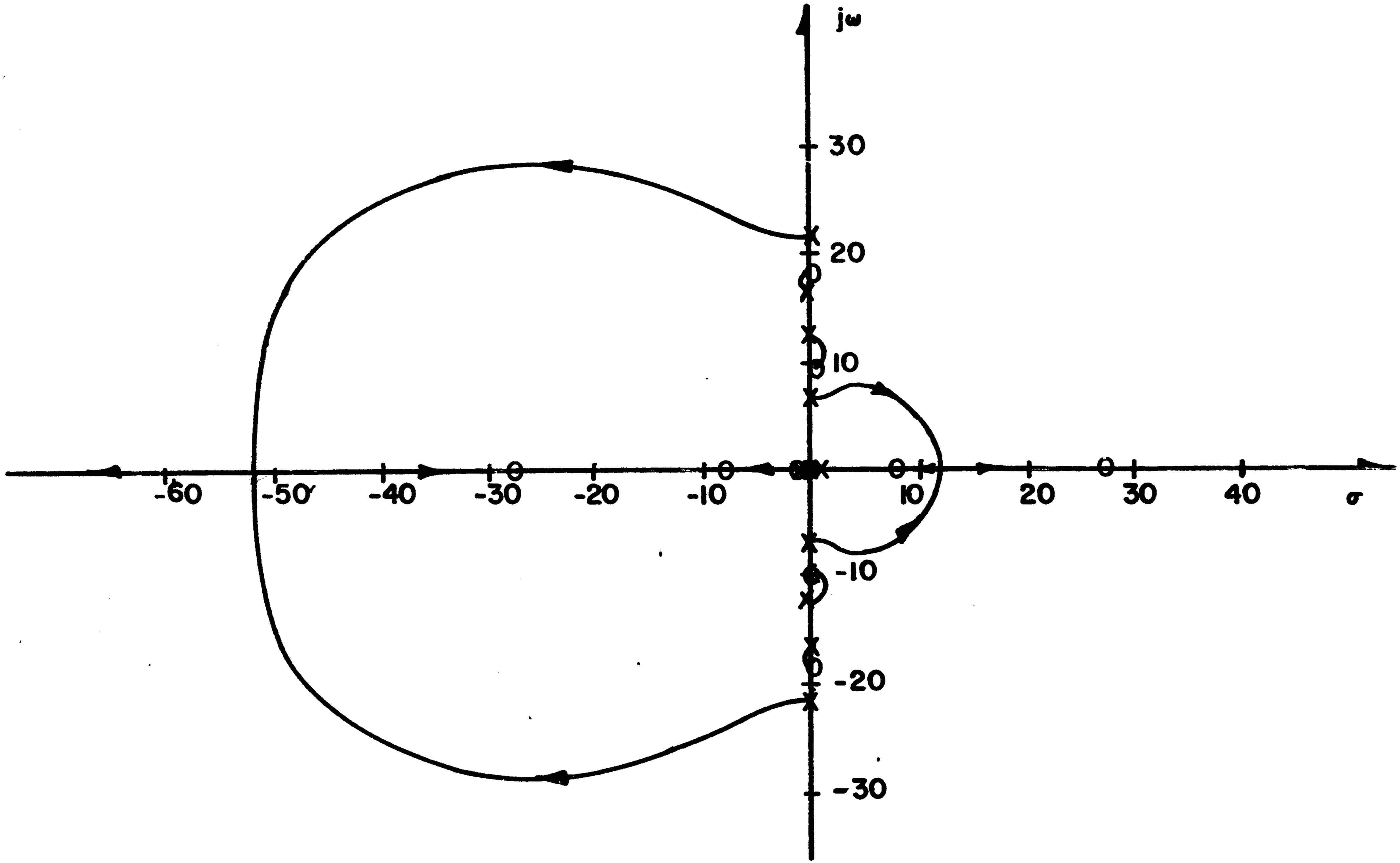

FIGURE 7 ROOT LOCUS PLOT FOR THE RIGID BODY
PLUS FIRST, SECOND, THIRD AND FOURTH BENDING MODE

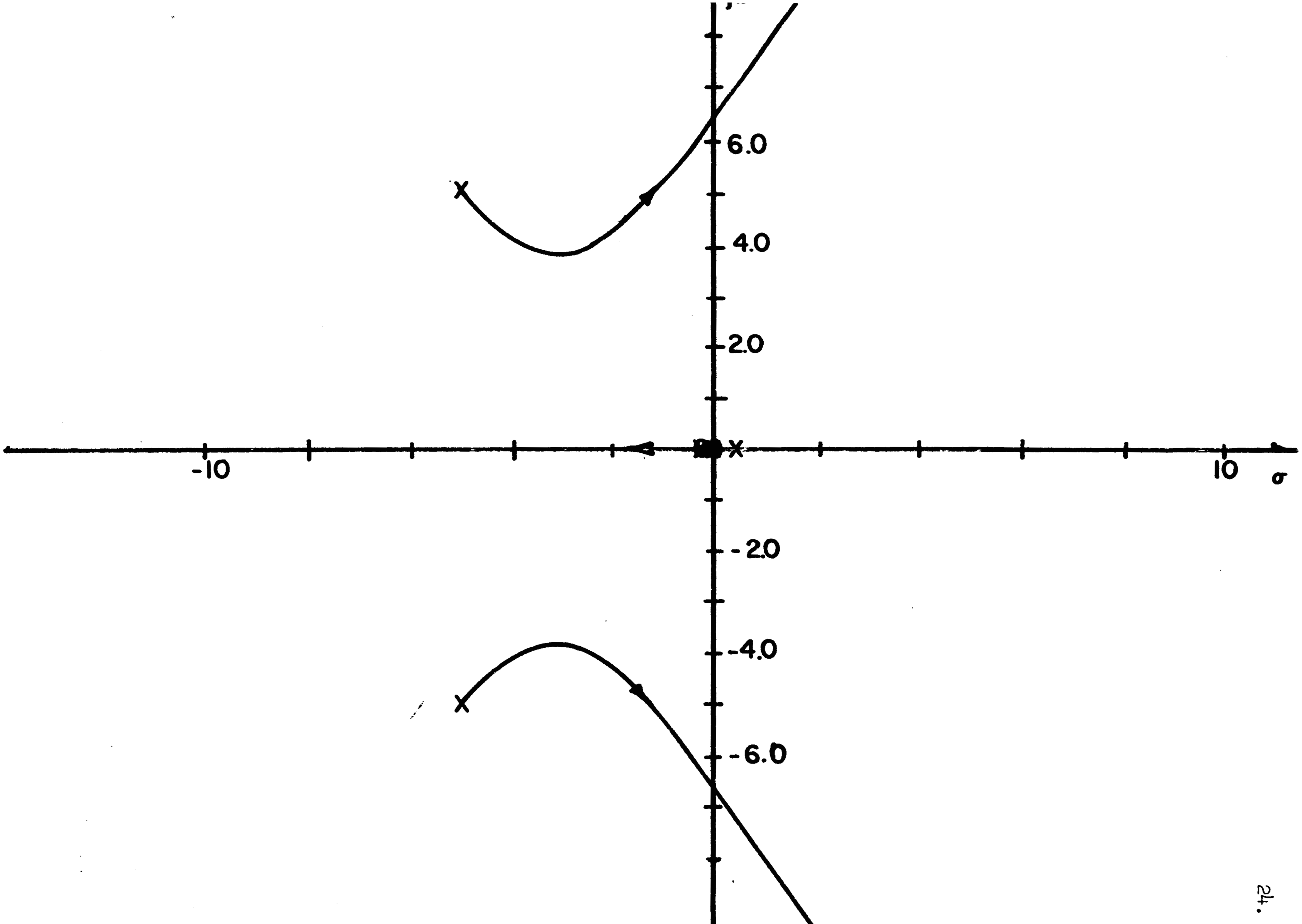

FIGURE 8 ROOT LOCUS PLOT FOR THE RIGID BODY MODE WITH FEEDBACK COMPENSATION

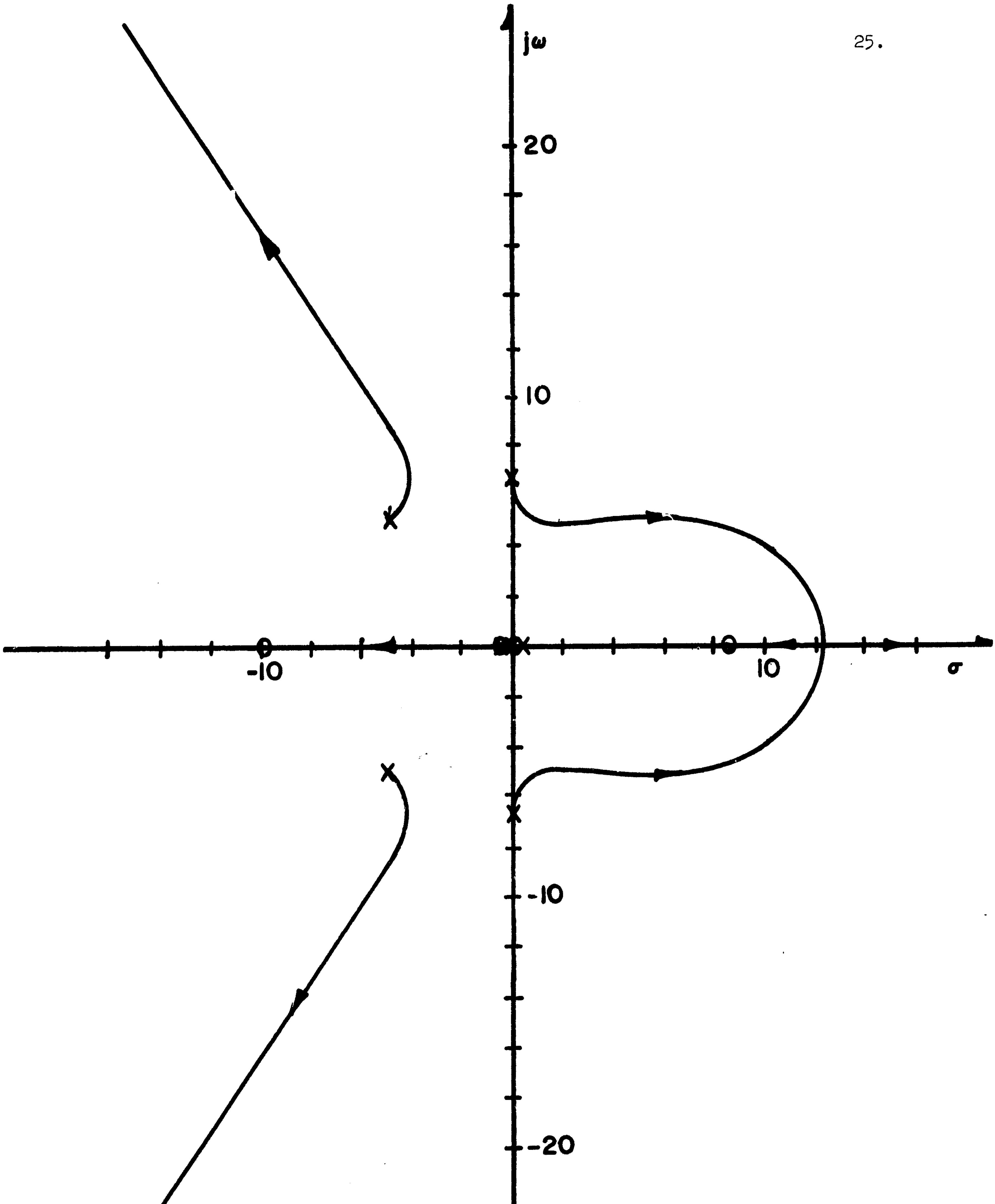

FIGURE 9 ROOT LOCUS PLOT FOR THE RIGID BODY PLUS FIRST BENDING MODE WITH FEEDBACK COMPENSATION

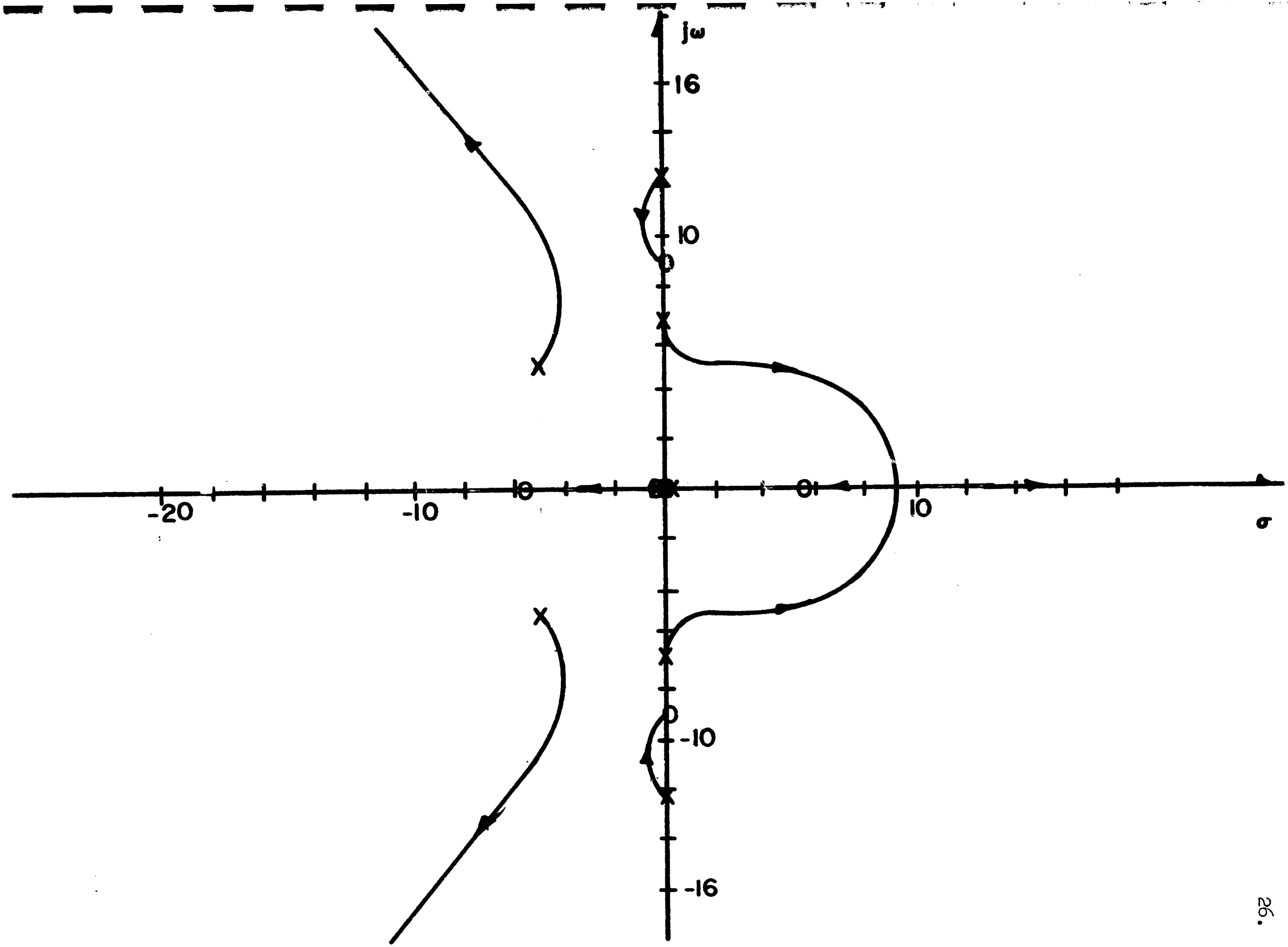

FIGURE 10 ROOT LOCUS PLOT FOR THE RIGID BODY PLUS FIRST AND SECOND BENDING MODE WITH FEEDBACK COMPENSATION

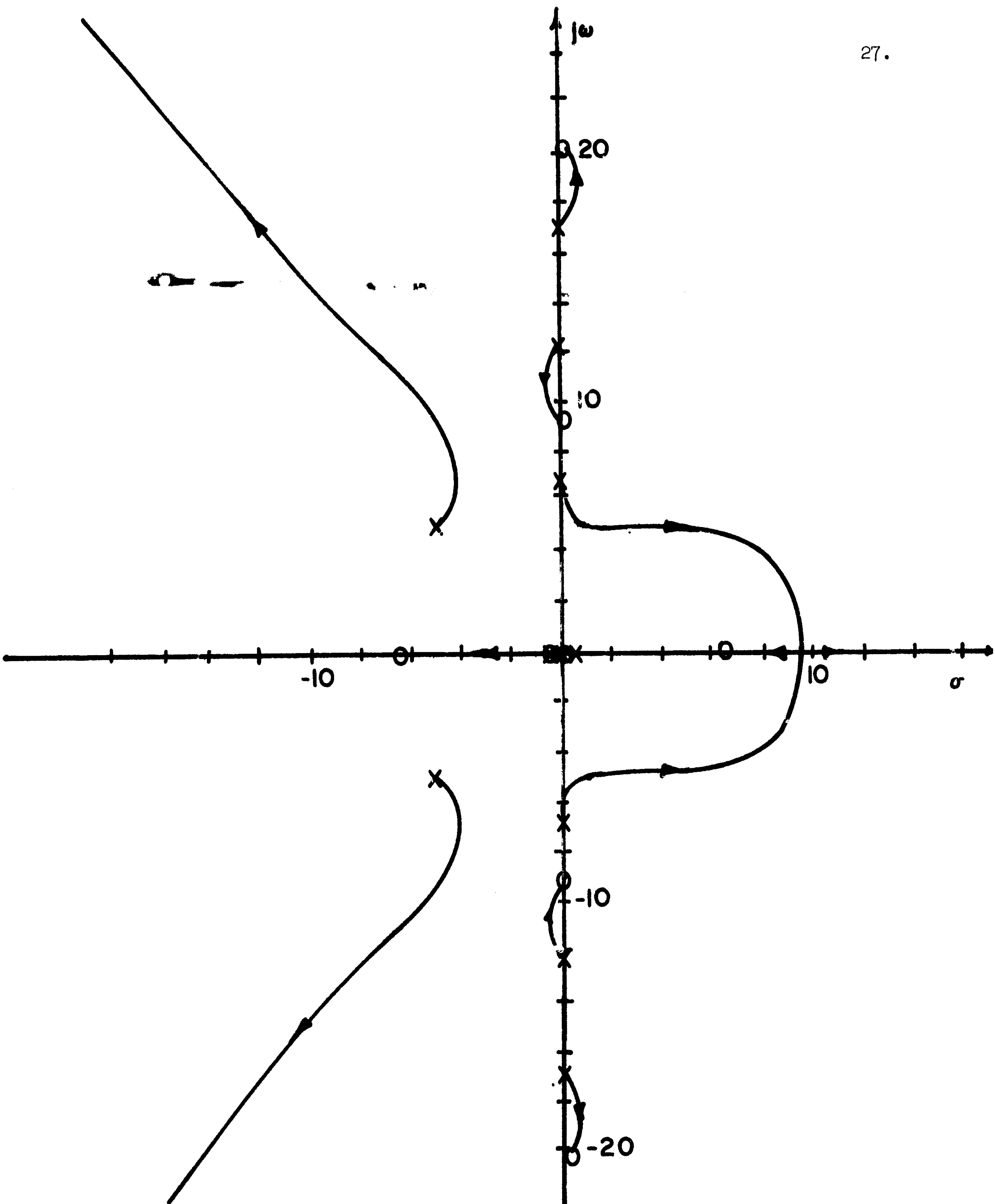

FIGURE 11 ROOT LOCUS PLOT OF RIGID BODY PLUS FIRST, SECOND AND THIRD BENDING MODE WITH FEEDBACK COMPENSATION

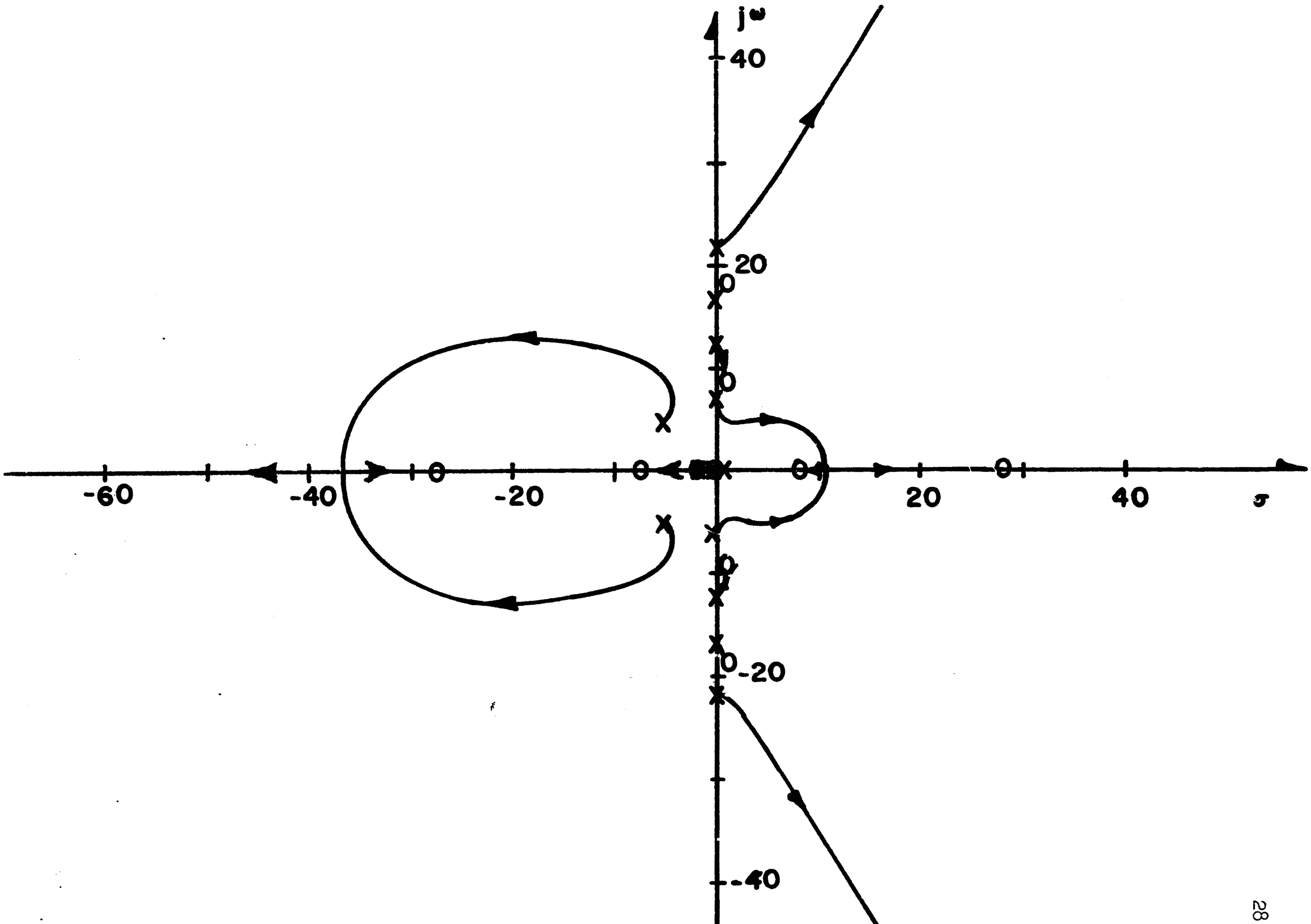

FIGURE 12 ROOT LOCUS PLOT OF THE RIGID BODY PLUS FIRST, SECOND THIRD AND FOURTH BENDING MODES WITH FEEDBACK COMPENSATION

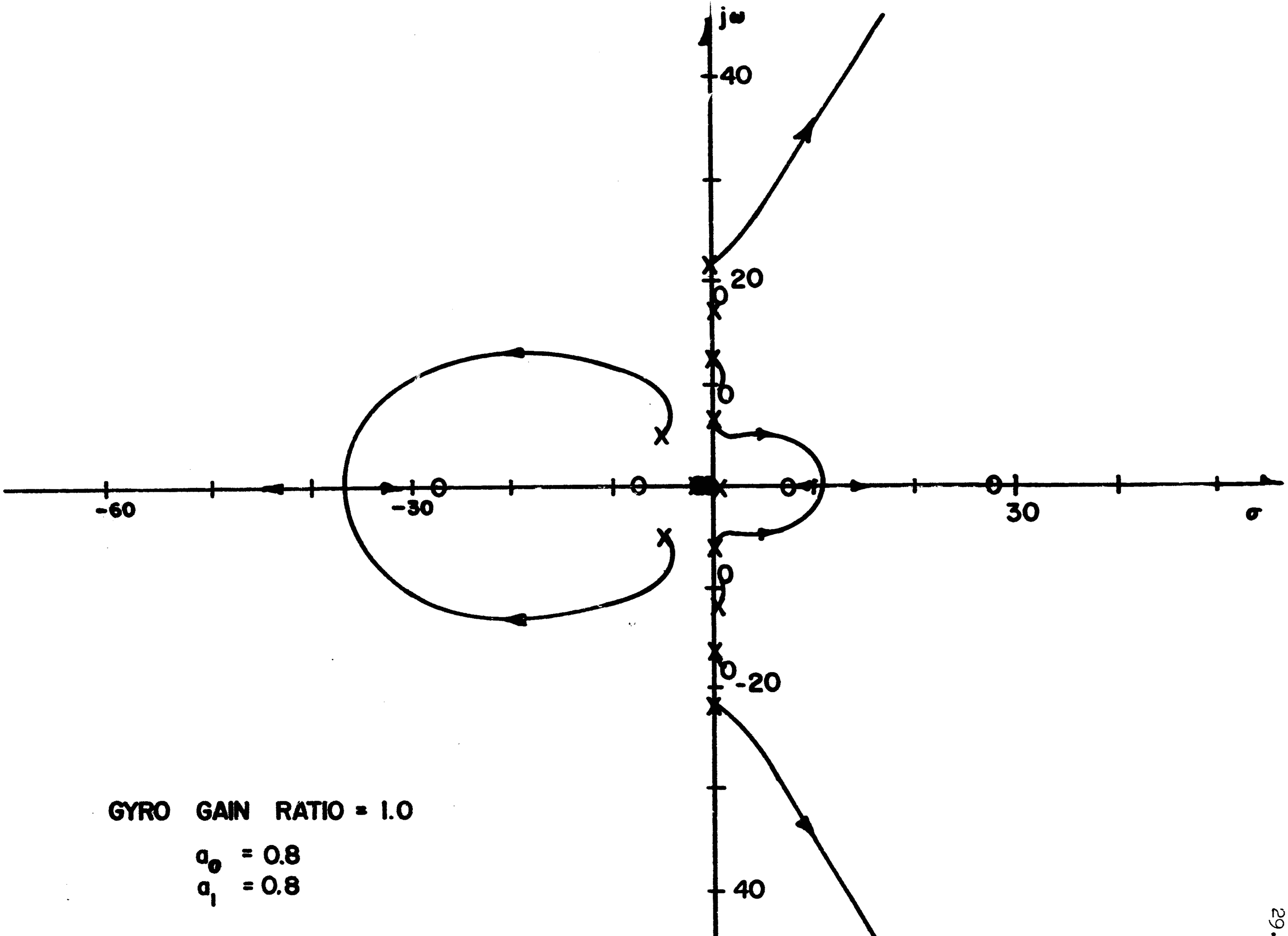

FIGURE 13 ROOT LOCUS PLOT OF THE RIGID BODY PLUS FIRST, SECOND, THIRD AND FOURTH BENDING MODES WITH FEEDBACK COMPENSATION

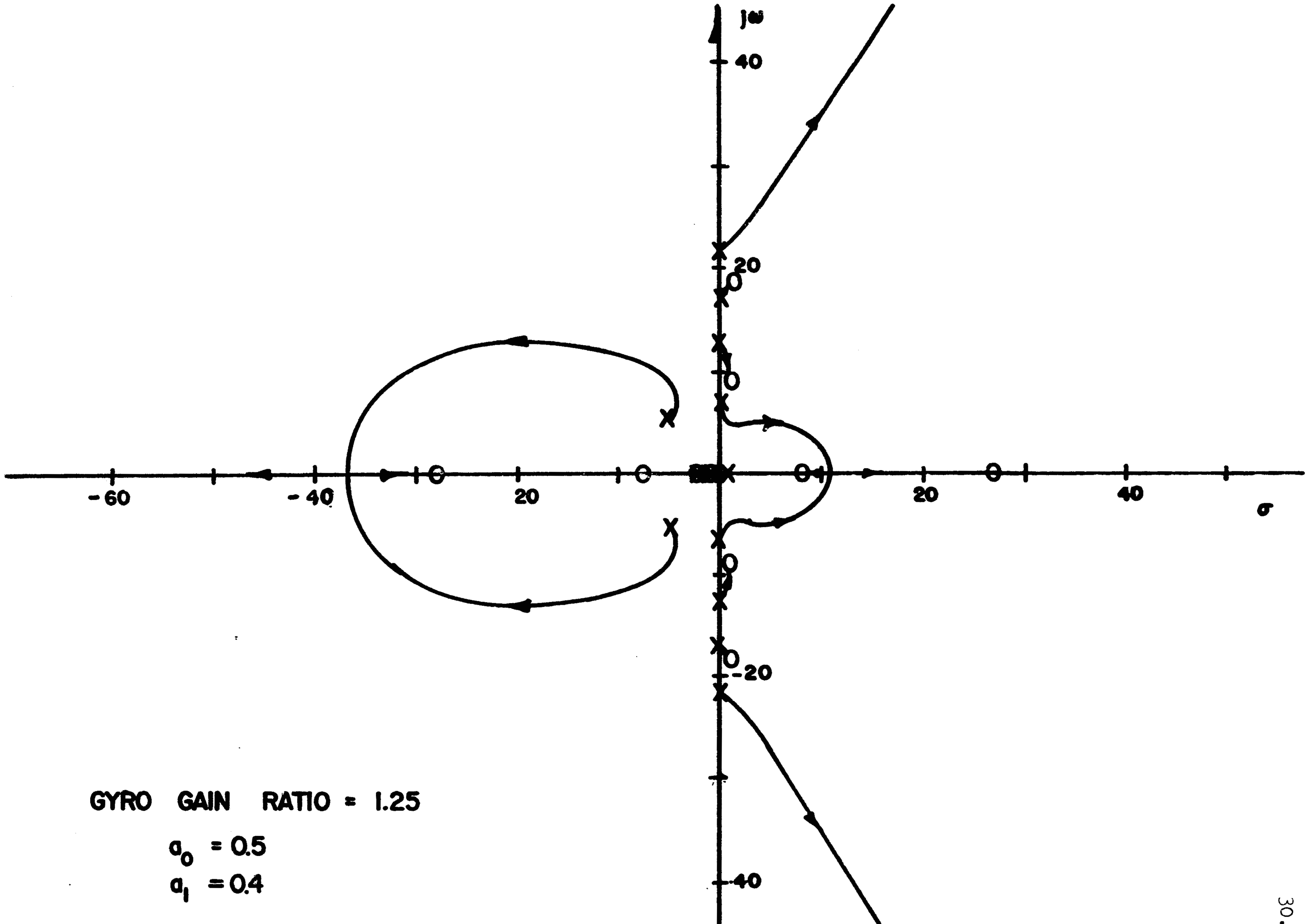

FIGURE 14 ROOT LOCUS PLOT OF THE RIGID BODY PLUS FIRST, SECOND, THIRD AND FOURTH BENDING MODES WITH FEEDBACK COMPENSATION

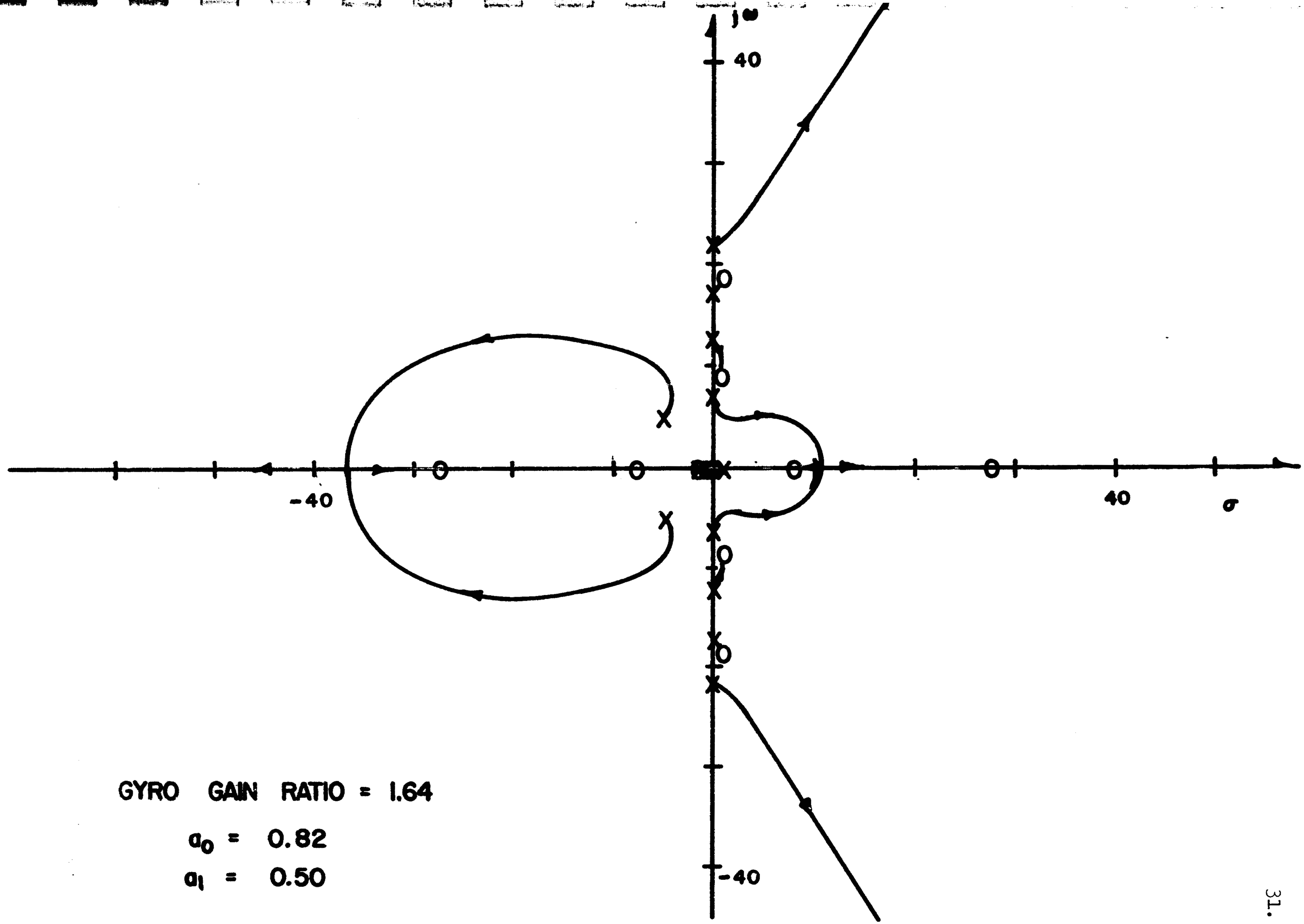

FIGURE 15 ROOT LOCUS PLOT OF THE RIGID BODY PLUS FIRST, SECOND, THIRD AND FOURTH BENDING MODES WITH FEEDING COMPENSATION

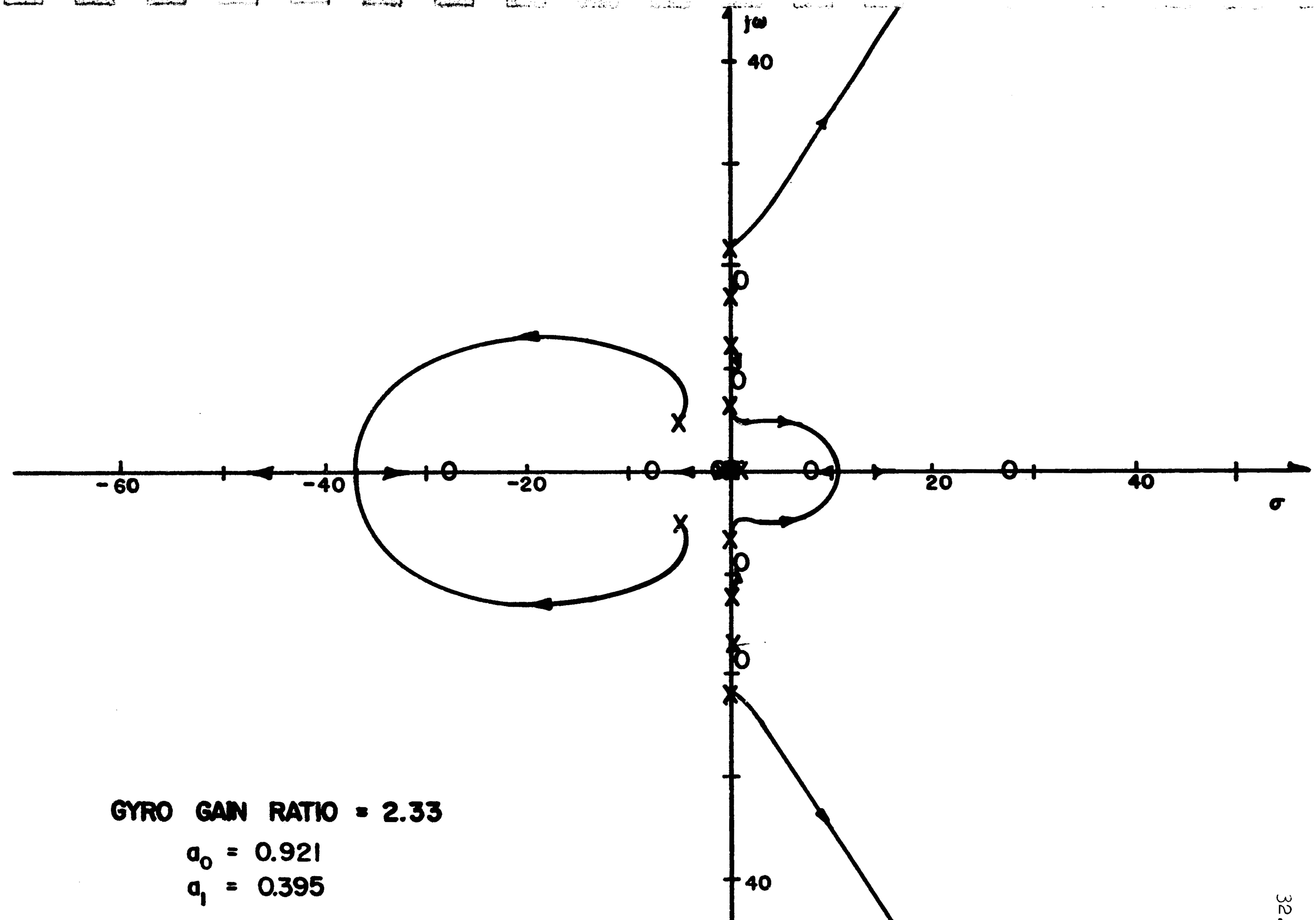

FIGURE 16 ROOT LOCUS PLOT OF THE RIGID BODY PLUS FIRST, SECOND, THIRD AND FOURTH BENDING MODES WITH FEEDBACK COMPENSATION

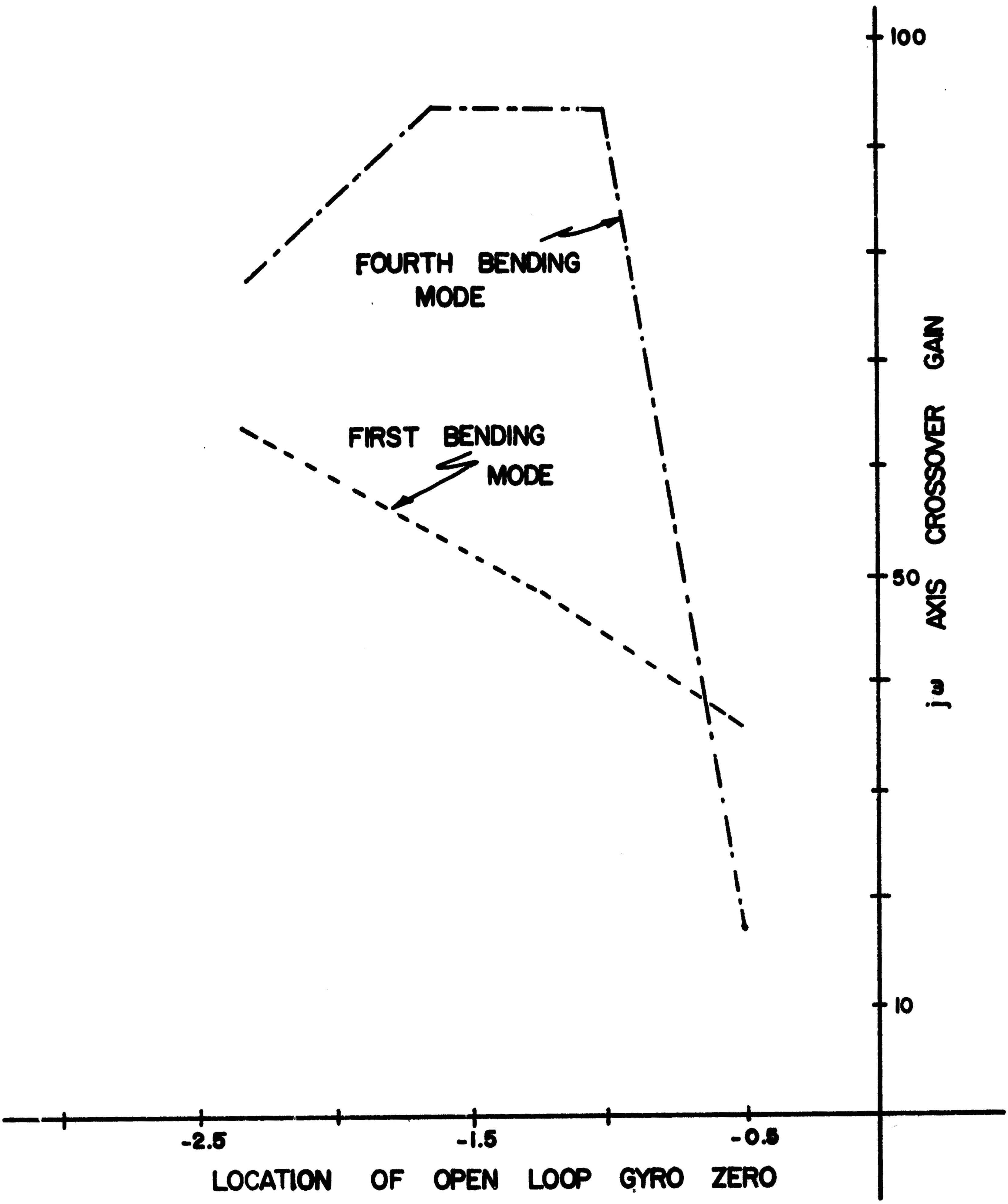

FIGURE 17 GAIN REQUIRED FOR INSTABILITY VS. POSITION OF OPENLOOP GYRO ZERO

APPENDIX A

ANALYSIS OF SATURN BOOSTER PERFORMANCE BY CONVENTIONAL CONTROL THEORY METHODS

The analysis of the Booster by conventional control theory techniques was conducted to provide a basis for comparison of the results obtained by the use of more sophisticated techniques. Routh-Hurwitz Criterion was used in conjunction with Root Locus techniques to evaluate system performance. A numerical analysis was conducted for the 80 second point on the trajectory since it represented the region close to the max q. point where stability was critical. Preliminary analysis indicated the need for compensation, and the simple second order lag filter, designed as part of the sensitivity study, was used here to check the validity of this choice of compensation.

A.1 Equations of Motion

The following equations of motion of the vehicle were used for this analysis:

$$\ddot{\phi} + C_1\alpha + C_2\beta = 0 \tag{A-1}$$

$$\ddot{Z} = \left(\frac{F - X}{m}\right)\phi + \left(\frac{N'}{m}\right)\alpha + \left(\frac{R'}{m}\right)\beta \tag{A-2}$$

$$\sum_i \ddot{\eta}_i + \sum_i 2\zeta_i\omega_i\dot{\eta}_i + \sum_i \eta_i\omega_i^2 = \left(\sum_i \frac{R' \; Y_i(x_\beta)}{M_i}\right)\beta \tag{A-3}$$

$$\alpha = \alpha_\omega + \phi - \frac{\dot{Z}}{V} \tag{A-4}$$

$$\beta = -a_o\,\phi_c + a_o\,\phi_D + a_1\,\dot{\phi}_{RG} \tag{A-5}$$

$$\dot{\phi}_{RG} = \dot{\phi} + \sum_i Y_i'\,(x_{RG})\,\dot{\eta}_i \tag{A-6}$$

$$\phi_D = \phi + \sum_i Y_i' (x_D) \eta_i \tag{A-7}$$

The following substitutions have been made to simplify the equations;

$$K_1 = \left(\frac{F - X}{m}\right) \tag{A-8}$$

$$K_2 = \frac{N'}{m} \tag{A-9}$$

$$K_3 = \frac{R'}{m} \tag{A-10}$$

$$K_{i5} = \sum_i 2 \zeta_i \omega_i \tag{A-11}$$

$$K_{i6} = \sum_i \omega_o^{\,2} \tag{A-12}$$

$$K_{i7} = \sum_i \frac{R' \; Y_i(x_\beta)}{M_i} \tag{A-13}$$

$$K_{i9} = \sum_i Y_i'(x_{RG}) \tag{A-14}$$

$$K_{i0} = \sum_i Y_i'(x_D) \tag{A-15}$$

The equations of motion can then be written as;

$$\ddot{\phi} + C_1\alpha + C_2\beta = 0 \tag{A-16}$$

$$\ddot{Z} = K_1\phi + K_2\alpha + K_3\beta \tag{A-17}$$

$$\ddot{\eta}_i + K_{i5} \dot{\eta}_i + K_{i6} \eta_i - K_{i7}\beta = 0 \tag{A-18}$$

$$\alpha = \alpha_\omega - \frac{\dot{Z}}{V} + \phi \tag{A-19}$$

$$\beta = -a_o \phi_c + a_o \phi_D + a_1 \dot{\phi}_{RG} \tag{A-20}$$

$$\dot{\phi}_{RG} = \dot{\phi} + K_{i9} \dot{\eta}_i \tag{A-21}$$

$$\phi_D = \phi + K_{i0} \eta_i \tag{A-22}$$

To reduce the number of variables from the equations, eliminate $\dot{Z}$. A further simplification can be accomplished by noting that two forcing functions are present, ϕ_c which is a command input and α_ω which is a wind disturbance input. Since we are dealing with an assumed linear system, the stability of the vehicle is not dependent upon the nature of the input. Therefore the vehicle response to only one input, ϕ_c, will be investigated. Assuming $\alpha_\omega = 0$ then;

$$\dot{Z} = V(\phi - \alpha) \tag{A-23}$$

differentiate with respect to time

$$\ddot{Z} = \dot{V}\,\phi + V\,\dot{\phi} - \dot{V}\,\alpha - V\,\dot{\alpha} \tag{A-24}$$

equating equations (A-17) and (A-24) yields

$$K_1\phi + K_2\alpha + K_3\beta = \dot{V}\,\phi + V\,\dot{\phi} - \dot{V}\,\alpha - V\,\dot{\alpha} \tag{A-25}$$

Grouping terms yields

$$(\dot{V} - K_1)\phi + V\,\dot{\phi} - (\dot{V} + K_2)\alpha - V\,\dot{\alpha} - K_3\beta = 0 \tag{A-26}$$

Equation (A-20), the control law, can be written in terms of the bending parameters as follows:

$$\beta = -a_o\,\phi_c + a_o\,\phi_D + a_1\,\dot{\phi}_{RG} = -a_o\,\phi_o + a_o\,\phi + K_{i0}\,a_i\,\eta_i + a_1\,\dot{\phi} + a_1\,x_{i9}\,\dot{\eta}_i \tag{A-27}$$

The equations of motion of the vehicle have now been reduced to a form where the open and closed loop transfer functions of the system may be obtained. It is expedient to work in the s-domain, therefore equations (A-16), (A-18), (A-26) and (A-27) are Laplace transformed assuming all initial conditions to be zero.

$$s^2\phi(s) + C_1\alpha(s) + C_2\beta(s) = 0 \tag{A-28}$$

$$(s^2 + (K_{i5}s) \qquad _i(s) - K_{i7}\beta(s) = 0 \tag{A-29}$$

$$\left[s + \left(\frac{\dot{V} - K_1}{V}\right)\right]\phi(s) - \left[s + \left(\frac{\dot{V} + K_2}{V}\right)\right]\alpha(s) - \frac{K_3}{V}\beta(s) = 0 \tag{A-30}$$

$$(a_o + a_1 s)\,\phi(s) + (K_{i10}\, a_o + K_{i9}\, a_1 s)\,\eta_i(s) - \beta(s) = a_o\phi_c(s) \tag{A-31}$$

The equations of motion can also be written in matrix form as,

$$\begin{bmatrix} s^2 & C_1 & C_2 & 0 \\ \left[s + \dfrac{\dot{V} - K_1}{V}\right] & -\left[s + \dfrac{\dot{V} + K_2}{V}\right] & \dfrac{-K_3}{V} & 0 \\ 0 & 0 & -K_{i7} & (s^2 + K_{i5}s + K_{i6}) \\ (a_o + a_1 s) & 0 & -1 & (a_o K_{i0} + K_{i9} a_1 s) \end{bmatrix} \begin{bmatrix} \phi \\ \alpha \\ \beta \\ \eta_i \end{bmatrix} = \begin{bmatrix} 0 \\ 0 \\ 0 \\ a_o\phi_c \end{bmatrix} \tag{A-32}$$

A.2 Development of System Transfer Functions

The vehicle bending modes are assumed to be decoupled from the rigid body and also from each other. This assumption permits the development of the transfer function of the vehicle rigid body dynamics independently from the bending dynamics. It follows that the dynamics of each bending mode can also be treated independently. This analysis will be conducted by first determining the Rigid Body transfer function and then adding the first, second, third and fourth Bending Modes.

A.2.1 Rigid Body Dynamics

The equations of motion for the rigid body reduce to;

$$\ddot{\phi} + C_1\alpha + C_2\beta = 0 \tag{A-33}$$

$$(\dot{V} - K_1)\,\phi + V\,\dot{\phi} - (\dot{V} + K_2)\,\alpha - V\,\dot{\alpha} - K_3\beta = 0 \tag{A-34}$$

$$\beta = -a_o\,\phi_c + a_o\phi + a_1\dot{\phi} \tag{A-35}$$

$$\phi_D = \phi \tag{A-36}$$

$$\dot{\phi}_{RG} = \dot{\phi} \tag{A-37}$$

These equations can be Laplace transformed, assuming zero initial conditions to yield;

$$s^2\phi(s) + C_1\alpha(s) + C_2\beta(s) = 0 \tag{A-38}$$

$$\left[s + \left(\frac{\dot{V} - K_1}{V}\right)\right]\phi(s) - \left[s + \left(\frac{\dot{V} + K_2}{V}\right)\right]\alpha(s) - \frac{K_3}{V}\,\beta(s) = 0 \tag{A-39}$$

$$(a_1 s + a_o)\,\phi(s) - \beta(s) = a_o\phi_c(s) \tag{A-40}$$

These equations can also be written in matrix form as:

$$\begin{bmatrix} s^2 & C_1 & C_2 \\ \left[s + \left(\frac{\dot{V} - K_1}{V}\right)\right] & -\left[s + \left(\frac{\dot{V} + K_2}{V}\right)\right] & \frac{-K_3}{V} \\ (a_o + a_1 s) & 0 & -1 \end{bmatrix} \begin{bmatrix} \phi(s) \\ \alpha(s) \\ \beta(s) \end{bmatrix} = \begin{bmatrix} 0 \\ 0 \\ a_o\phi_c \end{bmatrix} \tag{A-41}$$

The rigid body open loop transfer function ϕ/β is obtained by the use of determinants. The characteristic equation is the determinant of the coefficient matrix.

$$KG = \frac{\phi}{\beta} = \frac{-\left\{C_2\left[s + \left(\frac{\dot{V} + K_2}{V}\right)\right] - \frac{C_1 K_3}{V}\right\}}{s^3 + s^2\left(\frac{\dot{V} + K_2}{V}\right) + C_1 s + C_1\left(\frac{\dot{V} - K_1}{V}\right)} \qquad \text{(A-42)}$$

A block diagram of the closed loop system is shown in Figure 1.

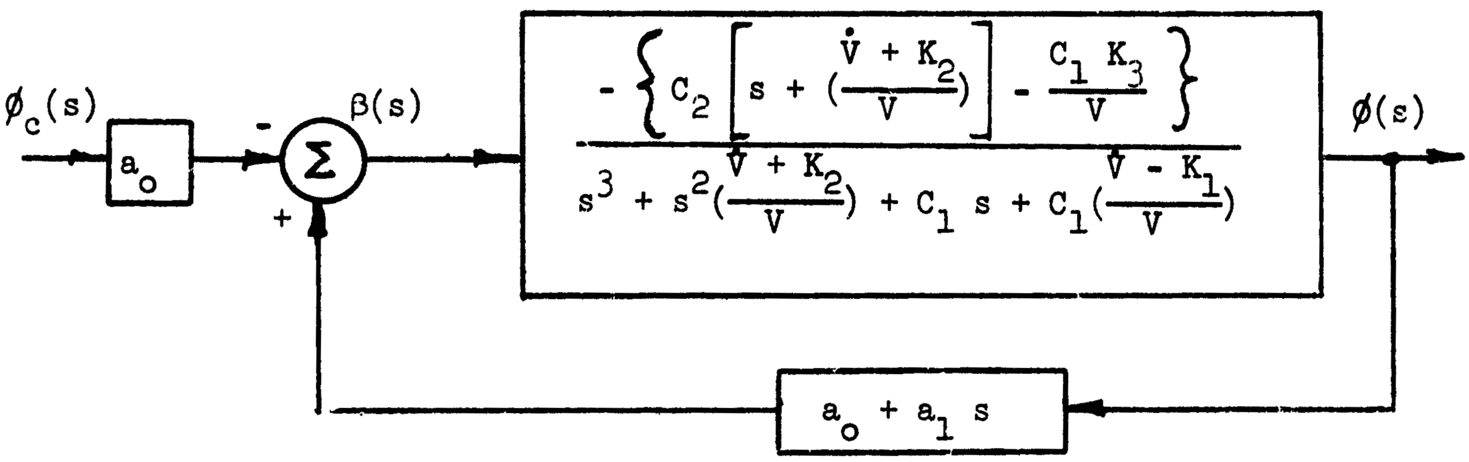

Figure 1 - Block Diagram of Closed Loop Control
with Only Rigid Body Dynamics

The closed loop transfer function may be written directly as

$$\frac{\phi(s)}{-\phi_o a_o} = \frac{KG(s)}{1 - KG(s)\,H(s)} \qquad \text{(A-43)}$$

The negative sign in the denominator indicates positive feedback. This arises because of the manner in which the control law (equation A-5) was written.

The Root Locus technique will be used to investigate the performance of the closed loop system. This requires that the characteristic equation be obtained in the proper form.

$$1 - KG(s)H(s) = 1 + \frac{\left\{ a_1\, C_2\, s^2 + \left[a_o\, C_2 + a_1\, C_2 \left(\frac{\dot{V} + K_2}{V}\right) - \frac{a_1\, C_1\, K_3}{V} \right] s + a_o \left[C_2 \left(\frac{\dot{V} + K_2}{V}\right) - \frac{C_1\, K_3}{V} \right] \right\}}{s^3 + \left(\frac{\dot{V} + K_2}{V}\right) s^2 + C_1\, s + \left(\frac{\dot{V} - K_1}{V}\right) C_1} \tag{A-44}$$

The numerator and denominator of the KGH function must be factored to obtain the zeros and poles required to plot the Root Locus diagram. The characteristic equation can now be obtained by algebraic manipulation.

$$1 - KGH = s^3 + \left[\left(\frac{\dot{V} + K_2}{V}\right) + a_1\, C_2 \right] s^2 + \left[C_1 + a_o\, C_2 + a_1\, C_2 \left(\frac{\dot{V} + K_2}{V}\right) - \frac{a_1\, C_1\, K_3}{V} \right] s + C_1 \left(\frac{\dot{V} - K_1}{V}\right) + a_o \left[C_2 \left(\frac{\dot{V} + K_2}{V}\right) - \frac{C_1 K_3}{V} \right] \tag{A-45}$$

Inspection of this equation indicates that system stability is strongly dependent upon the values of the gyro feedback gains a_o and a_1. Routh's Criteria can be used to determine the values of a_o and a_1 that will produce a stable, closed loop system.

The closed loop transfer function is given by the expression.

$$\frac{\phi}{-a_o \phi_c} = \frac{- \left\{ C_2 \left[s + \left(\frac{V + K_2}{V}\right) \right] - \frac{C_1\, K_3}{V} \right\}}{s^3 + \left[\left(\frac{\dot{V} + K_2}{V}\right) + a_1\, C_2 \right] s^2 + \left[C_1 + a_o\, C_2 + a_1\, C_2 \left(\frac{\dot{V} + K_2}{V}\right) - \frac{a_1\, C_1\, K_3}{V} \right] s + C_1 \left(\frac{\dot{V} - K_1}{V}\right) + a_o \left[C_2 \left(\frac{\dot{V} + K_2}{V}\right) - \frac{C_1 K_3}{V} \right]} \tag{A-46}$$

A.2.2 Rigid Body Plus First Bending Mode

The Rigid Body plus the first Bending Mode will be treated here to indicate the procedure used to analyze the bending modes in conjunction with the rigid body mode. This approach will be extended to four bending modes in the next section.

The equations of motion are given by the matrix equation (A-32) with i = 1.

$$\begin{bmatrix} s^2 & C_1 & C_2 & 0 \\ \left[s+\left(\frac{\dot{V}-K_1}{V}\right)\right] & -\left[s+\left(\frac{\dot{V}+K_2}{V}\right)\right] & \frac{-K_3}{V} & 0 \\ 0 & 0 & -K_{17} & (s^2+K_{15}s+K_{16}) \\ (a_0+a_1s) & 0 & -1 & (K_{10}a_0+K_{19}a_1s) \end{bmatrix} \begin{bmatrix} \phi(s) \\ \alpha(s) \\ \beta(s) \\ \eta_1(s) \end{bmatrix} = \begin{bmatrix} 0 \\ 0 \\ 0 \\ a_0\phi_c \end{bmatrix} \qquad \text{(A-47)}$$

The Bending Mode is decoupled from the Rigid Body Mode, therefore the open loop transfer function for the rigid body mode is the same as equation (A-42). The open loop bending mode equation can be found directly from equation (A-18).

$$\frac{\eta_1(s)}{\beta(s)} = \frac{K_{17}}{s^2 + K_{15}s + K_{16}} \qquad \text{(A-48)}$$

A block diagram of this system is shown in Figure 2.

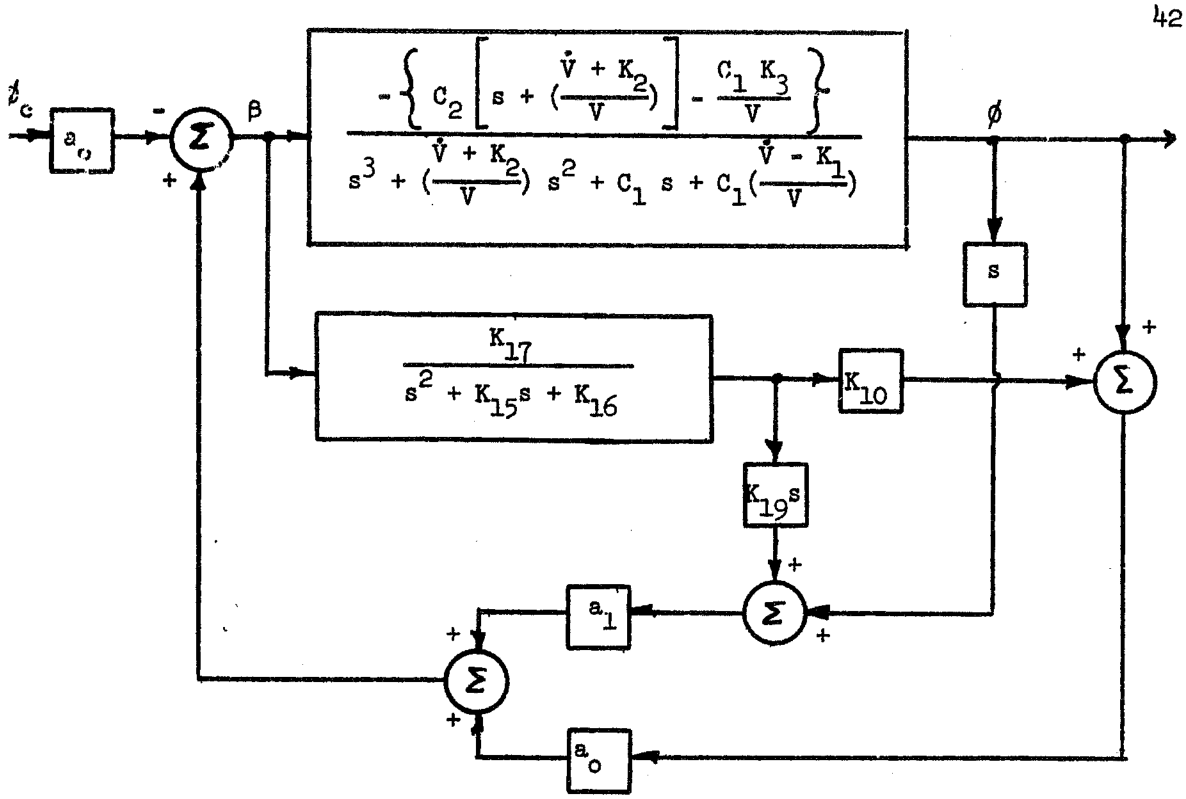

Figure 2 - Rigid Body Plus First Bending Mode Closed Loop Block Diagram

The closed loop transfer function is most readily found by block diagram reduction.

Let

$$G_0(s) = \frac{N_0}{D_0} = \frac{-\left\{C_2\left[s+\left(\frac{\dot{V}+K_2}{V}\right)\right]-\frac{C_1K_3}{V}\right\}}{s^3+\left(\frac{\dot{V}+K_2}{V}\right)s^2+C_1\,s+C_1\left(\frac{\dot{V}-K_1}{V}\right)} \tag{A-49}$$

$$G_1(s) = \frac{N_1}{D_1} = \frac{K_{17}}{s^2+K_{15}\,s+K_{16}} \tag{A-50}$$

The block diagram of Figure 2 may be altered by moving the gyro feedback gains into the Rigid Body and Bending Mode channels as shown in Figure 3. Only the open loop system is shown here. The output of the system is designated by the letter O.

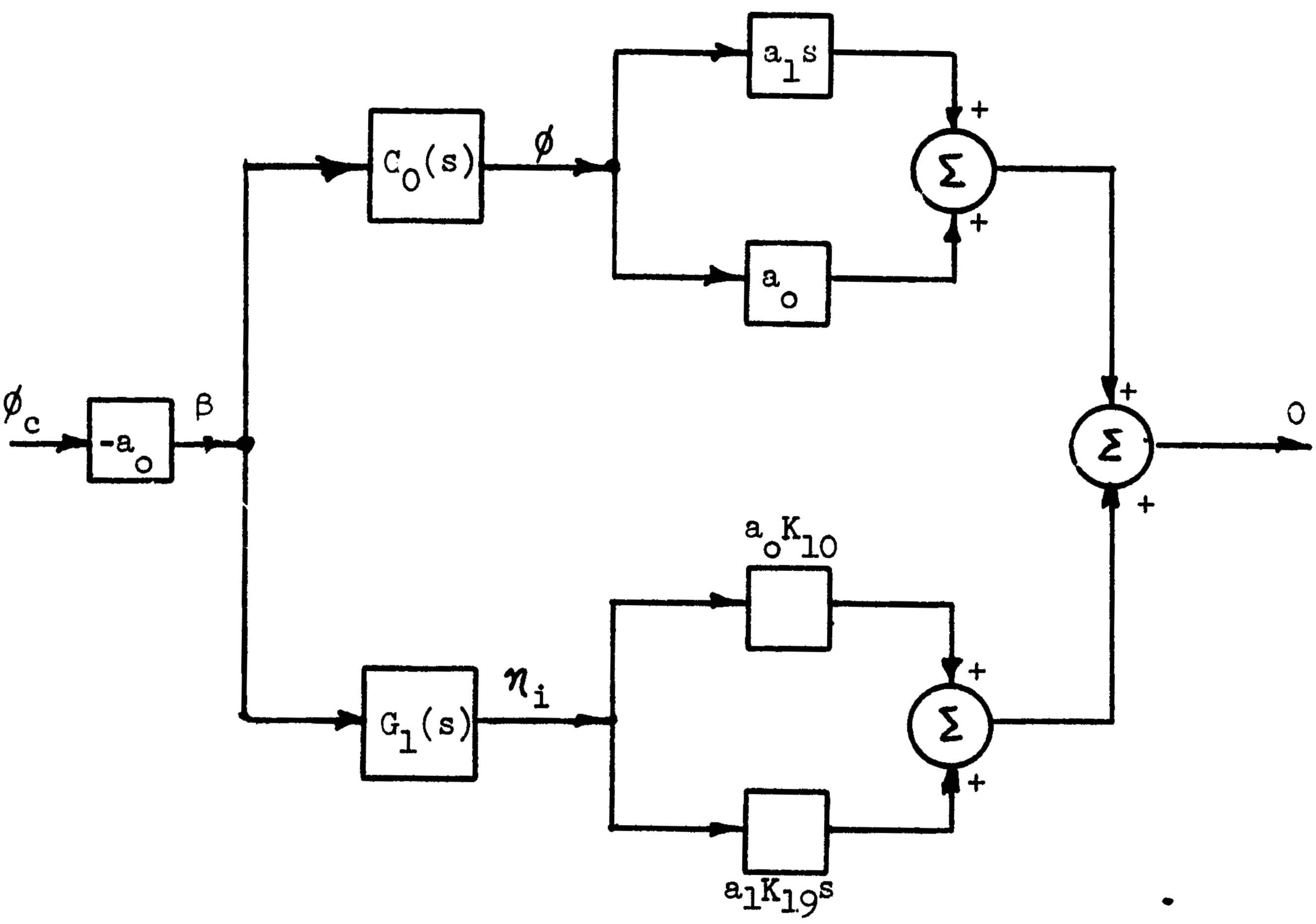

Figure 3 - Open Loop Block Diagram

This diagram can be further reduced to the form shown in Figure 4.

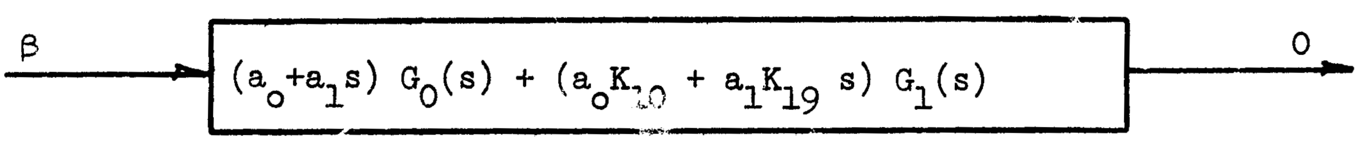

Figure 4 - Final Reduction of Block Diagram

The Open Loop transfer function becomes

$$KGH = \frac{O}{\beta} = (a_o + a_1 s)\ G_0(s) + (a_o\ K_{10} + a_1\ K_{19} s)\ G_1(s) \tag{A-51}$$

If the substitutions $G_0(s) = \frac{N_0}{D_0}$ and $G_1(s) = \frac{N_1}{D_1}$ are made in equation (A-51) the characteristic equation becomes

$$1 - KGH = 1 - \frac{(a_o + a_1 s)\, N_0\, D_1 + (a_o\, K_{10} + a_1\, K_{19})\, N_1\, D_0}{D_0\, D_1} \tag{A-52}$$

The numerator and denominator of the KGH function must then be factored to obtain a Root Locus Diagram for the system.

A.2.3 Rigid Body Plus First Four Bending Modes

The foregoing analysis for the Rigid Body plus First Bending mode may readily be extended to i uncoupled bending modes. In this particular analysis only the first four bending modes will be considered. The equations of motion for the four bending modes can be written as

$$\ddot{\eta}_1 + 2\zeta_1\, \omega_1 \dot{\eta}_1 + \omega_1^2 \eta_1 = \frac{R'\ Y_1(x_\beta)}{M_1}\ \beta \tag{A-53}$$

$$\ddot{\eta}_2 + 2\zeta_2\, \omega_2 \dot{\eta}_2 + \omega_2^2\, \eta_2 = \frac{R'\ Y_2(x_\beta)}{M_2}\ \beta \tag{A-54}$$

$$\ddot{\eta}_3 + 2\zeta_3\, \omega_3 \dot{\eta}_3 + \omega_3^2 \eta_3 = \frac{R\ Y_3(x_\beta)}{M_3}\ \beta \tag{A-55}$$

$$\ddot{\eta}_4 + 2\zeta_4\, \omega_4 \dot{\eta}_4 + \omega_4^2 \eta_4 = \frac{R'\ Y_4(x_\beta)}{M_4}\ \beta \tag{A-56}$$

In order to simplify the algebra, make the following substitutions,

$$K_{15} = 2\zeta_1\omega_1; \quad K_{25} = 2\,\zeta_2\omega_2; \quad K_{35} = 2\,\zeta_3\omega_3; \quad K_{\,5} = 2\zeta_4\omega_4$$

$$K_{16} = \omega_1^{\,2}\ ; \quad \omega_{26} = \omega_2^{\,2}\ ; \quad K_{36} = \omega_3^{\,2}\ ; \quad K_{46} = \omega_4^{\,2} \tag{A-57}$$

$$K_{17} = \frac{R'Y_1(x_\beta)}{M_1};\ K_{27} = \frac{R'Y_2(x_\beta)}{M_2};\ K_{37} = \frac{R'Y_3(x_\beta)}{M_3};\ K_{47} = \frac{R'Y_4(x_\beta)}{M_4}$$

The Laplace Transform of equations (A-53), (A-54), (A-55) and (A-56) is now taken, considering all initial conditions to be zero.

$$(s^2 + K_{15}s + K_{16})\eta_1(s) = K_{17}\,\beta(s) \tag{A-58}$$

$$(s^2 + K_{25}s + K_{26})\eta_2(s) = K_{27}\,\beta(s) \tag{A-59}$$

$$(s^2 + K_{35}s + K_{36})\eta_3(s) = K_{37}\,\beta(s) \tag{A-60}$$

$$(s^2 + K_{45}s + K_{46})\eta_4(s) = K_{47}\,\beta(s) \tag{A-61}$$

The equations for the outputs of the Position and Rate gyros are given as

$$\dot{\phi}_{RG} = \dot{\phi} + Y_1'(x_{RG})\dot{\eta}_1 + Y_2'(x_{RG})\dot{\eta}_2 + Y_3'(x_{RG})\dot{\eta}_3 + Y_4'(x_{RG})\dot{\eta}_4 \tag{A-62}$$

$$\phi_D = \phi + Y_1'(x_D)\eta_1 + Y_2'(x_D)\eta_2 + Y_3'(x_D)\eta_3 + Y_4'(x_D)\eta_4 \tag{A-63}$$

Make the following substitutions to simplify the algebra.

$$\begin{aligned} K_{19} &= Y_1'(x_{RG});\ K_{29} = Y_2'(x_{RG});\ K_{39} = Y_3'(x_{RG});\ K_{49} = Y_4'(x_{RG}) \\ K_{10} &= Y_1'(x_D)\ ;\ K_{20} = Y_2'(x_D)\ ;\ K_{30} = Y_3'(x_D)\ ;\ K_{40} = Y_4'(x_D) \end{aligned} \tag{A-64}$$

Taking the Laplace Transform of equations (A-62) and (A-63), assuming all initial conditions to be zero, yields;

$$s\phi_{RG}(s) = s\phi(s) + K_{19}s\,\eta_1(s) + K_{29}s\,\eta_2(s) + K_{39}s\,\eta_3(s) + K_{49}s\,\eta_4(s) \tag{A-65}$$

$$\phi_D(s) = \phi(s) + K_{10}\eta_1(s) + K_{20}\eta_2(s) + K_{30}\eta_3(s) + K_{40}\eta_4(s) \tag{A-66}$$

The open loop transfer function for each bending mode can now be written

$$G_1(s) = \frac{N_1}{D_1} = \frac{\eta_1}{\beta} = \frac{K_{17}}{s^2 + K_{15}s + K_{16}} \tag{A-67}$$

$$G_2(s) = \frac{N_2}{D_2} = \frac{\eta_2}{\beta} = \frac{K_{27}}{s^2 + K_{25}s + K_{26}} \tag{A-68}$$

$$G_3(s) = \frac{N_3}{D_3} = \frac{\eta_3}{\beta} = \frac{K_{37}}{s^2 + K_{35}s + K_{36}} \tag{A-69}$$

$$G_4(s) = \frac{N_4}{D_4} = \frac{\eta_4}{\beta} = \frac{K_{47}}{s^2 + K_{45}s + K_{46}} \tag{A-70}$$

The equations of motion of the system can now be written in matrix form.

A block diagram of the closed loop system is shown in Figure 5. Again this diagram can be reduced in the same fashion as indicated in Figures 3 and 4 to yield the open loop transfer function of the system.

$$\frac{0}{\beta} = (a_o + a_1 s)\, G_0(s) + (a_o K_{10} + a_1 K_{19} s)\, G_1(s) + (a_o K_{20} + a_1 K_{29} s)\, G_2(s)$$
$$+ (a_o K_{30} + a_1 K_{39} s)\, G_3(s) + (a_o K_{40} + a_1 K_{49} s)\, G_4(s) \tag{A-72}$$

If the substitutions $G_0(s) = \frac{N_0}{D_0}$; $G_1(s) = \frac{N_1}{D_1}$; $G_2(s) = \frac{N_2}{D_2}$; $G_3(s) = \frac{N_3}{D_3}$ and $G_4(s) = \frac{N_4}{D_4}$ are made in equation (A-72) the characteristic equation becomes

$$1 - KGH = 1 - \frac{\left\{ \begin{array}{l} (a_o + a_1 s) N_0 D_1 D_2 D_3 D_4 + (a_o K_{10} + a_1 K_{19} s) N_1 D_0 D_2 D_3 D_4 + (a_o K_{20} + a_1 K_{29} s) N_2 D_0 D_1 D_3 D_4 \\ + (a_o K_{30} + a_1 K_{39} s) N_3 D_0 D_1 D_2 D_4 + (a_o K_{40} + a_1 K_{49} s) N_4 D_0 D_1 D_2 D_3 \end{array} \right\}}{D_0 D_1 D_2 D_3 D_4} \tag{A-73}$$

$$
\begin{bmatrix}
s^2 & C_1 & C_2 & 0 & 0 & 0 & 0 \\
\left[s+\left(\frac{\dot{V}-K_1}{V}\right)\right] & -\left[s+\left(\frac{\dot{V}+K_2}{V}\right)\right] & \frac{-K_3}{V} & 0 & 0 & 0 & 0 \\
(a_o+a_1 s) & 0 & -1 & (K_{10}a_o+k_{19}a_1 s) & (K_{20}a_o+K_{29}a_1 s) & (K_{30}a_o+K_{39}a_1 s) & (K_{40}a_o+K_{49}a_1 s) \\
0 & 0 & -K_{17} & (s^2+K_{15}s+K_{16}) & 0 & 0 & 0 \\
0 & 0 & -K_{27} & 0 & (s^2+K_{25}s+K_{26}) & 0 & 0 \\
0 & 0 & -K_{37} & 0 & 0 & (s^2+K_{35}s+K_{36}) & 0 \\
0 & 0 & -K_{47} & 0 & 0 & 0 & (s^2+K_{45}s+K_{46})
\end{bmatrix}
\begin{bmatrix}
\phi \\ \alpha \\ \beta \\ \eta_1 \\ \eta_2 \\ \eta_3 \\ \eta_4
\end{bmatrix}
=
\begin{bmatrix}
0 \\ 0 \\ a_o\phi_c \\ 0 \\ 0 \\ 0 \\ 0
\end{bmatrix}
\tag{A-71}
$$

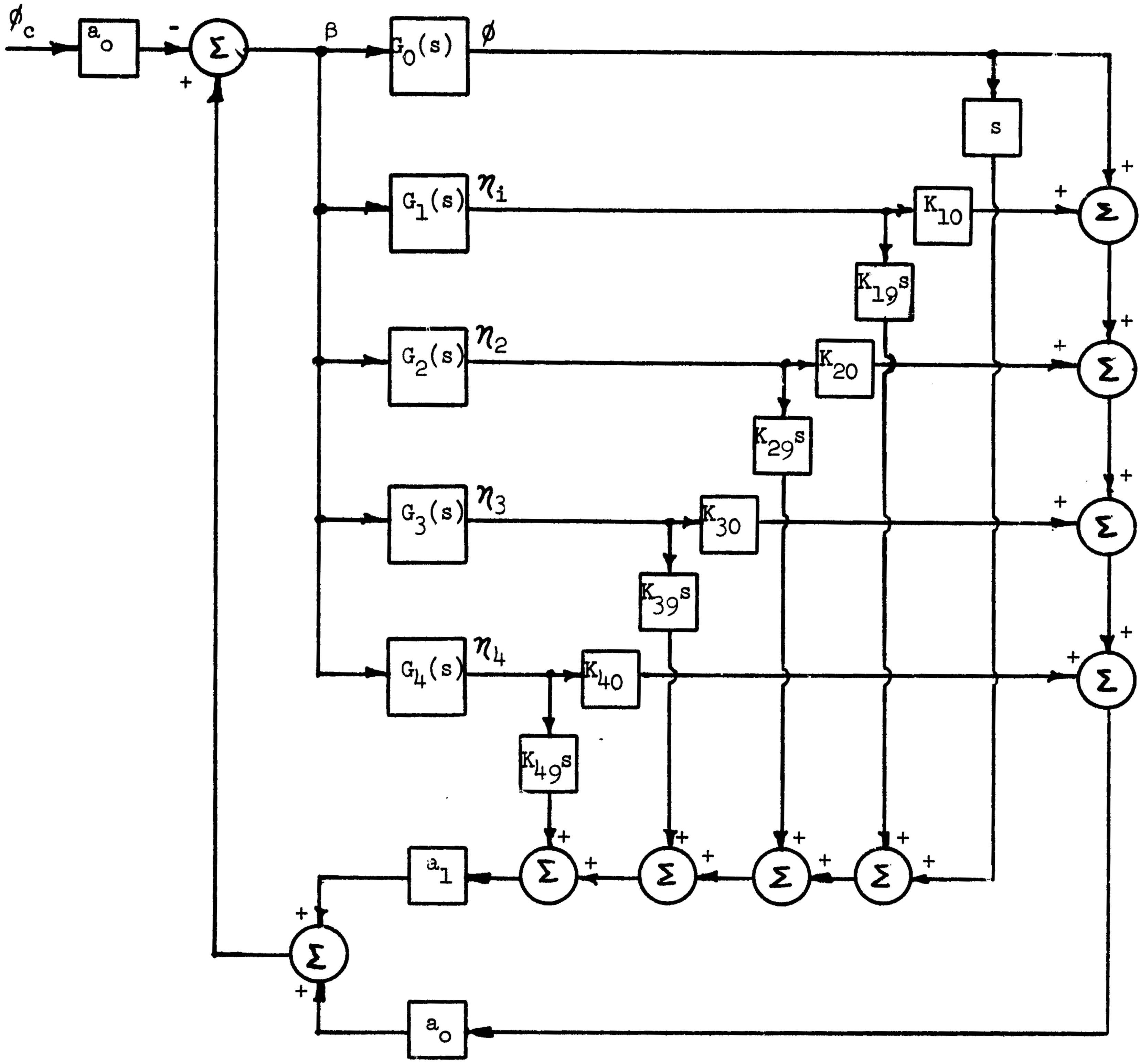

Figure 5 - Block Diagram of Rigid Body Plus Four Bending Modes.

The numerator and denominator of KGH can now be factored to draw the root locus.

A.3 Numerical Analysis at t = 80 Seconds

A.3.1 Rigid Body Mode

The open loop transfer function is

$$\frac{\phi}{\beta} = \frac{-\left\{C_2 s + \left[C_2\left(\frac{\dot{V}+K_2}{V}\right) - \frac{C_1 K_3}{V}\right]\right\}}{s^3 + \left(\frac{\dot{V}+K_3}{V}\right) s^2 + C_1 s + C_1\left(\frac{\dot{V}-K_1}{V}\right)} \qquad \text{(A-74)}$$

The coefficients are evaluated as follows;

$$C_1 = \frac{N' l_i}{I_{xx}} = \frac{C_{N\alpha} qs (x_{cg} - x_{cp})}{I_{xx}} = -\ 0.202 \text{ sec}^{-2}$$

$$C_2 = \frac{R' x_{cg}}{I_{xx}} = \frac{4}{5}\ \frac{F x_{cg}}{I_{xx}} = 1.17 \text{ sec}^{-2}$$

$$K_1 = \frac{F - x}{m} = 21.6 \text{ meters/sec}^2$$

$$K_2 = \frac{N'}{m} = \frac{C_{N\alpha} qs}{m} = 7.75 \text{ meters/sec}^2$$

$$K_3 = \frac{R'}{m} = \frac{4}{5}\ \frac{F}{m} = 18.1 \text{ meters/sec}^2$$

$$\frac{\dot{V} + K_2}{V} = 4.06 \times 10^{-2} \text{ sec}^{-1}$$

$$\frac{C_1 K_3}{V} = -6.76 \times 10^{-3} \text{ sec}^{-3}$$

$$\frac{\dot{V} - K_1}{V} = -1.37 \times 10^{-2} \text{ sec}^{-1}$$

Substitution of these values into the open loop transfer function of the rigid body yields

$$KG(s) = \frac{\phi}{\beta} = \frac{-1.17\ (s + 0.047)}{s^3 + 4.06 \times 10^{-2}\ s^2 - 2.02 \times 10^{-1} s + 2.77 \times 10^{-3}} \tag{A-75}$$

The system block diagram was shown in Figure 1. This is a positive feedback system because of the way the control law is written. The closed loop transfer function is

$$\frac{\phi}{-a_o \phi_c} = \frac{-KG}{1 - (-KG)H} = \frac{-KG}{1 + KGH} \tag{A-76}$$

the characteristic equation is

$$1 + KGH = 1 + \frac{1.17\ a_1 (s + a_o/a_1)\ (s + 0.047)}{s^3 + 4.06 \times 10^{-2}\ s^2 - 2.02 \times 10^{-1}\ s + 2.77 \times 10^{-3}} \tag{A-77}$$

It is obvious from equation (A-77) that a set of gyro feedback gains must be selected. To make a rational choice, the root locus plot of the rigid body mode with a feedback gain of unity will be investigated first. This condition would correspond to the use of only a position gyro in the feedback path, with a gain of unity. This condition is shown in block diagram form in Figure 6.

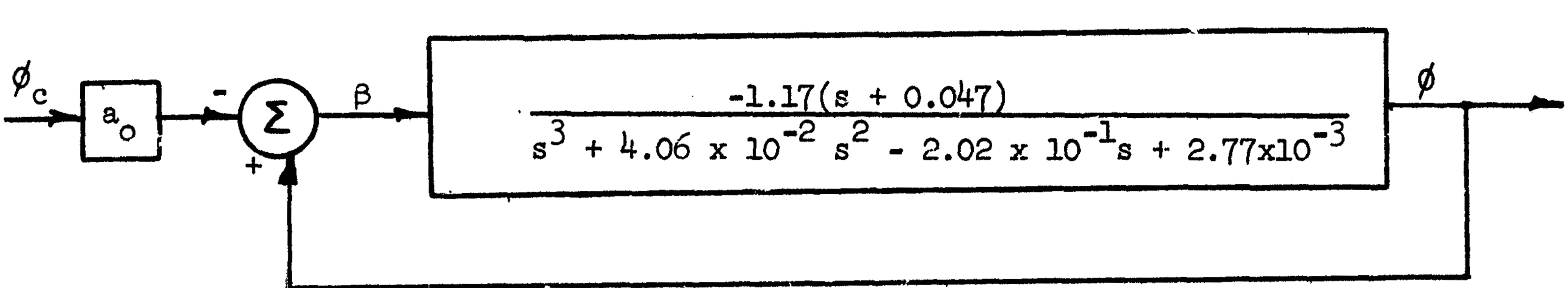

Figure 6 - Rigid Body Mode with Unity Feedback

The characteristic equation, in factored form is

$$1 + KGH = 1 + \frac{1.17\ (s + 0.047)}{(s + 0.48)\ (s - 0.014)(s - 0.422)} \tag{A-78}$$

A sketch of the pole-zero pattern for this configuration is shown in Figure 7.

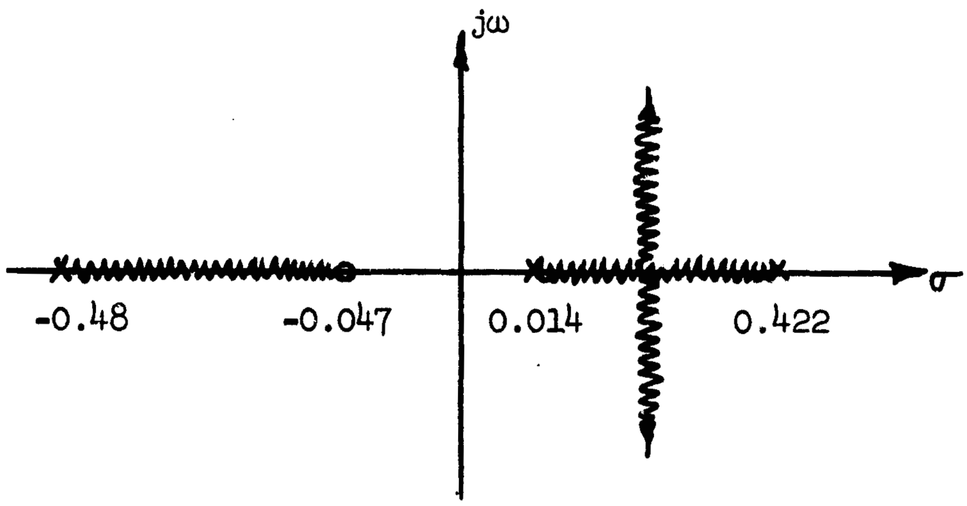

Figure 7 - Pole-Zero Pattern for Rigid Body Mode with Unity Feedback

The presence of the two poles in the right half plane is due to the location of the center of pressure above the center of gravity. As static gain is increased from zero to infinity the locus of the closed loop poles will have two branches that remain in the right half plane, yielding instability for all values of gain. When gyro feedback is introduced into the system, an open loop zero is inserted on the real axis in the left half plane. There are three possible locations for this zero. These locations and the resultant Root Locus diagrams are shown in Figure 8.

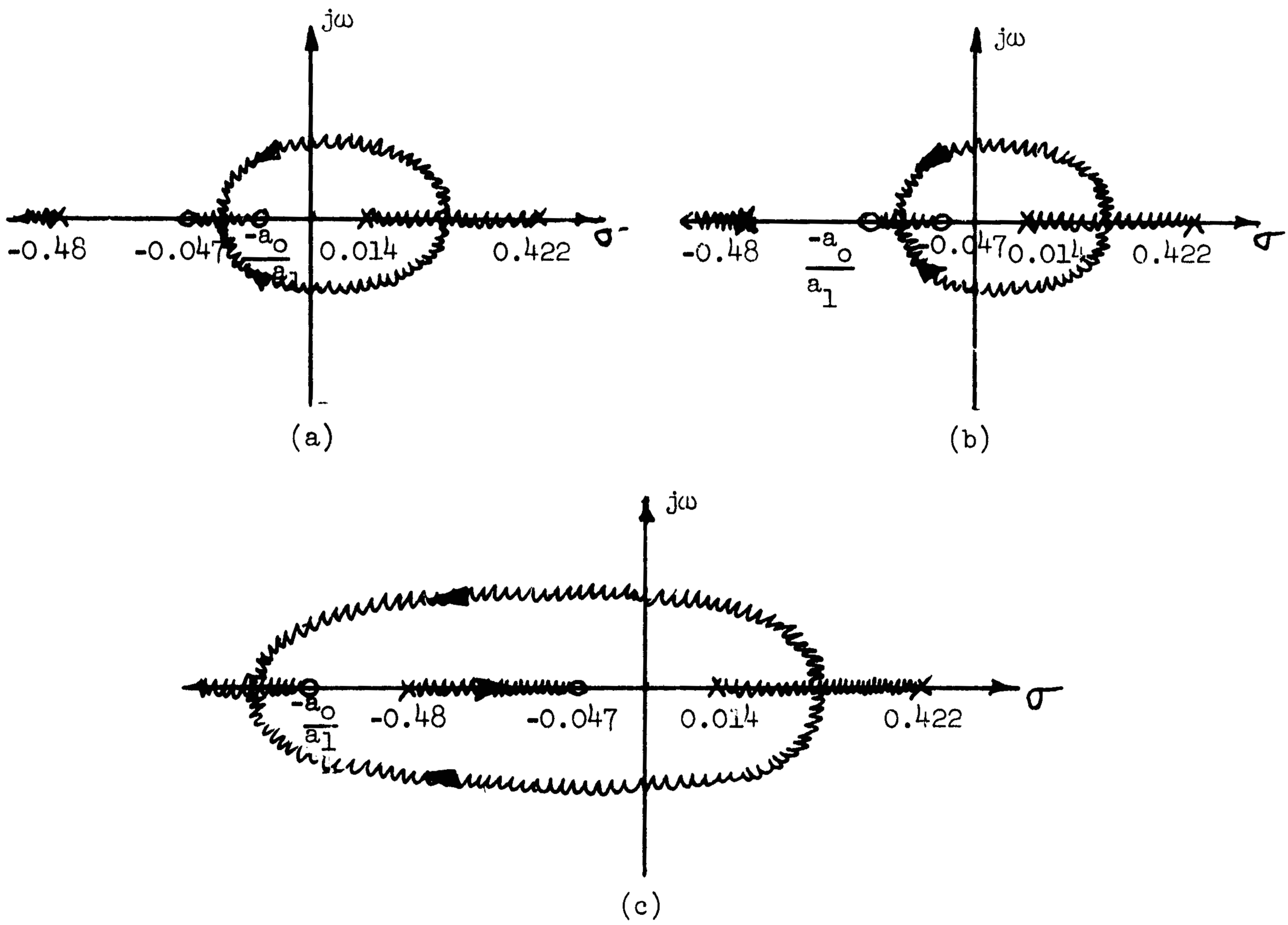

Figure 8 - Possible Gyro Open Loop Zero Locations on the S-Plane

The location of the zero in (c) yields a stable system for the lowest value of gain and for higher values of gain yields a higher damping ratio for a given value of gain. The zero therefore will be positioned to the left of the (s + 0.48) pole on the real axis in the left half plane. Routh's Criterion can now be used to determine the values of the gyro gains, a_o and a_1, required to produce a stable closed loop system. The first step in this process is to determine the characteristic equation.

$$1 - KGH = s^3 + (4.06 \times 10^{-2} + 1.17\, a_1)\, s^2 + (-2.02 \times 10^{-1} + 1.17\, a_o + 5.43 \times 10^{-2} a_1)s + (2.75 \times 10^{-3} + 5.43 \times 10^{-2} a_o) \qquad \text{(A-79)}$$

The Routhian array becomes

$$\begin{array}{lll} s^3 & 1 & (-2.02 \times 10^{-1} + 1.17a_o + 5.43 \times 10^{-2}a_1) \\ s^2 & (4.06 \times 10^{-2} + 1.17a_1) & (2.75 \times 10^{-3} + 5.43 \times 10^{-2}a_o) \\ s^1 & c_1 & c_2 \\ s^o & d_1 & d_2 \end{array} \qquad \text{(A-80)}$$

For simplicity let

$$b_1 = (4.06 \times 10^{-2} + 1.17\ a_1)$$

$$a_2 = (-2.02 \times 10^{-1} + 1.17\ a_o + 5.43 \times 10^{-2}\ a_1)$$

$$b_2 = (2.75 \times 10^{-3} + 5.43 \times 10^{-2}\ a_o)$$

The array can then be written as

$$\begin{array}{lll} s^3 & 1 & a_2 \\ s^2 & b_1 & b_2 \\ s^1 & c_1 & c_2 \\ s^o & d_1 & d_2 \end{array} \qquad \text{(A-81)}$$

where

$$c_1 = \frac{b_1\ a_2 - b_2}{b_1}$$

$$c_2 = 0 \qquad \text{(A-83)}$$

$$d_1 = \frac{c_1\ b_2}{c_1} = b_2 \qquad \text{(A-84)}$$

The Routhian array becomes

$$\begin{array}{lll} s^3 & 1 & a_2 \\ s^2 & b_1 & b_2 \\ s^1 & \dfrac{b_1a_2-b_2}{b_1} & 0 \\ s^o & b_2 & 0 \end{array} \qquad \text{(A-85)}$$

The only term that can yield a negative sign in the first column is $\dfrac{b_1a_2-b_2}{b_1}$. For a stable system then, it is necessary that

$$b_1a_2 > b_2 \qquad \text{(A-86)}$$

A further condition is that a_2 is positive. For this condition to hold.

$$(1.17\ a_o + 5.43 \times 10^{-2}\ a_1) > 2.02 \times 10^{-1} \qquad \text{(A-87)}$$

Now use an additional piece of information to determine the ratio a_o/a_1. Inspection of the root locus diagram of Figure 8-c indicates that the zero at $-\dfrac{a_o}{a_1}$ is to the left of the pole at s + 0.48 so that the following inequality holds.

$$\left|\frac{a_o}{a_1}\right| > |0.48| \qquad \text{(A-88)}$$

Assume

$$\frac{a_o}{a_1} > 0.5 \qquad \text{(A-89)}$$

or

$$a_o = 0.5\ a_1 \qquad \text{(A-90}$$

This value for a_o can now be substituted back into the equality of (A-87) to yield

$$a_1 > 0.315 \qquad \text{(A-91)}$$

Values for a_o and a_1 can now be assigned.

$$a_o = 0.2 \qquad \text{(A-92)}$$

$$a_1 = 0.4 \qquad \text{(A-93)}$$

The inequality $b_1 a_2 > b_2$ must also be checked. When the values of $a_o = 0.2$ and $a_1 = 0.4$ are substituted into (A-86) they yield the fact that

$0.0273 > 0.0136$ which checks.

The characteristic equation now becomes

$$1 - KGH = 1 + \frac{0.468\ (s + 0.5)\ (s + 0.047)}{(s + 0.48)\ s - 0.014)\ (s - 0.422)} \qquad \text{(A-94)}$$

The root locus plot for this characteristic equation is shown in Figure 9.

A.3.2 Rigid Body Plus First Bending Mode

In this analysis each mode will be added in turn and system performance evaluated. In this manner the effect on vehicle performance, of adding one bending mode at a time, can be more easily visualized.

Two alternatives must now be considered. First the gyro feedback gains that stabilized the Rigid Body Mode can be used, and the system compensated, if required, by appropriate filters. Or a new set of feedback gains can be determined, if they exist, that would stabilize the combined rigid body and first bending modes. The first alternative will

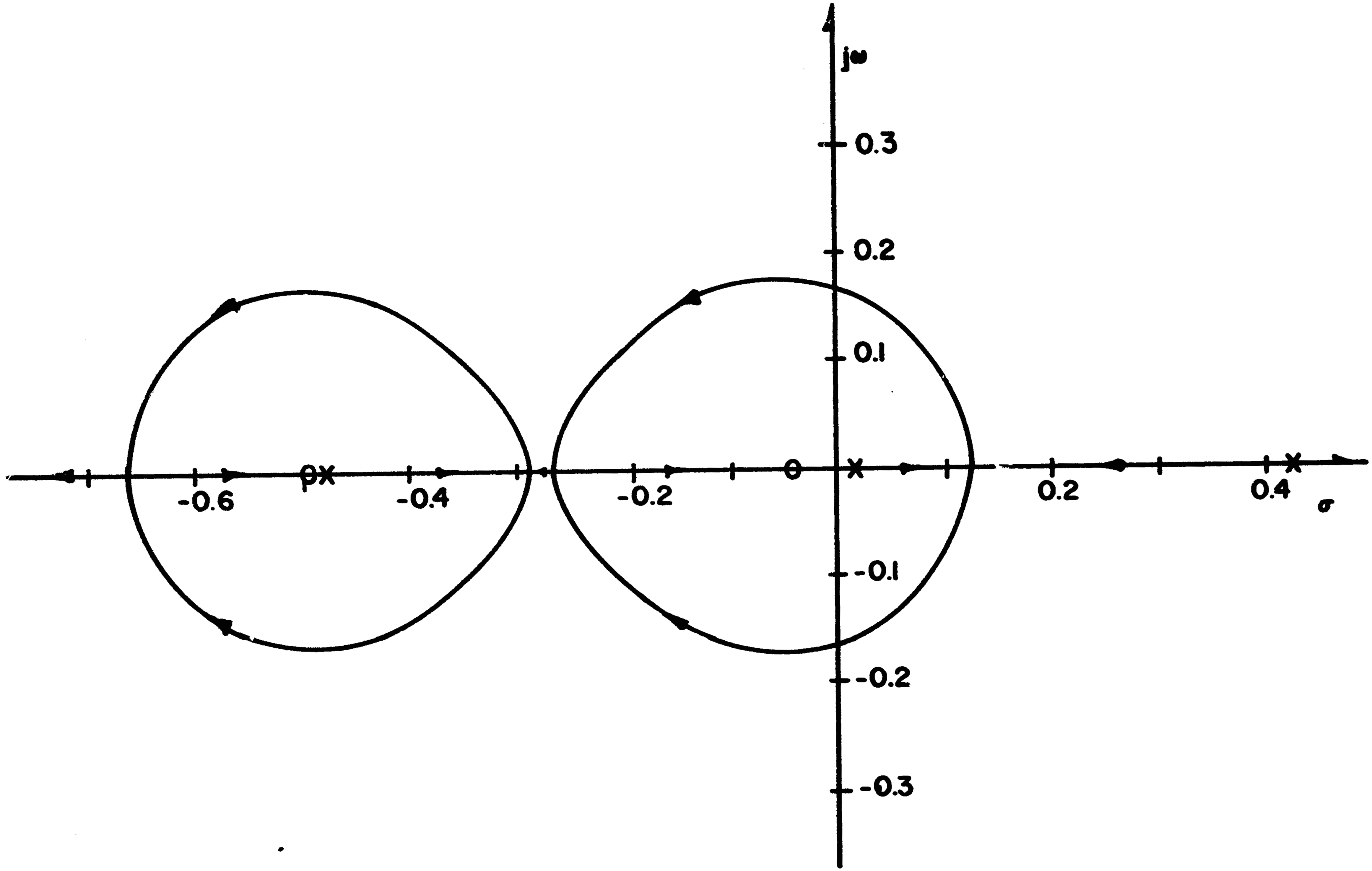

FIGURE 9 ROOT LOCUS PLOT OF RIGID BODY MODE

be used in this analysis.

The open loop, first bending mode, transfer function was given by equation (A-48) and is repeated here.

$$G_1(s) = \frac{N_1}{D1} = \frac{\eta_1}{\beta} = \frac{K_{17}}{s^2 + K_{15}s + K_{16}} \tag{A-95}$$

where

$$K_{17} = \frac{R' \; Y_1(x_\beta)}{M_1} = 254 \text{ meters/sec}^2$$

$$K_{15} = 2\zeta_1\omega_1 = 1.34 \times 10^{-1} \text{ sec}^{-1}$$

$$K_{16} = \omega_1^{\,2} = 44.9 \text{ rad/sec}^2$$

$$\zeta_1 = 0.01$$

The open loop transfer function becomes

$$G_1(s) = \frac{N_1}{D_1} = \frac{\eta_1}{\beta} = \frac{254}{s^2 + 1.34 \times 10^{-1}s + 44.9} = \frac{254}{(s + 0.067 + j\,6.7)\,(s + 0.067 - j\,6.7)} \tag{A-96}$$

A block diagram of this system was shown in Figure 2. The system characteristic equation is given by

$$1 - KGH = 1 - \left[(a_o + a_1 s)\; G_0(s) + (a_o K_{10} + a_1 K_{19} s)\; G_1(s)\right] \tag{A-97}$$

where

$$K_{10} = Y_1' \; (x_D) = 1.463 \times 10^{-2} \text{ meters}^{-1}$$

$$K_{19} = Y_1' \; (x_{RG}) = 7.01 \times 10^{-3} \text{ meters}^{-1}$$

if the su itutions

$$G_0(s) = \frac{N_0}{D_0}$$

and

$$G_1(s) = \frac{N_1}{D_1}$$

are made the characteristic equation assumes the form

$$1 - KGH = 1 - \left[\frac{(a_0 + a_1 s)\, N_0 D_1 + (a_0 K_{10} + a_1 K_{19} s)\, N_1 D_0}{D}\right] \tag{A-98}$$

Substitution for the various constants yields

$$1 - KGH = 1 - \frac{2.44 + 10^{-1}(s^4 + 1.87s^3 - 8.65 \times 10^{+1}s^2 - 4.77 \times 10^{+1}s - 2.02)}{s^5 + 1.75 \times 10^{-1}s^4 + 4.47 \times 10^{+1}s^3 + 1.8s^2 - 9.06s + 1.25 \times 10^{-1}} \tag{A-99}$$

In factored form

$$1 - KGH = 1 - \frac{2.44 \times 10^{-1}(s - 8.7)(s + 0.046)(s + 0.5)(s + 10)}{(s + 0.48)(s - 0.014)(s - 0.422)(s + 0.067 + j\,6.7)(s + 0.067 - j\,6.7)} \tag{A-100}$$

The root locus plot for this system is shown in Figure 10.

A.3.3 Rigid Body Plus First and Second Bending Modes

The open loop, second bending mode, transfer function was given by equation (A-68) and is repeated here.

$$G_2(s) = \frac{N_2}{D_2} = \frac{\eta_2}{\beta} = \frac{K_{27}}{s^2 + K_{25}s + K_{26}} \tag{A-101}$$

where

$$K_{27} = \frac{R'Y_2(x_\beta)}{M_2} = -485 \text{ meters/sec}^2$$

$$K_{25} = 2\,\zeta_2\,\omega_2 = 2.44 \times 10^{-1} \text{ rad/sec}$$

$$K_{26} = \omega_2^{\,2} = 149 \text{ rad/sec}^2$$

$$\zeta_2 = 0.01$$

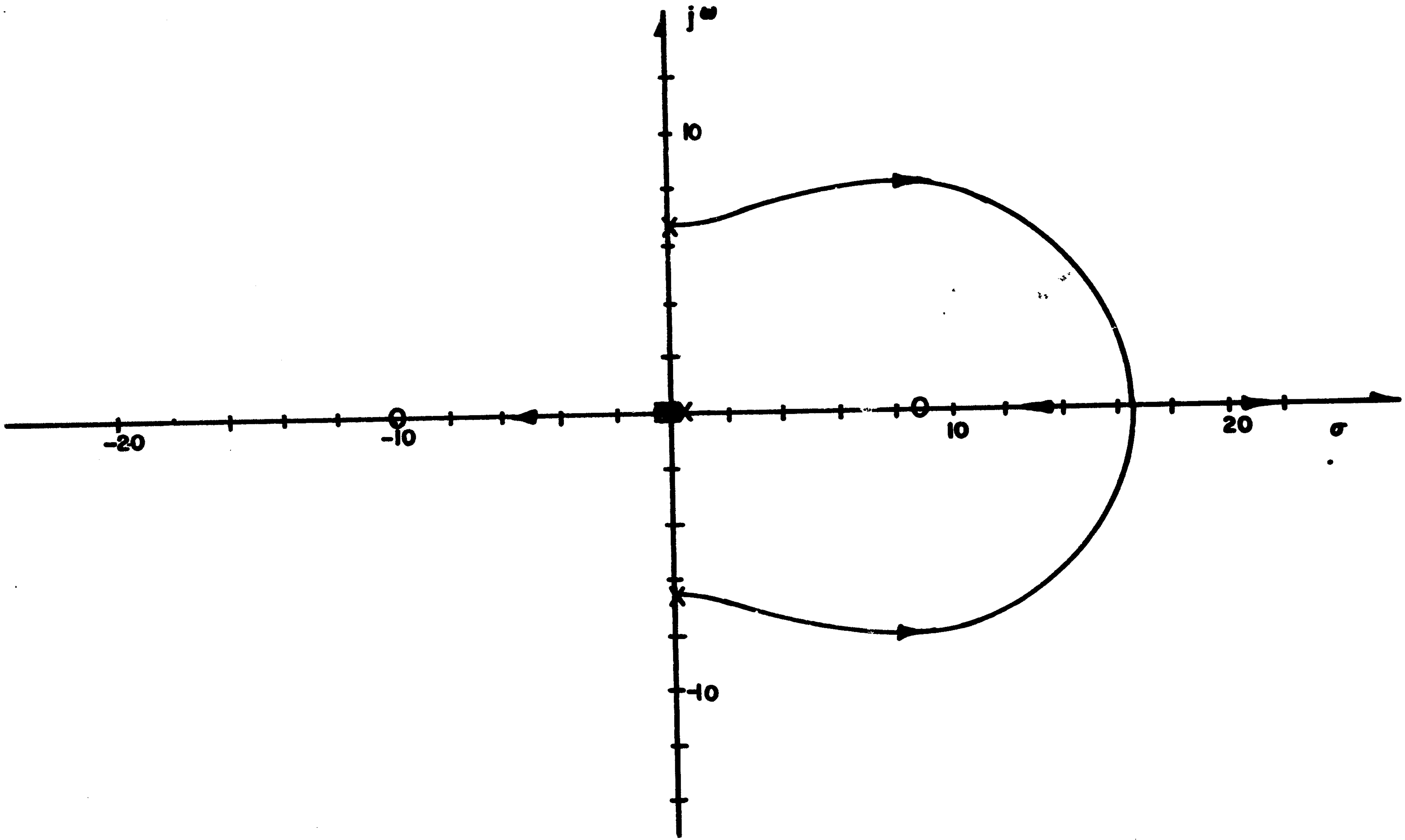

FIGURE 10 ROOT LOCUS PLOT OF RIGID BODY PLUS FIRST BENDING MODE

The open loop transfer function becomes

$$G_2(s) = \frac{N_2}{D_2} = \frac{\gamma_2}{\beta} = \frac{-485}{s^2 + 2.44 \times 10^{-1}s + 149} = \frac{-485}{(s + 0.122 + j12.25)(s + 0.122 - j12.25)} \tag{A-102}$$

A block diagram of this system is shown in Figure 11. The system characteristic equation is given by

$$1 - KGH = 1 - \left[(a_o + a_1 s)\, G_0(s) + (a_o K_{10} + a_1 K_{19} s)\, G_1(s) + (a_o K_{20} + a_1 K_{29} s) G_2(s)\right] \tag{A-103}$$

where

$$K_{20} = Y_2'(x_D) = 1.27 \times 10^{-3} \text{ meters}^{-1}$$

$$K_{29} = Y_2'(x_{RG}) = -5.13 \times 10^{-3} \text{ meters}^{-1}$$

Again substitute the following expressions into equation (A-103)

$$G_0(s) = \frac{N_0}{D_0}$$

$$G_1(s) = \frac{N_1}{D_1}$$

$$G_2(s) = \frac{N_2}{D_2}$$

The characteristic equation is then written as

$$1 - KGH = 1 - \left[\frac{(a_o + a_1 s)N_0 D_1 D_2 + (a_o K_{10} + a_1 K_{19} s)N_1 D_0 D_2 + (a_o K_{20} + a_1 K_{29} s)N_2 D_0 D_1}{D_0 D_1 D_2}\right] \tag{A-104}$$

Substitution for the various constants yields

$$1 - KGH = 1 - \frac{1.24(s^6 + 4.57 \times 10^{-1}s^5 + 4.8 \times 10^{+1}s^4 + 3.89 \times 10^{+1}s^3 - 2.56 \times 10^{+3}s^2 - 1.41 \times 10^{+3}s - 5.95 \times 10^{+1})}{s^7 + 4.19 \times 10^{-1}s^6 + 1.94 \times 10^{+2}s^5 + 3.88 \times 10^{+1}s^4 + 6.65 \times 10^{+3}s^3 + 2.66 \times 10^{+2}s^2 - 3.35 \times 10^{+3}s + 1.86 \times 10^{+1}} \qquad \text{(A-105)}$$

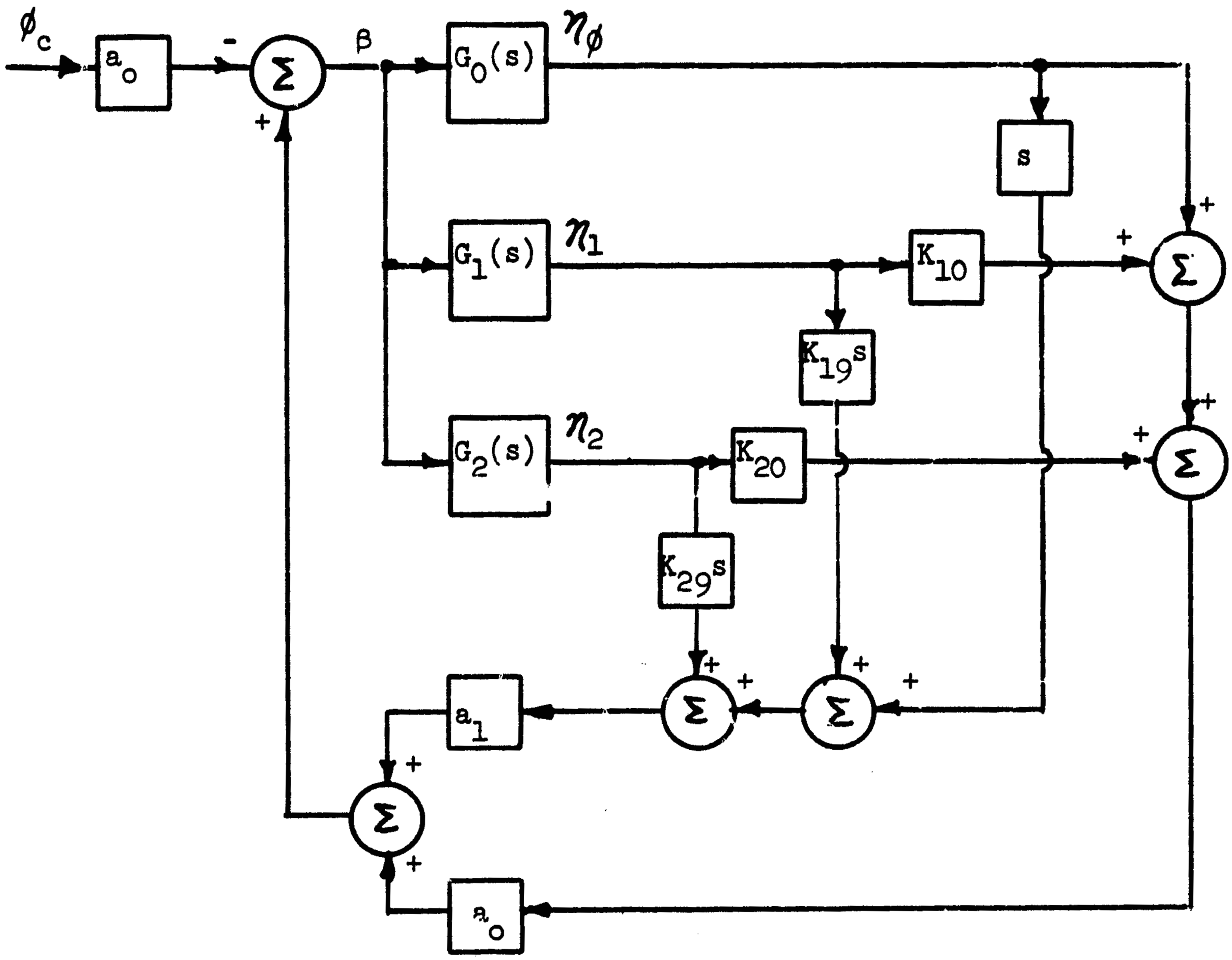

Figure 11 - Block Diagram of Rigid Body Plus First and Second Bending Modes.

In factored form this becomes

$$1 - KGH = 1 - \frac{1.24(s - 5.62)(s - 0.089 \pm j\,8.95)(s + 0.046)(s + 0.5)(s + 5.7)}{(s + 0.48)(s - 0.014)(s - 0.422)(s + 0.067 \pm j\,6.7)(s + 0.122 \pm j\,12.3)}$$

(A-106)

The root locus plot for this system is shown in Figure 12.

A.3.4 Rigid Body Plus First, Second and Third Bending Modes

The open loop third bending mode transfer function was given by equation (A-69) and is repeated here.

$$G_3(s) = \frac{N_3}{D_3} = \frac{\eta_3}{\beta} = \frac{K_{37}}{s^2 + K_{35}s + K_{36}} \tag{A-107}$$

where

$$K_{37} = \frac{R'Y_3(x_\beta)}{M_3} = 494 \text{ meters/sec}^2$$

$$K_{36} = \omega_3^{\,2} = 285.5 \text{ rad/sec}^2$$

$$K_{35} = 2\zeta_3\omega_3 = 3.38 \times 10^{-1} \text{ rad/sec}$$

$$\zeta_3 = 0.01$$

The open loop transfer function becomes

$$G_3(s) = \frac{N_3}{D_3} = \frac{\eta_3}{\beta} = \frac{494}{s^2 + 3.38 \times 10^{-1}s + 2.86 \times 10^{+2}} = \frac{494}{(s + 0.17 + j\,17)(s + 0.17 - j17)} \tag{A-108}$$

A block diagram of this system is shown in Figure 13. The system characteristic equation is given by

$$1 - KGH = 1 - \Big[(a_o + a_1s)\, G_0(s) + (a_oK_{10} + a_1K_{19}s)\, G_1(s) + (a_oK_{20} + a_1K_{29}s)\, G_2(s) + (a_oK_{30} + a_1K_{39}s)\, G_3(s)\Big] \tag{A-109}$$

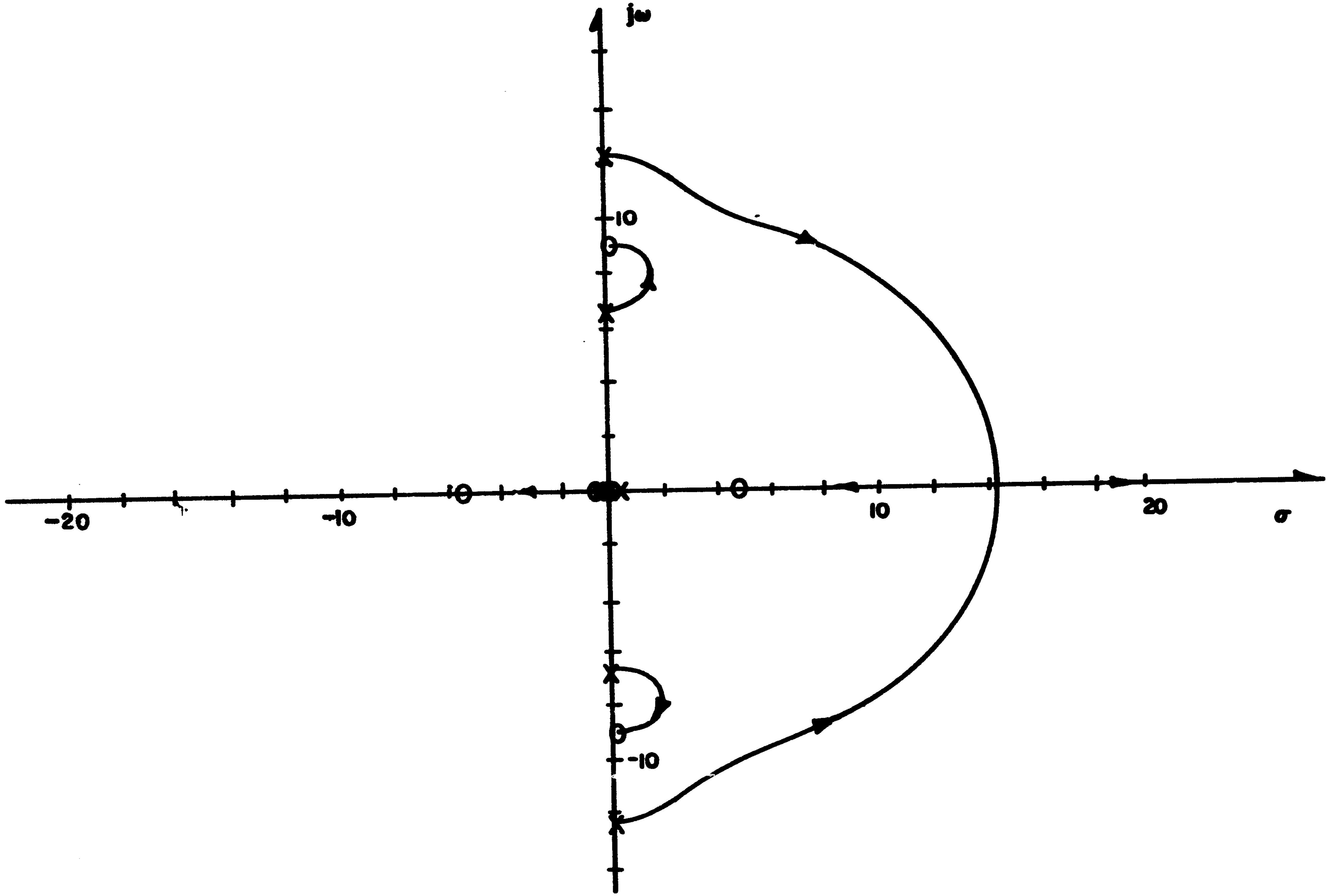

FIGURE 12 ROOT LOCUS PLOT OF RIGID BODY PLUS FIRST AND SECOND BENDING MODE

where

$$_{30} = Y_3'(x_D) = -1.051 \times 10^{-2} \text{ meters}^{-1}$$

$$K_{39} = Y_3'(x_{RG}) = -2.95 \times 10^{-3} \text{ meters}^{-1}$$

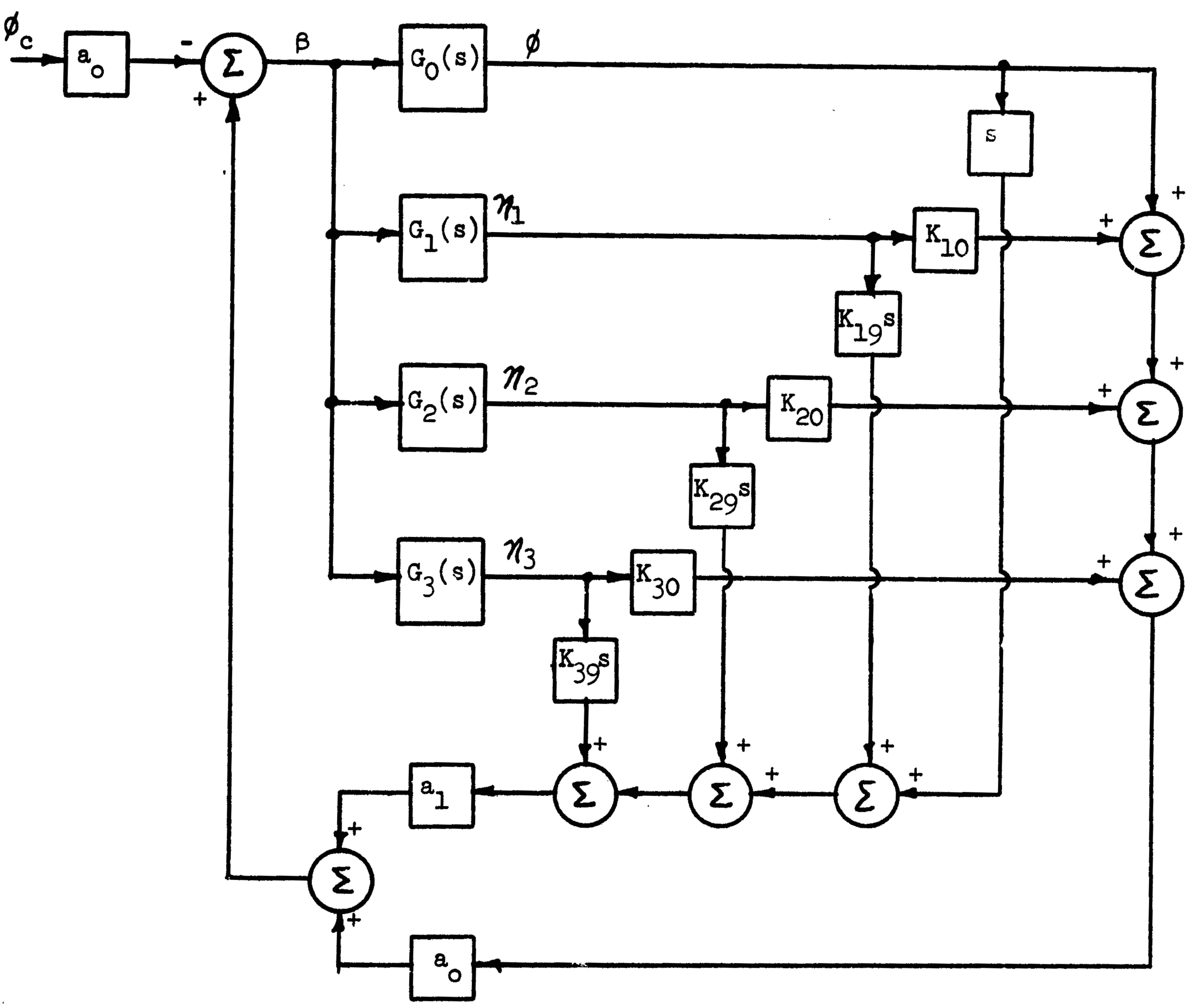

Figure 13 - Block Diagram of Rigid Body Plus First, Second and Third Bending Modes

Again make the following substitutions into equation (A-109)

$$G_0(s) = \frac{N_0}{D_0} \; ; \; G_1(s) = \frac{N_1}{D_1} \; ; \; G_2(s) = \frac{N_2}{D_2} \; ; \; G_3(s) = \frac{N_3}{D_3}$$

The characteristic equation is then written as;

$$1 - KGH = 1 - \frac{\left[(a_o + a_1 s)N_0 D_1 D_2 D_3 + (a_o K_{10} + a_1 K_{19} s)N_1 D_0 D_2 D_3 + (a_o K_{20} + a_1 K_{29} s)N_2 D_0 D_1 D_3 + (a_o K_{30} + a_1 K_{39} s)N_3 D_0 D_1 D_2\right]}{D_0 D_1 D_2 D_3} \qquad \text{(A-110)}$$

Substitution for the various constants yields

$$1 - KGH = 1 - \frac{6.54 \times 10^{-1}\left[\begin{array}{l}(s^8 - 4.6 \times 10^{-1} s^7 + 4.55 \times 10^{+2} s^6 + 2.45 s^5 + \\ 1.48 \times 10^{+4} s^4 + 5.96 \times 10^{+3} s^3 - 1.4 \times 10^{+6} s^2 \\ -7.66 \times 10^{+5} s - 3.23 \times 10^{+4})\end{array}\right]}{\left[\begin{array}{l}(s^9 + 7.57 \times 10^{-1} s^8 + 4.8 \times 10^{+2} s^7 + 2.24 \times 10^{+2} s^6 + 6.22 \times 10^{+4} s^5 \\ + 1.36 \times 10^{+4} s^4 + 1.9 \times 10^{+6} s^3 + 7.57 \times 10^{+4} s^2 - 3.86 \times 10^{+5} s + \\ 5.32 \times 10^{+3})\end{array}\right]} \qquad \text{(A-111)}$$

in factored form this becomes

$$1 - KGH = 1 - \frac{6.54 \times 10^{-1}\left[\begin{array}{l}(s - 6.46)(s - 0.24 + j\,20.3)(s - 0.24 - j\,20.3) \\ (s - 0.14 + j\,9.2)(s - 0.14 - j\,9.2)(s + 0.046) \\ (s + 0.5)(s + 6.23)\end{array}\right]}{\left[\begin{array}{l}(s + 0.48)(s - 0.014)(s - 0.422)(s + 0.067 + j\,6.7)(s + 0.067 - j\,6.7) \\ (s + 0.122 + j\,12.3)(s + 0.122 - j\,12.3)(s + 0.17 + j\,17)(s + 0.17 - j\,17)\end{array}\right]}$$

(A-112)

The root locus plot for this system is shown in Figure 14.

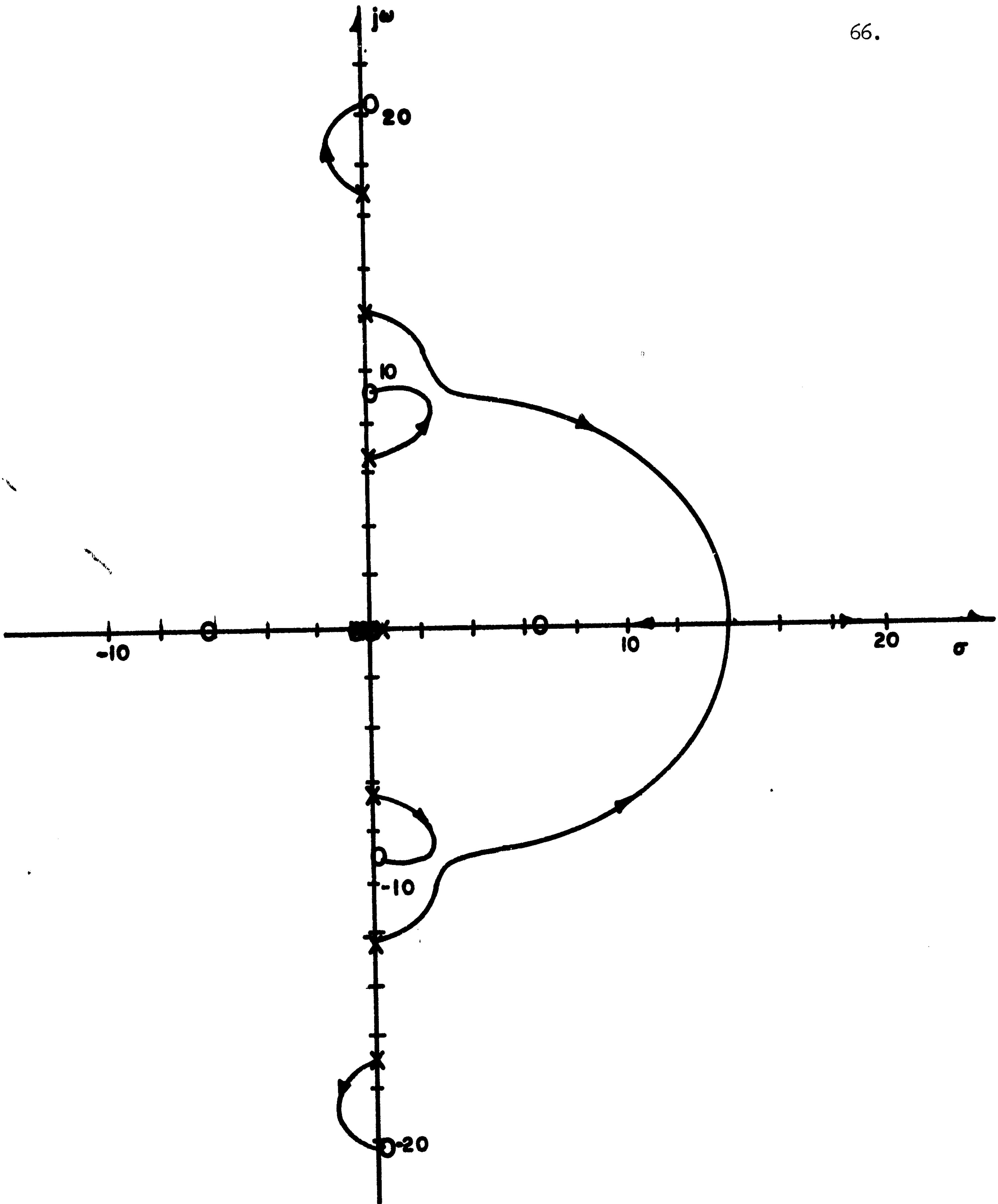

FIGURE 14 ROOT LOCUS PLOT OF RIGID BODY MODE PLUS FIRST, SECOND, AND THIRD BENDING MODE

A.3.5 Rigid Body Plus First, Second, Third and Fourth Bending Modes

The open loop fourth bending mode transfer function was given by equation (A-70) and is repeated here.

$$G_4(s) = \frac{N_4}{D_4} = \frac{\eta_4}{\beta} = \frac{K_{47}}{s^2 + K_{45}s + K_{46}} \qquad \text{(A-113)}$$

where

$$K_{47} = \frac{R'Y_4(x_\beta)}{M_4} = -206 \text{ meters/sec}^2$$

$$K_{46} = \omega_4{}^2 = 459 \text{ rad/sec}^2$$

$$K_{45} = 2\zeta_4\omega_4 = 4.28 \times 10^{-1} \text{ rad/sec}$$

$$\zeta_4 = 0.01$$

The open loop transfer function becomes

$$G_4(s) = \frac{N_4}{D_4} = \frac{\eta_4}{\beta} = \frac{459}{s^2 + 4.28 \times 10^{-1}s + 4.59 \times 10^{+2}} = \frac{459}{(s + 0.21 + j21.5)(s + 0.21 - j21.5)} \qquad \text{(A-114)}$$

A block diagram of this system has previously been drawn in Figure 5. The system characteristic equation is given by

$$1 - KGH = 1 - \Big[(a_o + a_1 s)\, G_0(s) + (a_o K_{10} + a_1 K_{19} s)\, G_1(s) + (a_o K_{20} + a_1 K_{29} s)\, G_2(s) + (a_o K_{30} + a_1 K_{39} s)\, G_3(s) + (a_o K_{40} + a_1 K_{49} s)\, G_4(s)\Big] \qquad \text{(A-115)}$$

where

$$K_{40} = Y_4'(x_D) = -1.524 \times 10^{-2} \text{ meters}^{-1}$$

$$K_{49} = Y_4'(x_{RG}) = 1.196 \times 10^{-2} \text{ meters}^{-1}$$

Again make the following substitutions into equation (A-115)

$$G_0(s) = \frac{N_0}{D_0}; \quad G_1(s) = \frac{N_1}{D_1}; \quad G_2(s) = \frac{N_2}{D_2}; \quad G_3(s) = \frac{N_3}{D_3}; \quad G_4(s) = \frac{N_4}{D_4}$$

The characteristic equation can then be written as

$$1 - KGH = 1 - \left[\frac{(a_o + a_1 s)N_0 D_1 D_2 D_3 D_4 + (a_o K_{10} + a_1 K_{19} s)N_1 D_0 D_2 D_3 D_4 + (a_o K_{20} + a_1 K_{29} s) N_2 D_0 D_1 D_3 D_4 + (a_o K_{30} + a_1 K_{39} s)N_3 D_0 D_1 D_2 D_4 + (a_o K_{40} + a_1 K_{49} s)N_4 D_0 D_1 D_2 D_3}{D_0 D_1 D_2 D_3 D_4}\right] \tag{A-116}$$

Substitution for the various constants yield;

$$1 - KGH = 1 + 3.31 \times 10^{-1} \frac{\left[s^{10} + 4.02 \times 10^{-1} s^9 - 3.83 \times 10^{+2} s^8 + 7.14 \times 10^{+2} s^7 - 2.59 \times 10^{+5} s^6 - 1.03 \times 10^{+5} s^5 - 5.35 \times 10^{+6} s^4 - 6.21 \times 10^{+6} s^3 + 1.26 \times 10^{+9} s^2 + 6.92 \times 10^{+8} s + 2.94 \times 10^{+7}\right]}{\left[s^{11} + 1.19 s^{10} + 9.39 \times 10^{+2} s^9 + 7.77 \times 10^{+2} s^8 + 2.82 \times 10^{+5} s^7 + 1.43 \times 10^{+5} s^6 + 3.05 \times 10^{+7} s^5 + 7.13 \times 10^{+6} s^4 + 8.72 \times 10^{+8} s^3 + 3.45 \times 10^{+7} s^2 - 1.77 \times 10^{+8} s + 2.44 \times 10^{+6}\right]} \tag{A-117}$$

In factored form this becomes

$$1 - KGH = 1 + 3.31 \times 10^{-1} \frac{\left[(s - 26.8)(s - 7.67)(s - 0.45 \pm j\,18.1)(s + 0.43 \pm j\,9.46)(s + 0.046)(s + 0.5)(s + 7.61)(s + 27.59)\right]}{\left[(s + 0.48)(s - 0.014)(s - 0.422)(s + 0.067 \pm j\,6.7)(s + 0.122 \pm j\,12.3)(s + 0.17 \pm j\,17)(s + 0.21 \pm j\,21.5)\right]} \tag{A-118}$$

The root locus plot for this system is shown in Figure 15.

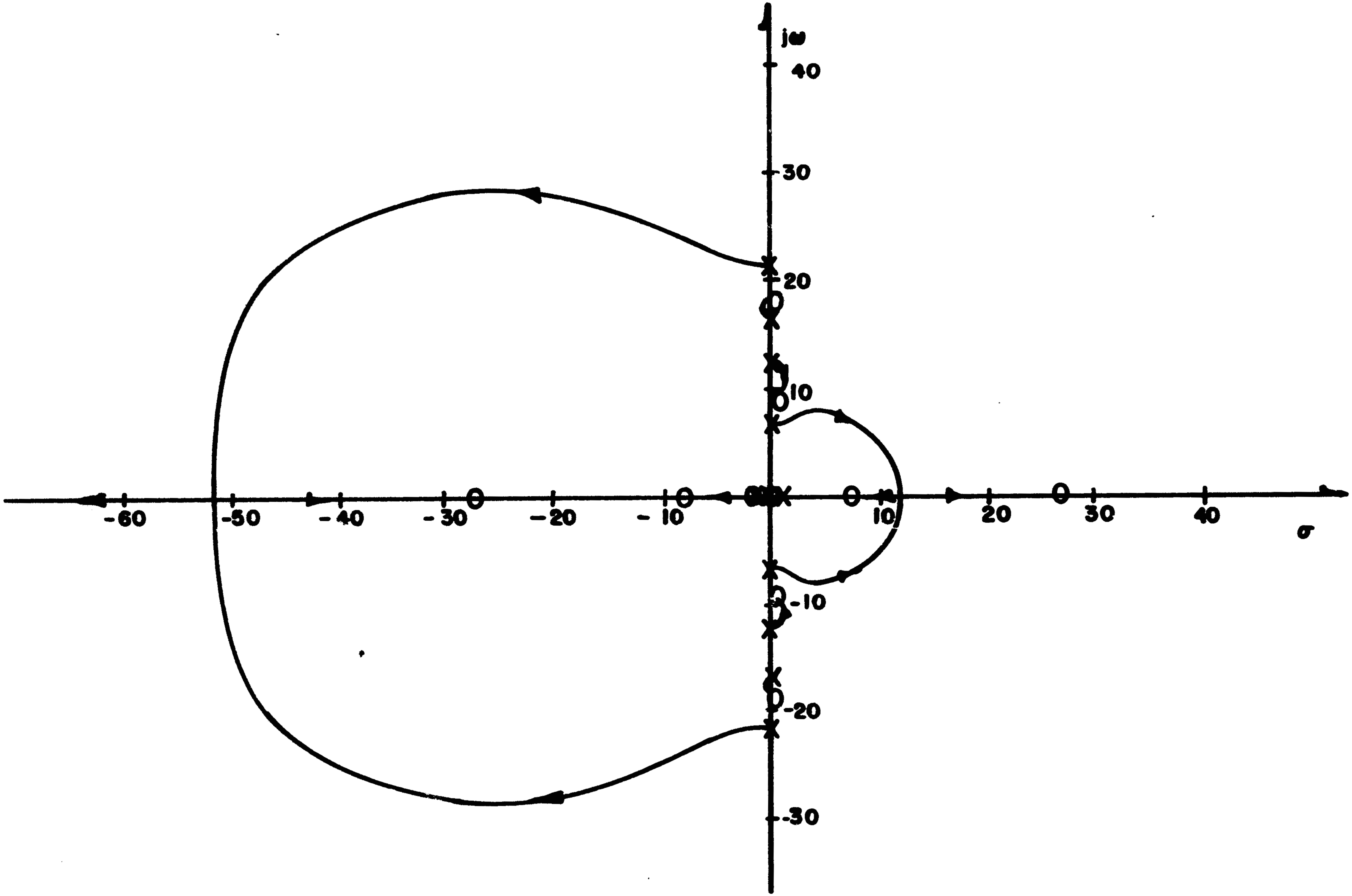

FIGURE 15 ROOT LOCUS PLOT FOR THE RIGID BODY
PLUS FIRST, SECOND, THIRD AND FOURTH BENDING MODES

A.3.6 Evaluation of results

With the gyro gains chosen (a_o = 0.2 and a_1 = 0.4) the closed loop control system is unstable for the rigid body plus the first four bending modes. The analysis was conducted in five steps. The rigid body was investigated first then the bending modes were added one at a time. This was done so that the system sensitivity to each bending mode could be ascertained.

Figure 9 is a root locus diagram for the rigid body mode. For the gyro feedback gains chosen the system forward loop gain is K = 0.468. This value of gain yields a pair of dominant closed loop poles at s = -0.026 $\pm$ j 0.17. This system is lightly damped and has a low frequency response.

Figure 10 is a root locus diagram of the rigid body plus first bending mode. The gyro feedback gains chosen for this analysis yield a pair of complex conjugate closed loop poles in the right half plane at s = 0.29 $\pm$ j 6.65. This produces an unstable system and it is obvious that the system is very sensitive to the first bending mode at this point in the trajectory.

Figure 12 is a root locus plot of the rigid body plus the first and second bending modes. For the gyro gains chosen, the closed loop poles associated with the first bending mode lie in the right half plane at s = 0.29 $\pm$ j 6.64. The closed loop poles associated with the second bending mode also lie in the right half plane at s = 0.38 $\pm$ j 12.24. The first and second bending mode produce system instability.

The root locus plot of the rigid body plus the first, second and third bending modes is shown in Figure 14. For the gyro gains chosen the open loop gain is K = 0.654. The closed loop poles associated with the third bending mode lie in the left half plane at $s = -0.46 \pm j\ 16.9$. The third bending mode does not contribute to system instability, but the closed loop poles associated with the first and second bending modes are located in the right half plane at $s = 0.29 \pm 6.3$ and $s = 0.38 \pm j\ 12.3$ respectively. The system is again unstable.

The root locus plot of the rigid body plus first, second, third and fourth bending modes is shown in Figure 15. The locus of the closed loop pole associated with the fourth bending mode never leaves the left half plane and therefore the fourth bending mode dynamics cannot lead to system instability. However the first and second bending modes dominate the control system performance and produce an unstable system for very low gains.

In summary, it appears that the first and second bending modes are the principle causes of instability at this point in the trajectory. The need for compensation is apparent. Investigation of the root locus diagram of Figure 10, for the Rigid Body plus first bending mode, revealed that the entry of the locus into the right half plane could be delayed if the angle of exit of the locus from the complex open loop poles located at $s = 0.067 \pm j\ 6.7$ could be rotated by 180°. This could be accomplished by the addition of a second order filter of the form

$$G_c(s) = \frac{\omega_c^{\ 2}}{s^2 + 2\,\zeta_c \omega_c\, s + \omega_c^{\ 2}} \qquad \text{(A-119)}$$

into the feedback loop. This filter will degenerate the performance of the Rigid Body mode, but this trade-off was practical, since the rigid body could be made stable by the proper choice of gain. Values of $\omega_c^{\ 2} = 50$ and $\zeta_c = 0.707$ were chosen for the filter parameters.

A.4 Feedback Compensation

A.4.1 Rigid Body Mode:

A block diagram of the rigid body mode with gyro and feedback compensation is shown in Figure 16.

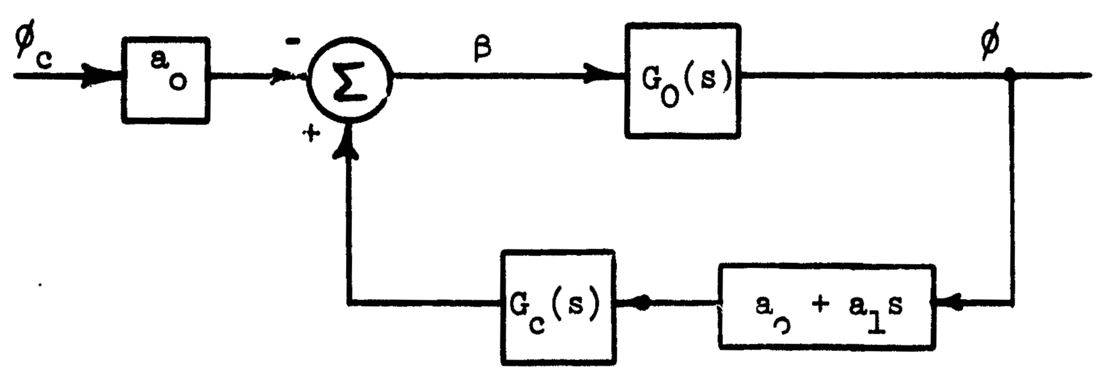

Figure 16 - Block Diagram of Rigid Body Mode Plus Feedback Compensation

where

$$G_0(s) = \frac{-1.17\,(s + 0.0465)}{s^3 + 4.06 \times 10^{-2}s^2 - 2.02 \times 10^{-1}s + 2.77 \times 10^{-3}} \tag{A-120}$$

$$G_c(s) = \frac{50}{s^2 + 10s + 50} \tag{A-121}$$

The system characteristic equation is

$$1 - KGH = 1 + \frac{1.17a_1\,(50)(s + a_o/a_1)(s + 0.0465)}{(s^3 + 4.06 \times 10^{-2}s^2 - 2.02 \times 10^{-1}s + 2.77 \times 10^{-3})(s^2 + 10s + 50)} \tag{A-122}$$

For feedback gains of

$$a_o = 0.2$$

$$a_1 = 0.4$$

The characteristic equation becomes

$$1 - KGH = 1 + \frac{23.4\ (s + 0.5)(s + 0.047)}{(s + 0.48)(s - 0.014)(s - 0.422)(s + 5 \pm j\ 5)} \tag{A-123}$$

The root locus plot for this system is shown in Figure 17.

A.4.2 Rigid Body Plus First Bending Mode

A block diagram of the rigid body mode plus the first bending mode with gyro feedback and feedback compensation is shown in Figure 18.

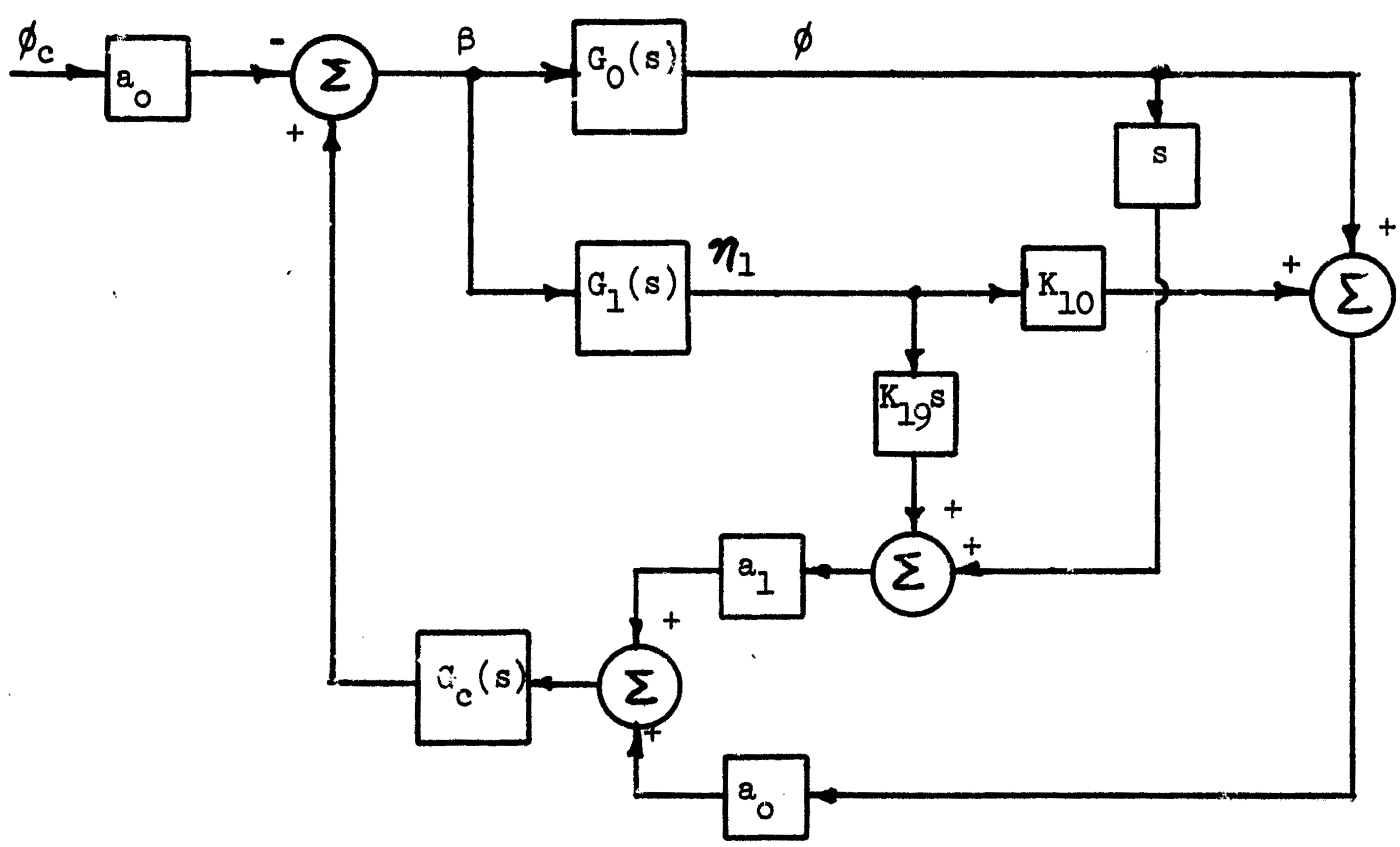

Figure 18 - Block Diagram of Rigid Body Plus First Bending Mode with Feedback Compensation

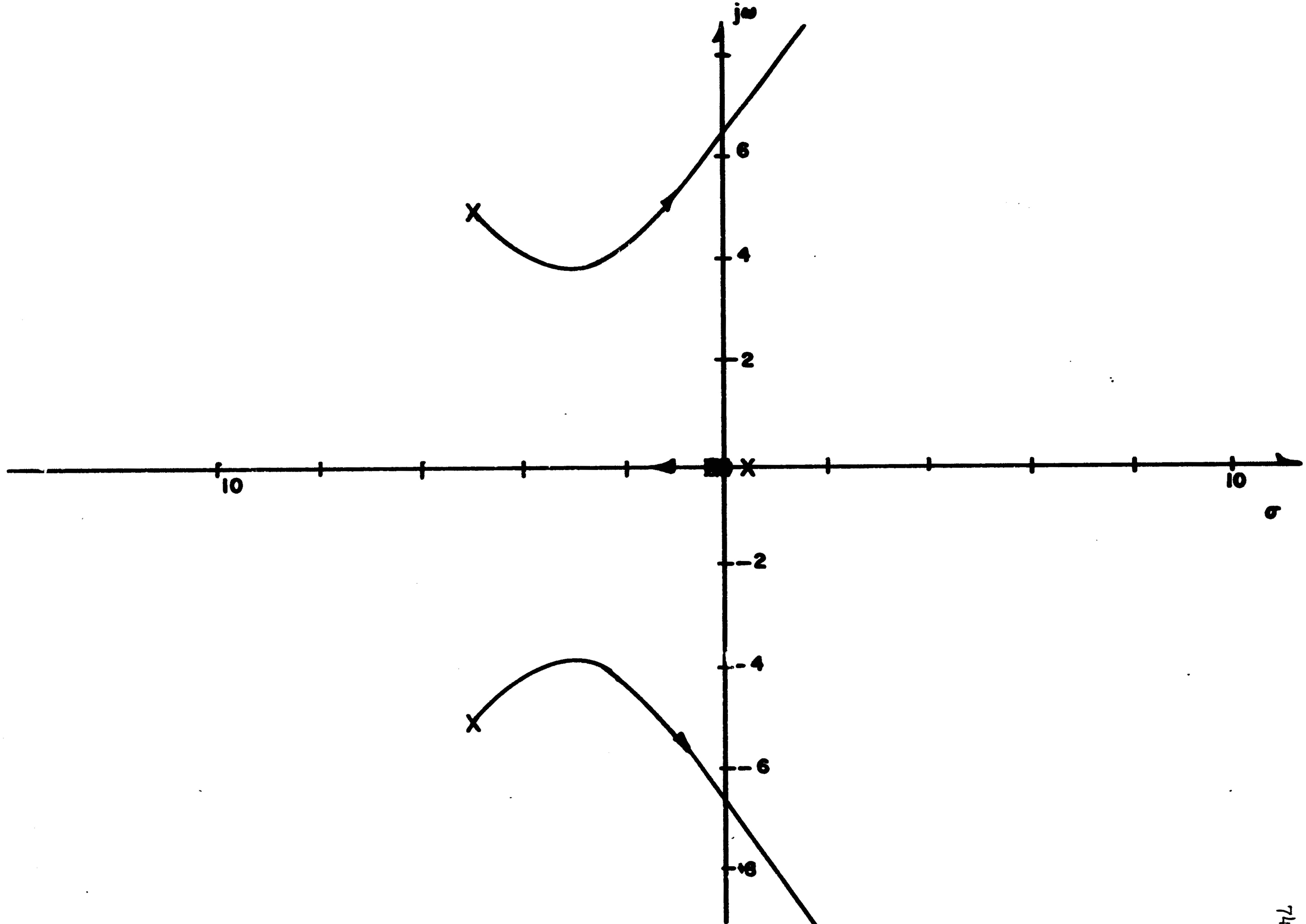

FIGURE 17 ROOT LOCUS PLOT FOR THE RIGID BODY MODE WITH FEEDBACK COMPENSATION

Block diagram reduction results in the diagram shown in Figure 19.

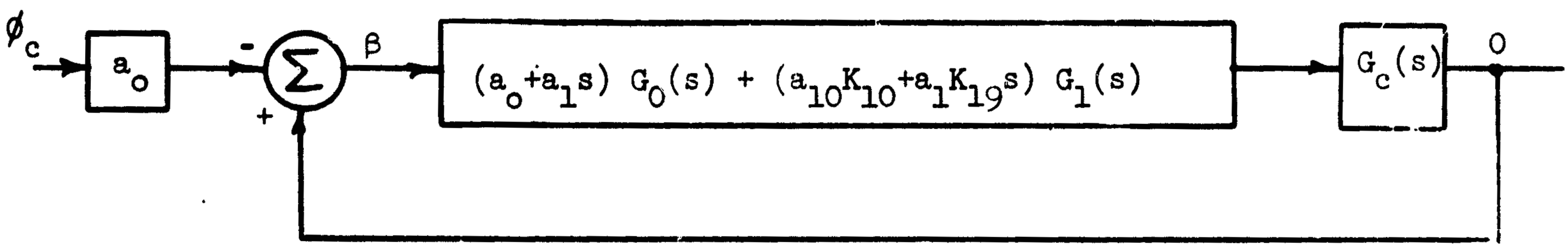

Figure 19 - Reduced Block Diagram

The characteristic equation for this system is:

$$1 - KGH = 1 - G_c(s)\ \left[(a_o + a_1 s)\ G_0(s) + (a_o K_{10} + a_1 K_{19} s)\ G_1(s)\right] \tag{A-124}$$

$$1 - KGH = 1 - \frac{12.2(s^4 + 1.87s^3 - 8.65 \times 10^{+1}s^2 - 4.77 \times 10^{+1}s - 2.02)}{s^7 + 10.2s^6 + 9.65 \times 10^{+1}s^5 + 4.58 \times 10^{+2}s^4 + 2.55 \times 10^{+3}s^3 - 4.7 \times 10^{-1}s^2 - 4.54 \times 10^{+2}s + 6.25} \tag{A-125}$$

In factored form this becomes

$$1 - KGH = 1 - \frac{12.2(s - 8.7)(s - 0.046)(s + 0.5)(s + 10)}{(s + 0.48)(s - 0.014)(s - 0.422)(s + 0.067 \pm j\ 6.7)(s + 5 \pm j\ 5)} \tag{A-126}$$

The root locus plot for this system is shown in Figure 19.

A.4.3 Rigid Body Plus First and Second Bending Mode

The block diagram for this system is similar to that of Figure 11 with the addition of the filter in the feedback loop. The system characteristic equation is

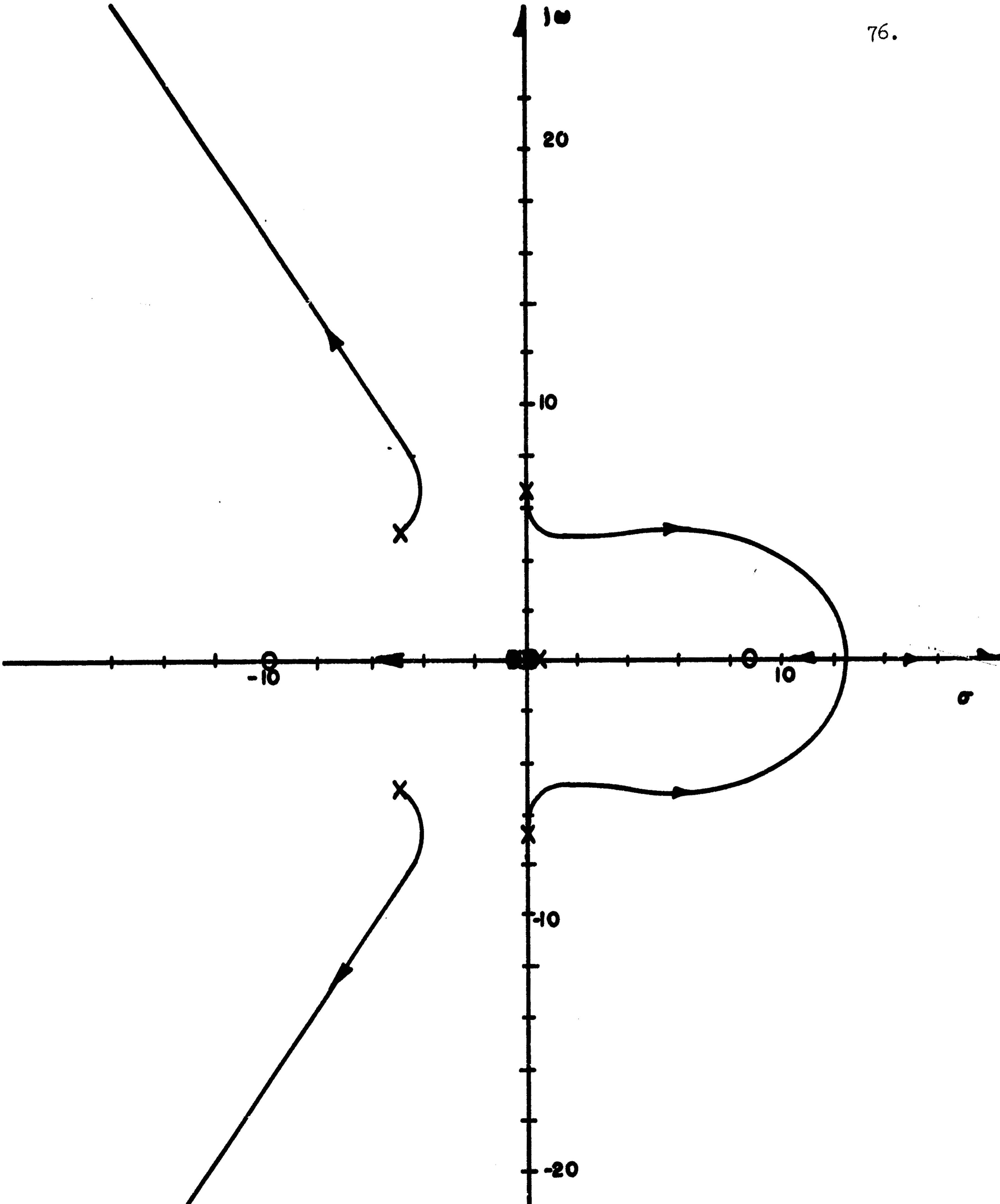

FIGURE 19 ROOT LOCUS PLOT FOR THE RIGID BODY PLUS FIRST BENDING MODE WITH FEEDBACK COMPENSATION

$$1 - KGH = 1 - G_c(s)\left[(a_o + a_1 s)\, G_0(s) + (a_o K_{10} + a_1 K_{19} s)\, G_1(s) + (a_o K_{20} + a_1 K_{29} s)\, G_2(s)\right] \quad \text{(A-127)}$$

$$1 - KGH = 1 - 62.5 \frac{\left[\begin{array}{l} s^6 + 4.57 \times 10^{-1} s^5 + 4.8 \times 10^{+1} s^4 + 3.89 \times 10^{+1} s^3 \\ - 2.56 \times 10^{+3} s^2 - 1.41 \times 10^{+3} s - 5.95 \times 10^{+1} \end{array}\right]}{\left[\begin{array}{l} s^9 + 1.04 \times 10^{+1} s^8 + 2.48 \times 10^{+2} s^7 + 2 \times 10^{+3} s^6 \\ + 1.67 \times 10^{+4} s^5 + 6.87 \times 10^{+4} s^4 + 3.33 \times 10^{+5} s^3 \\ - 1.8 \times 10^{+2} s^2 - 6.73 \times 10^{+4} s + 9.3 \times 10^{+2} \end{array}\right]} \quad \text{(A-128)}$$

In factored form this is

$$1 - KGH = 1 - \frac{62.5(s - 5.62)(s - 0.089 \pm j\, 8.95)(s + 0.046)(s + 0.5)(s + 5.7)}{(s + 0.48)(s - 0.014)(s - 0.422)(s + 0.067 \pm j\, 6.7)(s + 0.122 \pm j12.3)(s + 5 \pm j\, 5)} \quad \text{(A-129)}$$

The root locus plot for this system is shown in Figure 20.

A.4.4 Rigid Body Plus First, Second and Third Bending Mode

The block diagram for this system is similar to that of Figure 13 with the addition of the filter in the feedback loop.

The system characteristic equation is given by

$$1 - KGH = 1 - G_c(s)\left[(a_o + a_1 s)\, G_0(s) + (a_o K_{10} + a_1 K_{19} s)\, G_1(s) + (a_o K_{20} + a_1 K_{29} s)\, G_2(s) + (a_o K_{30} + a_1 K_{39} s)\, G_3(s)\right] \quad \text{(A-130)}$$

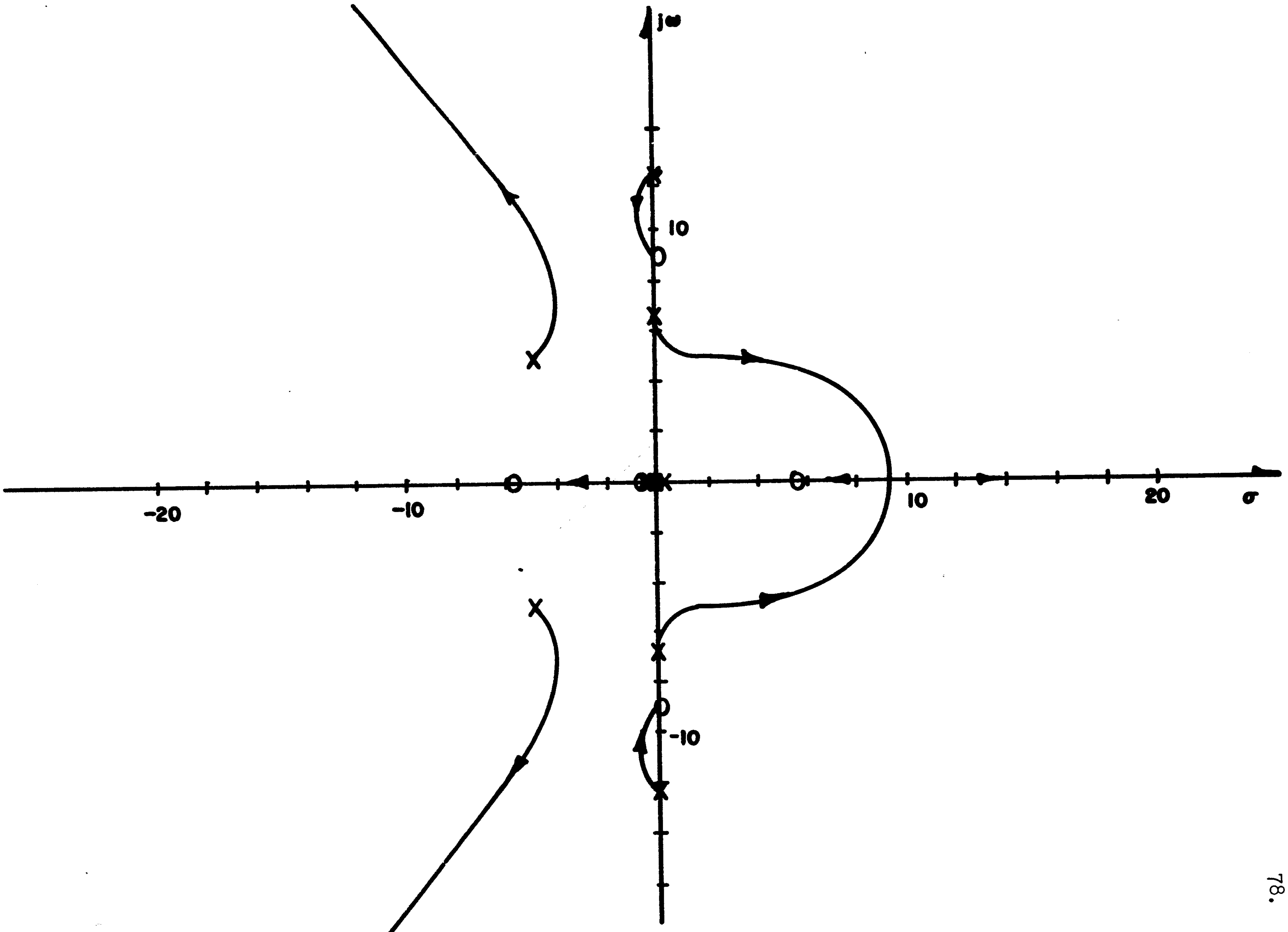

FIGURE 20 ROOT LOCUS PLOT FOR THE RIGID BODY PLUS FIRST AND SECOND BENDING MODE WITH FEEDBACK COMPENSATION

$$1 - KGH = 1 - 32.7 \frac{\left[\begin{array}{l} s^8 - 4.6 \times 10^{-1} s^7 + 4.55 \times 10^{+2} s^6 + 2.45\, s^5 + 1.48 \times 10^{+4} s^4 \\ + 5.96 \times 10^{+3} s^3 - 1.4 \times 10^{+6} s^2 - 7.66 \times 10^{+5} s - 3.23 \times 10^{+4} \end{array}\right]}{\left[\begin{array}{l} s^{11} + 1.08 \times 10^{+1} s^{10} + 5.38 \times 10^{+2} s^9 + 5.06 \times 10^{+3} s^8 + 8.84 \\ \times 10^{+4} s^7 + 6.69 \times 10^{+5} s^6 + 5.15 \times 10^{+6} s^5 + 1.98 \times 10^{+7} s^4 + \\ 9.54 \times 10^{+7} s^3 - 6.47 \times 10^{+4} s^2 - 1.93 \times 10^{+7} s + 2.66 \times 10^{+5} \end{array}\right]} \tag{A-131}$$

In factored form this equation becomes

$$1 - KGH = 1 - 32.7 \frac{\left[\begin{array}{l} (s - 6.46)(s - 0.24 \pm j\, 20.3)(s - 0.14 \pm j\, 9.2) \\ (s + 0.046)(s + 0.5)(s + 6.23) \end{array}\right]}{\left[\begin{array}{l} (s + 0.48)(s - 0.014)(s - 0.422)(s + 0.067 \pm j\, 6.7) \\ (s + 0.122 \pm j\, 12.3)(s + 0.17 \pm j\, 17)(s + 5 \pm j\, 5) \end{array}\right]} \tag{A-132}$$

The root locus plot for this system is shown in Figure 21.

A.4.5 <u>Rigid Body Plus First, Second, Third and Fourth Bending Mode</u>

The block diagram for this system is similar to that of Figure 5 with the addition of the filter in the feedback loop.

The system characteristic equation is given by

$$1 - KGH = 1 - G_c(s) \Big[(a_o + a_1 s)\, G_0(s) + (a_o K_{10} + a_1 K_{19} s)\, G_1(s) + (a_o K_{20} + a_1 K_{29} s)\, G_2(s) + (a_o K_{30} + a_1 K_{39} s)\, G_3(s) + (a_o K_{40} + a_1 K_{49} s)\, G_4(s) \Big] \tag{A-133}$$

In factored form this equation becomes

$$1 - KGH = 1 + 16.6 \frac{\left[\begin{array}{l} (s - 26.8)(s - 7.67)(s - 0.45 \pm j\, 18.1)(s + 0.013 \pm j\, 9.46) \\ (s + 0.046)(s + 0.5)(s + 7.61)(s + 27.59) \end{array}\right]}{\left[\begin{array}{l} (s + 0.48)(s - 0.014)(s - 0.422)(s + 0.067 \pm j\, 6.7) \\ (s + 0.122 \pm j\, 12.3)(s + 0.17 \pm j\, 17)(s + 0.21 \pm j\, 21.5) \\ \qquad (s + 5 \pm j\, 5) \end{array}\right]} \tag{A-134}$$

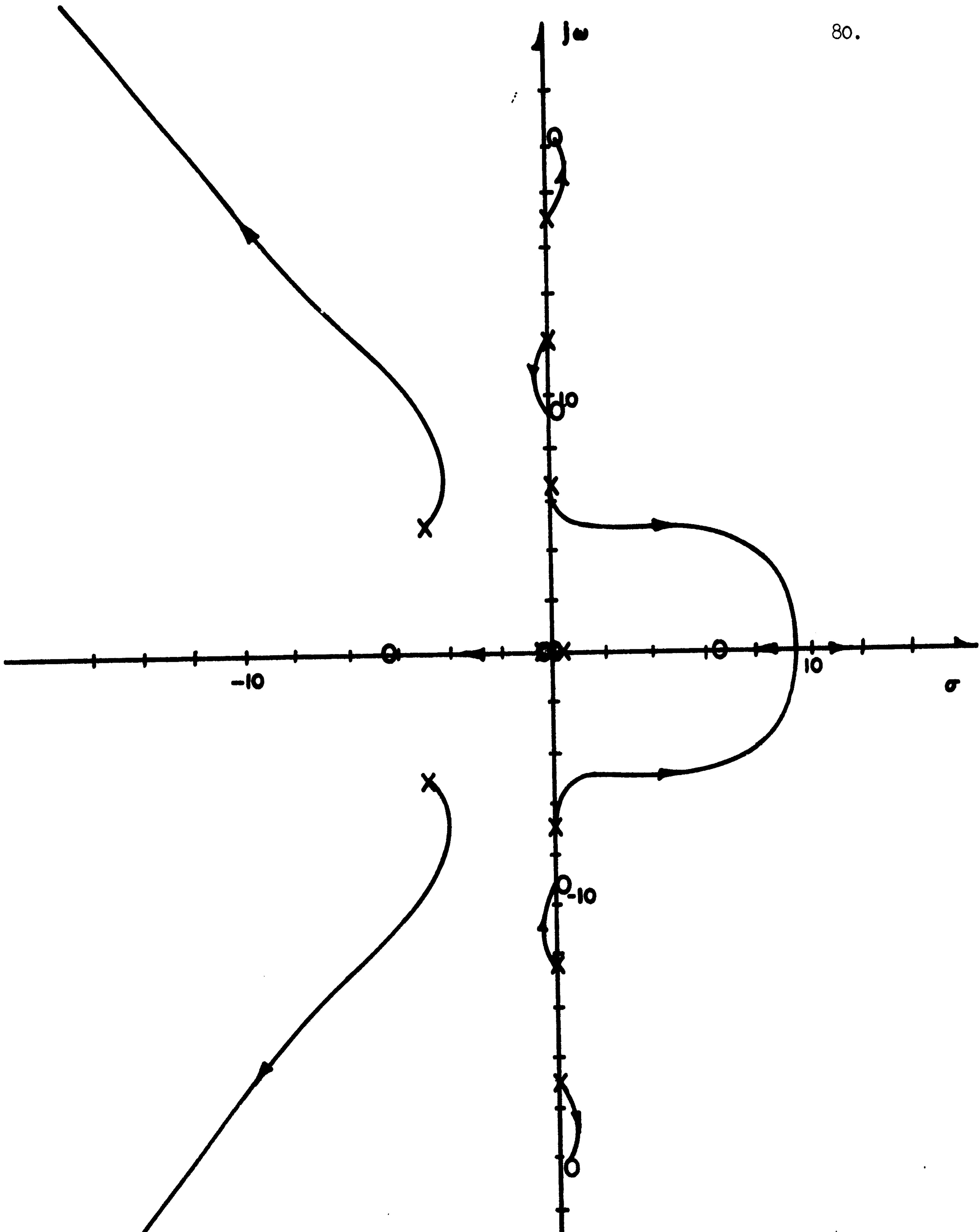

FIGURE 21 ROOT LOCUS PLOT RIGID BODY PLUS FIRST, SECOND AND THIRD BENDING MODES WITH FEEDBACK COMPENSATION

The root locus plot for this system is shown in Figure 22.

A.4.6 Evaluation of Results

The insertion of the second order lag filter in the feedback loop has little effect upon the performance of the Rigid Body mode at lower gains. This is apparent from the root locus plot of Figure 17. The location of the closed loop poles for a gain of $K = 23.4$ (a combination of a filter gain of 50 and a gyro feedback gain of 0.468) indicates that the dominant pair of closed loop poles are located at $s = 0.026 \pm j\,0.18$ and one due to the rigid body dynamics. The effect of the filter complex closed loop poles located at $s = -4.8 \pm j\,4.8$ is negligible on the overall response because the transient due to these poles dies out very quickly compared to the long transient associated with the rigid body poles. However as gain is increased the effect of the filter is more noticable and the possibility of instability exists for high gain as the locus will move from the left half plane to the right half plane along the direction of the asymptotes located at 60° and 300°.

Figure 19 shows the effect of the compensation filter on the locus of closed loop poles for the Rigid Body plus First Bending mode. The locus generated from the open loop poles located at $s = -0.067 \pm j\,6.7$ again moves from the left half plane to the right half plane but the $j\omega$ axis crossover is accomplished at a higher gain ($K = 36.4$) than the uncompensated system ($K = .0335$). This results in a "stiffer" system.

The root locus plots of the Rigid Body plus First and Second Bending modes and Rigid Body plus First, Second and Third Bending modes are shown in Figures 20 and 21. Here the additional angle added by the compensation

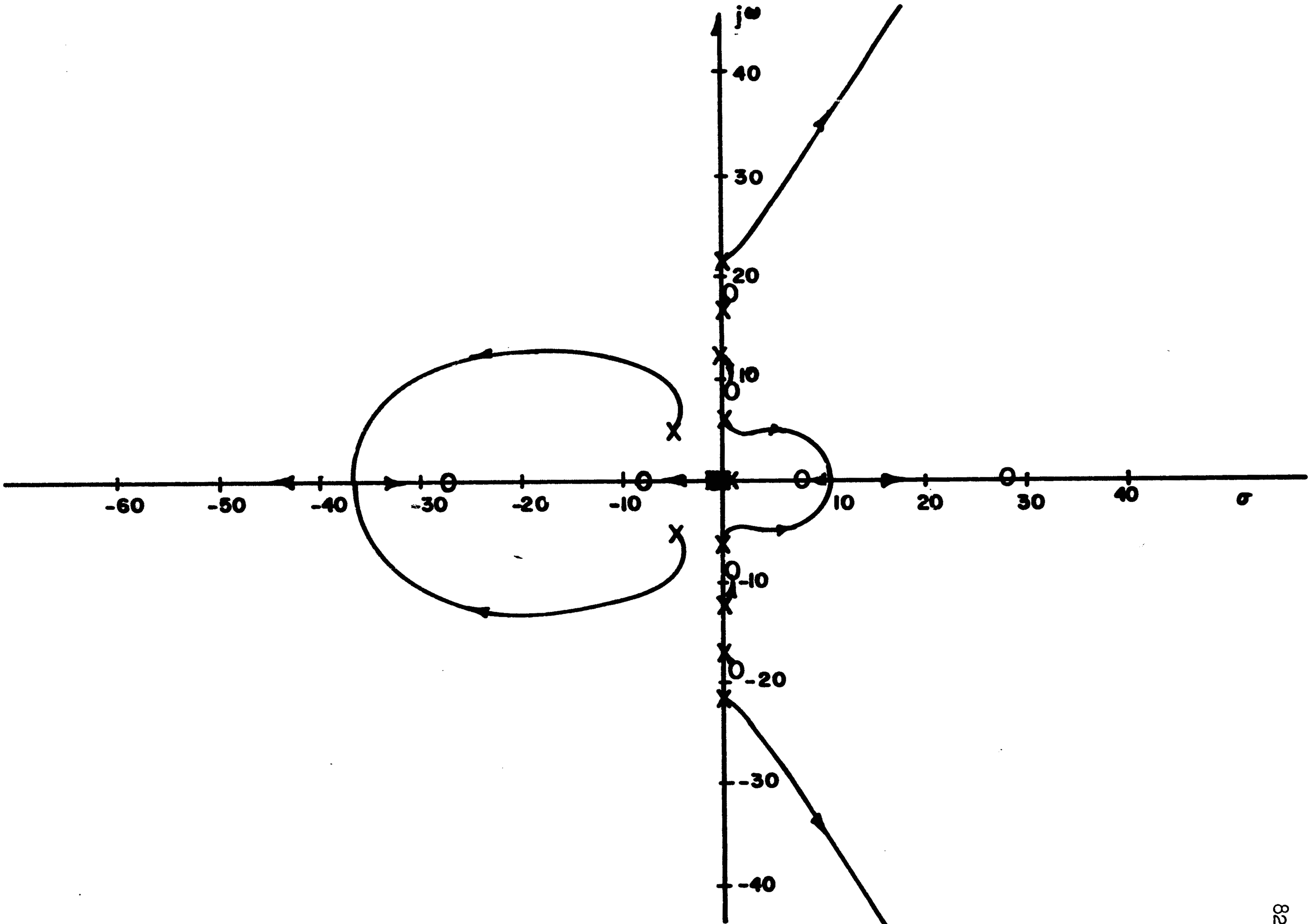

FIGURE 22 ROOT LOCUS PLOT OF THE RIGID BODY PLUS FIRST, SECOND, THIRD, AND FOURTH BENDING MODES WITH FEEDBACK COMPENSATION

filter alters the locus between the mode pole-zero pairs, reversing the path 180° from the uncompensated system. Again $j\omega$ crossover is accomplished at higher gains.

Finally the root locus for the Rigid Body plus four bending modes is shown in Figure 22. Here a stability problem is introduced by the addition of the compensation filter. In the uncompensated case the locus from the pair of complex open loop poles associated with the Fourth Bending mode migrates to the real axis in the left half plane. The locus never leaves the left half plane and the fourth bending mode does not compromise stability. However with the addition of the compensation network, the locus now migrates into the right half plane, for a gain of $K = 17.3$. The filter acts as a destabilizing influence on the Fourth Bending mode dynamics.